Habilitation à diriger des recherches :
Université Toulouse III - Paul Sabatier
LABORATOIRE COLLISIONS AGRÉGATS RÉACTIVITÉ

Spécialité : PHYSIQUE

Atom interferometer experiments using large spatial separations.

Alexandre Gauguet

Soutenue le 15 juillet 2024 devant le jury composé de :

M. Markus ARNDT	University of Vienna	Rapporteur
M. Nicola POLI	University of Florence	Rapporteur
Mme Saïda GUELLATI-KHELIFA	Sorbonne Université	Rapporteuse
M. Arnaud LANDRAGIN	Observatoire de Paris	Examinateur
M. Mark KASEVICH	University of Stanford	Examinateur
M. David GUÉRY-ODELIN	Université Toulouse 3 - Paul Sabatier	Examinateur
M. Carlo RIZZO	Université Toulouse 3 - Paul Sabatier	Examinateur

Remerciements

Lorem ipsum dolor sit amet, consectetuer adipiscing elit. Ut purus elit, vestibulum ut, placerat ac, adipiscing vitae, felis. Curabitur dictum gravida mauris. Nam arcu libero, nonummy eget, consectetuer id, vulputate a, magna. Donec vehicula augue eu neque. Pellentesque habitant morbi tristique senectus et netus et malesuada fames ac turpis egestas. Mauris ut leo. Cras viverra metus rhoncus sem. Nulla et lectus vestibulum urna fringilla ultrices. Phasellus eu tellus sit amet tortor gravida placerat. Integer sapien est, iaculis in, pretium quis, viverra ac, nunc. Praesent eget sem vel leo ultrices bibendum. Aenean faucibus. Morbi dolor nulla, malesuada eu, pulvinar at, mollis ac, nulla. Curabitur auctor semper nulla. Donec varius orci eget risus. Duis nibh mi, congue eu, accumsan eleifend, sagittis quis, diam. Duis eget orci sit amet orci dignissim rutrum.

Résumé

Les expériences d'interférométrie à ondes de matière ont marqué une avancée dans l'étude expérimentale de la physique quantique, permettant de dépasser les simples expériences de pensée. À Toulouse, nous développons des interféromètres atomiques dont la particularité réside dans une grande séparation spatiale entre les bras de l'interféromètre. Cette caractéristique offre possibilité de contrôler les potentiels électromagnétiques et gravitationnels le long des bras de l'interféromètre, ouvrant ainsi de nouvelles perspectives dans le domaine de la physique fondamentale.

Nous avons développé un interféromètre exploitant un jet supersonique de lithium et la diffraction de Bragg sur une onde laser stationnaire. La distance maximale entre les deux chemins atomiques dans cet interféromètre est d'environ 100 micromètres, ce qui permet l'insertion d'un septum (une fine feuille d'aluminium) entre ces deux chemins. Cela nous a permis d'appliquer des champs électriques et magnétiques distincts sur les deux bras de l'interféromètre. Ces fonctionnalités ont été exploitées dans une série d'expériences à visée métrologique, telles que la mesure de la polarisabilité électrique du lithium, ou dans l'exploration de phénomènes quantiques, tels que les phases géométriques He-McKellar-Wilkens et Aharonov-Casher, ou encore la modulation de phase des ondes atomiques du lithium.

Nous travaillons actuellement sur le développement d'un nouvel interféromètre atomique utilisant des condensats de Bose-Einstein de rubidium manipulés à l'aide d'un réseau optique vertical. Pour augmenter la séparation entre les bras de l'interféromètre, nous explorons une solution fondée sur l'utilisation de séparatrices dites à grands transferts d'impulsion (LMT). Dans ce contexte, je présente une nouvelle technique reposant sur une séquence d'impulsions laser dans le régime de diffraction de quasi-Bragg. Nous avons démontré des mesures interférométriques avec un transfert total de 200 $\hbar k$. Ce travail a des applications dans le développement de capteurs inertiels. De plus, de tels interféromètres, avec des séparations spatiales macroscopiques, ouvrent la voie à de nouveaux types d'interféromètres atomiques envisagés pour des tests de physique fondamentale, tels que la recherche de matière noire, les tests de neutralité atomique et les tests de gravitation.

Mots clés : Interférométrie atomique, Physique quantique expérimentale, Atomes ultra-froids

Abstract

Matter-wave interferometry experiments are a milestone in the experimental study of quantum physics, allowing to go beyond simple thought experiments. In our group in Toulouse, we are developing atom interferometers with a high degree of spatial separation between the arms of the interferometer. This feature makes it possible to control electromagnetic and gravitational potentials along the interferometer arms, opening new perspectives in fundamental physics.

An interferometer using a supersonic lithium beam and Bragg diffraction on a stationary light wave has been developed. The maximum separation of the two atomic paths in this interferometer is about 100 micrometers, which allows the insertion of a septum (a thin aluminum foil) between the two atomic paths. This configuration enables different electric and magnetic fields to be applied to the two paths. These possibilities have been exploited in a number of metrological experiments. For example, the electrical polarizability of lithium has been measured, and quantum phenomena such as the He-McKellar-Wilkens and Aharonov-Casher geometric phases and the phase modulation of lithium atomic waves have been studied.

We are currently developing a new atom interferometer using Bose-Einstein condensates of rubidium manipulated with a vertical optical lattice. An attractive solution to increase the arm separation is to use large momentum transfer (LMT) beamsplitters. I present a promising technique based on a sequence of laser pulses in the quasi-Bragg diffraction regime. In particular, we have demonstrated interferometers with a total transfer of 200 $\hbar k$. This work has applications in the field of quantum technologies with the development of inertial sensors. In addition, interferometers with macroscopic spatial separations pave the way for new atomic interferometers proposed in various fundamental physics tests, such as the search for dark matter, atomic neutrality tests, and gravitational tests.

Keywords : Atom interferometry, Experimental quantum physics, Ultra-cold atoms

Table des matières

Chapitre 1

Summary of the work

> All in all it is just
> Another brick in the wall.
>
> — Pink Floyd

T<small>HIS</small> thesis summarizes my research activities at the Laboratoire Collisions Agrégats et Réactivité (LCAR) since I was recruited as a lecturer at Paul Sabatier University in 2010. My research focuses on the development of atom interferometers for precision measurements, with applications in geophysics, navigation and fundamental physics. As some of my research work prior to 2010 is directly related to atom interferometry and metrology, I begin this chapter with a brief description.

My research activity started in 2004 with my PhD thesis in the "Atom Interferometry and Inertial Sensors" group of the SYRTE (SYstème Référence Temps Espace) laboratory, under the supervision of Philip Tuckey and Arnaud Landragin. My thesis focused on the characterization of a gyroscope based on the measurement of the Sagnac effect with cold atoms. The experiment is based on the differential measurement of the interference signals of two atom interferometers sharing the same laser beams. The main results concern an improvement of the sensitivity of the atom interferometer and an evaluation of the accuracy of the rotation measurements. This work confirmed the utility of cold atoms for controlling systematic effects. When I defended my thesis in 2008, few studies had been published on the metrological limits of dual interferometers, so this work contributed to the dimensioning of large-scale instruments based on dual interferometers, such as those intended for gravitational testing, gravitational wave detection, or geophysical measurements.

During the academic year 2007-2008, I worked as an ATER (attaché temporaire d'enseignement et de recherche) at the University Paris 13 in the "Metrology, molecules and fundamental tests" team at the Laboratoire de Physique des Lasers (LPL). Under the supervision of Christophe Daussy, I participated in the determination of the Boltzmann constant by measuring the Doppler broadening of a molecular absorption line. The spectroscopy was performed in the mid-infrared, around 10 μm, in a low-pressure molecular ammonia gas placed inside a thermostat.

I then spent two years (2008-2010) as a postdoctoral fellow at Durham University in the group of Charles Adams, where we demonstrated the possibility of "cooperative optical nonlinearities" induced by dipole-dipole interactions between Rydberg atoms. A first experimental setup based on optically induced transparency (EIT) allowed us to demonstrate these cooperative optical nonlinearities induced by interactions between atoms. I also designed and set up an experiment to trap atoms in a micrometric optical trap to achieve the Rydberg blockade regime. This experiment allowed us to demonstrate optical single photon trapping in the form of Rydberg polaritons and their manipulation by microwave fields.

In 2010, I joined the LCAR atom interferometry group led by Jacques Vigué. We used a large spatial separation interferometer based on a supersonic beam of lithium atoms to study He-McKellar-Wilkens and Aharonov-Casher geometric phase shifts, matter wave beating, decoherence, and measurements of electrical polarizabilities. These experiments are presented in Sec.3.

Since 2015, the team I lead has focused on the study of atom interferometers using Bose-Einstein condensates manipulated by optical lattices. I supervise two experimental setups. The first focuses on interferometers with very large spatial separation. These interferometers are used in fundamental physics to test the foundations of quantum physics and its relation to gravity, the neutrality of matter, and models of energy and dark matter. The device we are developing offers a new approach to these tests by using geometric phase shifts. The second is to develop on-chip Bose-Einstein condensate sources with a view to space missions using cold atoms.

Figure 1.1 summarizes the main experimental setups I've worked on since my recruitment in Toulouse, the corresponding research contracts, and the Ph.D. students I've supervised. In September 2016, Baptiste Allard was recruited as a lecturer in the team. Together, we provide the scientific leadership of the team.

In addition to this general presentation, the manuscript consists of four chapters. Chapter 2 gives a historical overview of the field and introduces the basics of atom interferometry. Chapter 3 presents the results obtained with the lithium interferometer. Chapter 4 presents the development of the new interferometer and the prospects in terms of performance limits, as well as a number of applications, in particular for matter neutrality testing. I also present the technological developments of on-chip ultracold atom sources that we are carrying out in the laboratory.

2010	2011	2012	2013	2014	2015	2016	2017	2018	2019	2020	2021	2022	2023	2024	2025	2026

J. Gillot

B. Decamps

J. Alibert (co.dir.)

M. Bordoux (dir.)

A. Béguin (co. dir.)

T. Rodzinka (co. dir.)

R. Calviac

L. Calmels (co. Dir.)

S. Beldjoudi

Interféromètre lithium

Interféromètre BEC rubidium

Puce hybride

ANR-HIPATI

CNES-Pancha

NEXT CORSAIR

ANR-TANAI

IDEX CORSAIR

NanoX- Asgard

ANR-MiniXQuanta

CNES-Puce

CNES-Puce

ANR-AGAPES

PEPR - QAFCA

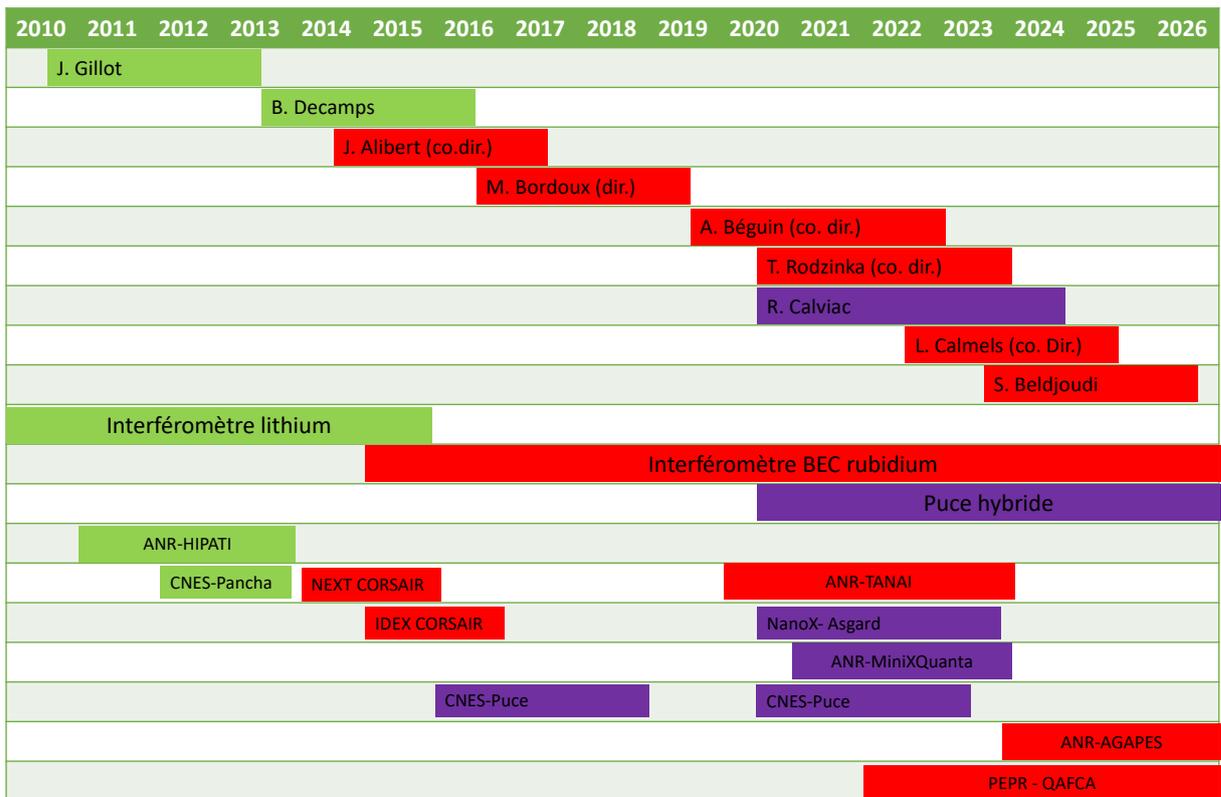FIGURE 1.1 – Supervision of graduate students and research projects

Chapitre 2

Basic concepts of atom interferometry

Bazinga!

Sheldon Cooper

Objectifs

This chapter presents the context of my research on atom interferometry. Atom interferometry was first published in 1991. Since then, it has developed very rapidly, thanks in particular to developments in atom cooling techniques, which have made entirely new experiments possible. This chapter briefly introduces the basics of atom interferometry and some of the recent advances that have inspired me.

Sommaire

1 Principles of atom interferometry

1.1 Matter-wave interferometer

Optical interferometry developed throughout the 19th century, with the work of Young, Fresnel, Fizeau, and Michelson, to name just a few famous names. After the discovery of quantum physics by L. de Broglie [De Broglie, 1924], E. Schrödinger [Schrödinger, 1926] and W. Heisenberg [Heisenberg, 1925], the idea of the matter wave optics developed very rapidly. These theoretical predictions were confirmed for electrons three years later by the observation of electron diffraction in two independent experiments by G. P. Thomson at the University of Aberdeen [Thomson, 1928] and by C. J. Davisson and L. H. Germer at Bell Laboratories [Davisson, 1927]. In 1930, diffraction experiments with atoms were performed by I. Estermann and O. Stern [Estermann, 1930]. These experiments contributed to the development of matter-wave interferometers, first with electron interferometers [Marton, 1952; Möllenstedt, 1955] and then with neutron interferometers [Rauch, 1974]. A detailed history of these developments is given in the book [Rauch, 2015].

Atom interferometry has its roots in studies of coherent manipulation of the internal states of atoms, in particular Ramsey's separate-field excitation [Ramsey, 1950][1], as well as advances in optical spectroscopy and the need to consider the quantization of the external degrees of freedom of atoms. These advances led to the first atom interferometers in the late 1980s. Four pioneering experiments, all published in Physical Review Letters (PRL), marked this advent. These included an experiment using Young's slits [Carnal, 1991], an interferometer exploiting the diffraction by material nanograting of a supersonic beam [Keith, 1991], an interferometer based on Raman diffraction of cold atoms [Kasevich, 1991], and finally a Ramsey-Bordé interferometer using a thermal beam and single-photon transitions [Riehle, 1991]. Details of these advances can be found in various books and review articles [Berman, 1997; Miffre, 2006a; Cronin, 2009; Tino, 2014]. Before discussing certain aspects of atom interferometry, it is worth mentioning the advances in matter-wave interferometry, where more complex objects, such as macromolecules, have been successfully used [Fein, 2019; Brand, 2020], contributing in particular to the search for either the limits of quantum mechanics or the ultimate processes of matter-wave decoherence [Arndt, 2014].

1.2 Two-wave atom interferometer

Most recent atom interferometers share similarities with two-wave optical interferometers (see figure 2.1). In both cases, an incident wave is coherently split into two paths by a first beamsplitter and interferes at a last beamsplitter. The populations in the output states depend on the phase in each of the output ports. In the case of a two-wave interferometer, the population measured at one of the two interferometer outputs oscillates as a function of the phase accumulated between the two interferometer paths:

$$P = P_0 \big[1 + V \cos(\Delta\phi) \big] \tag{2.1}$$

---

1. This technique was later reinterpreted as a real atom interferometry experiment [Bordé, 1984].
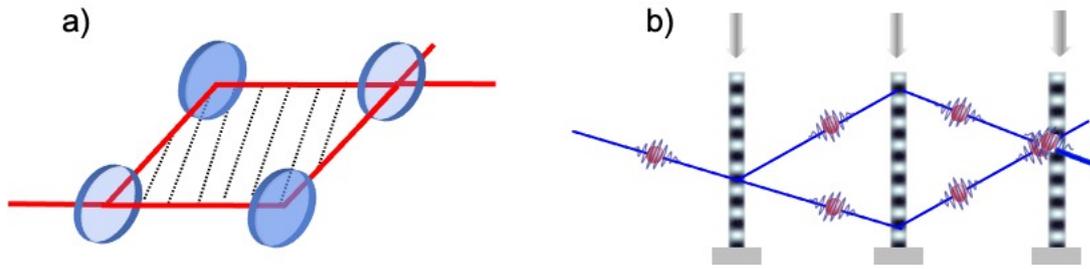
FIGURE 2.1 – Principle of a two-wave interferometer. a) In optics, a laser beam is split along two paths and, after reflection at mirrors, converges on a 2nd splitter, which recombines the beams and closes the interferometer. b) In an atom interferometer, matter waves are manipulated coherently using diffraction gratings (material or light).

P_0 is the average detected signal and $V = \frac{P_{\max} - P_{\min}}{P_{\max} + P_{\min}}$ is the visibility.

By measuring the atomic populations at the output, we can determine the phase shift between the two arms and thus the interaction potentials responsible for this phase shift. To calculate these phase shifts as a function of the interaction potentials, several approaches are available. The most common approach is to calculate the propagator in the position space representation using a semi-classical approximation [Bordé, 1990 ; Pippa Storey, 1994 ; Bongs, 2006]. In the case of interaction potentials at most quadratic in r and p, exact solutions are available [Bordé, 1990 ; Antoine, 2003]. This approach has been incorporated into a five-dimensional formalism corresponding to propagation in ordinary space-time plus one dimension corresponding to proper time [Bordé, 2008]. Despite its complexity, this formalism, to which C.J. Bordé devoted his efforts until the end of his life, sheds new light on the significance of atom interferometry measurements within the framework of general relativity [Jaekel, 2013 ; Overstreet, 2023]. Consequently, it is of great significance for understanding new proposals to test general relativity with atom interferometers [Lamine, 2002 ; Dimopoulos, 2007 ; Zych, 2011 ; Loriani, 2019]. These ideas are also explored using descriptions based on operator evolution, without the need for specific representations [Kleinert, 2015]. As the accuracy of the interferometer improves, theoretical models must include effects that are increasingly complex to describe precisely, such as propagation effects during atom beamsplitters [Antoine, 2006], as well as non-quadratic potentials [Bertoldi, 2019 ; Ufrecht, 2020 ; Overstreet, 2021], which become significant when the interferometer arms are very far apart [Bertoldi, 2019 ; Ufrecht, 2020 ; Overstreet, 2021].

The interferometers I describe in this manuscript have a configuration similar to the Mach-Zehnder interferometer in optics (see figure 2.1). In this configuration, both arms of the interferometer close regardless of the initial velocity, allowing us to use atomic ensembles characterized by a broad velocity distribution σ_v (corresponding to a short coherence length $\xi = \frac{\hbar}{m\sigma_v}$). Furthermore, this geometry is robust to various perturbations, such as constant frequency shifts, making it attractive for measuring inertial effects and interaction potentials applied to each interferometer arm. Variants of this configuration are used for specific measurements, such as the Ramsey-Bordé geometry [Bordé, 1984 ; Riehle, 1988 ; Weiss, 1994] for h/m measurements, as well as more advanced configurations, such as multi-loop configurations, which are of growing
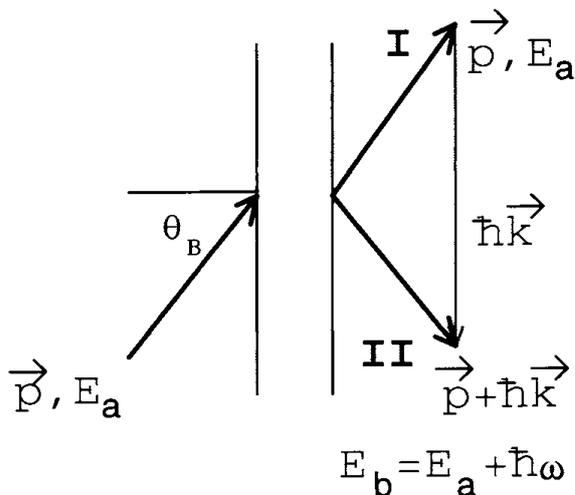
Figure 2.2 – Figure taken from C.J. Bordé's article in the book [Berman, 1997], showing the exchange of energy and momentum between an atom and a light wave. For a sufficiently long interaction, the conservation of energy and momentum allows us to consider two exit paths (I and II). An incident atom in its initial state of energy E_a and momentum $\vec{p}$ interacts with a light wave. It can remain in its initial state (path I), or it can gain momentum $\hbar\vec{k}$ and energy $\hbar\omega$ by exchange processes with photons of the light wave and emerge in state II with energy E_a and momentum $\vec{p} + \hbar\vec{k}$.

interest in metrology [Graham, 2016 ; Sidorenkov, 2020 ; Schubert, 2021].

1.3 Atomic Beamsplitter

To achieve coherent separation of atomic wave functions, atom interferometers first exploited diffraction from material gratings [Keith, 1991]. Although these approaches are relatively simple to implement and robust, they suffer from low efficiency and limited control over the diffracted states. Today, most metrology experiments use laser-based atom beamsplitters, which have the advantage of excellent transmission and phase control. In this case, spatial separation is achieved by momentum exchange during the interaction between the atom and the light field. The principle is shown schematically in figure 2.2, taken from the article by C.J. Bordé in [Berman, 1997]. The atom can either remain in the initial $|a, \vec{p}\rangle$ state of total energy E_a and momentum $\vec{p}$, or it can emerge in the $\left|b, \vec{p} + \hbar\vec{k}\right\rangle$ and gain energy $\pm\hbar\omega$ and momentum $\pm\hbar\vec{k}$ by absorption $(+)$ or stimulated emission $(-)$ of photons from the light wave. It is possible to distinguish between inelastic processes that couple two different internal states, such as single-photon transitions (Figure 2.3(a)) and two-photon Raman transitions (Figure 2.3(b)), and elastic processes, such as Bragg transitions (Figure 2.3(c)), where the momentum states are coupled without the atom changing its internal state.

Atomic beamsplitters using single-photon optical transitions, $|a, p\rangle \longleftrightarrow |b, p + \hbar k\rangle$ (figure 2.3(a)), were already implemented in the first Ramsey-Bordé interferometers [Bordé, 1984 ; Riehle, 1988]. These beamsplitters use Rabi oscillations between the two coupled states to control a coherent superposition of the form $\alpha\,|a, p\rangle + \beta\,|b, p + \hbar k\rangle\,e^{i\phi_L}$. A $\pi/2$ pulse creates an equiprobable superposition between the two momentum states, thus realizing the equivalent of beamsplitters for atomic wave functions, while a π pulse is used to deflect atomic paths with a probability ideally 100%, thus playing the role of mirrors. It is important to note that these atomic beamsplitters require long-lived states (e.g., the clock transition in strontium 87) to avoid losses due to spontaneous emission. In addition, these beamsplitters require strict control of the optical phase ϕ_L, since this phase is transferred to the atomic wave, and the stability of this phase over the time spent in the interferometer is crucial [Chiarotti, 2022]. This requi-

rement necessitates the use of lasers with spectral properties equivalent to those of the best optical clocks. For this reason, these devices are often referred to as "clock-atom interferometers". Single-photon separators are the subject of renewed interest [Hu, 2017b; Rudolph, 2020], especially in the context of dark matter research and gravitational wave detection [Badurina, 2020; Schlippert, 2020; Abe, 2021].

To circumvent spontaneous emission and mitigate the critical dependence on laser phase control, one solution is to use multiphoton transitions between long-lived internal ground states (Figure 2.3(b and c)). The atom interacts with two counterpropagating optical waves of wavevectors $k_{1,2}$, which couple internal ground states $|a\rangle$ and $|b\rangle$ via an intermediate excited state $|i\rangle$. This two-photon process is accompanied by a momentum exchange with the two counterpropagating traveling waves $\hbar(\vec{k_1} - \vec{k_2} \sim 2\hbar\vec{k})$, where the momentum state of the atoms changes from $|\vec{p}\rangle$ to $\left|\vec{p} + 2\hbar\vec{k}\right\rangle$. By choosing a sufficiently large detuning of the lasers with respect to the optical transition Δ, it is possible to neglect the population in the intermediate state $|i\rangle$ and thus to reduce the dynamics to an effective two-level system between the ground states $|a, \vec{p}\rangle \longleftrightarrow \left|b, \vec{p} + 2\hbar\vec{k}\right\rangle$. To create the atomic waves equivalent of mirrors and beam splitters, we can perform π and $\pi/2$ laser pulses, as in single-photon transitions.

Among the two-photon transitions, stimulated Raman transitions involve coupling between two different internal states. In the case of alkali, the two internal states can be the two hyperfine ground states. The frequency difference between these two states is typically several GHz, which is much larger than the shifts associated with recoil effects of a few kHz[2]. Consequently, in contrast to Bragg diffraction, which will be discussed later, it is possible to restrict the dynamics to an effective two-level system $|a, \vec{p}\rangle$ and $\left|b, \vec{p} + 2\hbar\vec{k}\right\rangle$. Moreover, the coupling between the two pulse states implies a dependence of the resonance condition on the atomic velocity due to the Doppler effect. This dependence gives a selectivity of the Raman transitions with respect to the atomic velocity parallel to $\vec{k}$. This selectivity increases with the length of the laser pulse used. Pulses of duration τ are characterized by a spectrum whose width is proportional to τ^{-1}. These pulses can induce efficient Raman transitions for initial velocity classes that become larger as τ^{-1} increases. In this way, a resonant Raman transition can be achieved for a velocity distribution whose width is several times the recoil velocity ($v_r = \hbar k/m$). In addition, Raman transitions offer the advantage that the transmitted and diffracted waves are not in the same internal state: selective detection in the internal state makes it possible to separate the output channels of an atom interferometer, eliminating the need for spatially separated atom clouds. Currently, Raman transitions are widely used in atom interferometry for high precision measurements [Gauguet, 2009; Hu, 2013; Rosi, 2014; Fang, 2016; Freier, 2016; Morel, 2020].

The principle of Bragg transitions is similar to that of Raman transitions. The main difference is that the momentum states are coupled without changing the internal state of the atoms, as shown in figure 2.3(c). Consequently, to satisfy the resonance condition, it is necessary to tune the frequency difference between the two waves of the optical lattice to multiples of the recoil frequency $\omega_r/(2\pi)$ (a few kHz). This adjustment can be done with a single laser combined with

---

2. The recoil frequency associated with the D2 transition, $\omega_r = \frac{\hbar k^2}{2m}$, is ~ 3.77 kHz for rubidium 87 and ~ 63 kHz for lithium 7.
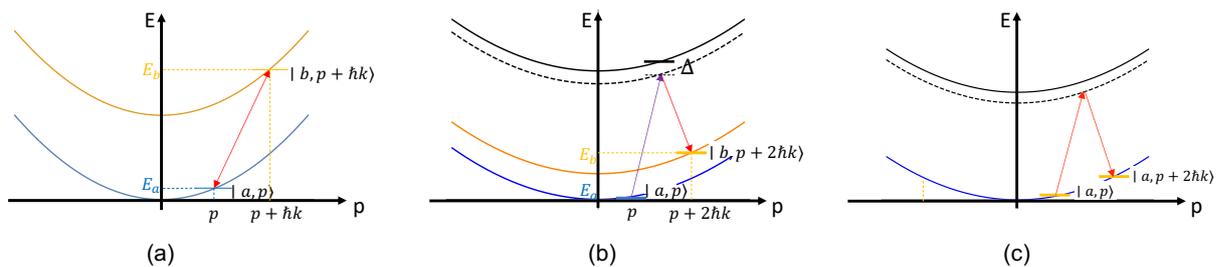
FIGURE 2.3 – (a) Energy momentum diagrams corresponding to a one-photon transition between two states (a), a Raman transition (b), and a Bragg transition (c).

acousto-optic modulators (AOM) (see chapter 4), or by tilting the standing wave with respect to the atomic trajectory to induce a Doppler effect that compensates for the detuning associated with the recoil. This tilt angle is known as the Bragg angle, as explained in chapter 3. In addition, a peculiarity of Bragg diffraction is that it allows coupling to higher diffraction orders associated with 2n photon transitions $|p\rangle \leftrightarrow |p + 2n\hbar k\rangle$. However, the two-photon coupling to the next non-resonant pulse state $|p + 2(n + 1)\hbar k\rangle$ shows a relatively small detuning of $\delta_{n+1} \sim 4(n+1)\omega_r$ (see figure 2.4(a)). Consequently, to limit the population in unwanted diffraction orders, the spectral width of the transition must be well below $4\omega_r$. It is therefore essential to have a source of atoms with a velocity distribution less than v_r to select a single diffraction order. This condition is also essential to facilitate the spatial separation of the output ports, which is necessary for the detection of interference fringes, since with the internal state unchanged it is no longer possible to distinguish the output states other than by their momentum. Despite these limitations, Bragg diffraction offers some interesting features for atom interferometry. Atoms propagate in the same internal state, which is essential for certain measurements of atomic properties [Décamps, 2020] that cannot be obtained by spectroscopy, as well as for Aharonov-Bohm-type measurements of geometric phases (chapter 3). In addition, high-order Bragg diffraction can be used to increase the separation between the interferometer arms, thereby increasing the sensitivity of inertial sensors. In addition, as we will see in chapter 4, Bragg diffraction is particularly well suited for even higher order pulse transfers based on the use of sequences of successive Bragg pulses.

Atomic diffraction through an optical lattice in the quasi-Bragg regime. The diffraction of an atom by an optical lattice formed by a standing wave of light has been the subject of many theoretical studies. An introduction to the subject can be found in [Meystre, 2001]. A description adapted to the experimental configuration of the chapter 3 can be found in the thesis of S. Lepoutre [Lepoutre, 2011]. M. Bordoux's thesis [Bordoux, 2019] and A. Béguin's [Beguin, 2023] also deal with Bragg diffraction, but in the context of an experiment with ultra-cold atoms, described in chapter 4. In the following, I briefly introduce the elements used in the rest of this manuscript.

The optical lattice consists of two counter-propagating beams, characterized in the laboratory reference frame by their frequency ($\omega_{1,2}$), their wave vector ($\vec{k}_{1,2}$) opposite $\vec{k}_1 \sim -\vec{k}_2$, and a phase ($\phi_{1,2}$) (see figure 2.4). The frequency difference between these two beams is denoted by

$\delta\omega = \omega_1 - \omega_2$, and the mean wave vector is defined as $k = (k_1 + k_2)/2$. When these two waves are superimposed, they form a quasi-stationary wave moving with velocity $v = \delta\omega/2k$ relative to the laboratory reference frame.

In our experimental setups, the laser is detuned far from the frequencies of the atomic transitions, allowing for adiabatic elimination of the excited state. The atom-light interaction is then reduced to a light shift proportional to the light intensity. This leads to an interaction potential of the form $2\hbar\Omega(t)\sin^2(kz - \phi(t)/2)$, where $\Omega(t)$ represents the two-photon Rabi frequency. The Hamiltonian describing the evolution of the atom is the sum of a kinetic energy term, the potential associated with the standing wave, and a Doppler term corresponding to the relative velocity between the optical lattice and the atom, denoted $\tilde{v}$.

$$H = \frac{\hat{p}^2}{2M} - \tilde{v}\hat{p} - \frac{\hbar\Omega(t)}{2}\left(e^{2ik\hat{z}} + e^{-2ik\hat{z}}\right) \tag{2.2}$$

The operators $e^{\pm 2ik\hat{z}}$ couple momentum states differing by $2\hbar k$. The periodic potential can thus be interpreted as a two-photon process in which a photon is absorbed in one traveling wave and re-emitted by stimulated emission in the other wave, resulting in a momentum transfer of $2\hbar k$. This two-photon process can be repeated n times, transferring $2n$ photon recoils corresponding to higher diffraction orders, as shown in the figure 2.4. Because of the spatial periodicity of the Hamiltonian, it is possible to expand the wave function over the plane waves basis $\{|2l\hbar k\rangle\}$. In this basis, the Hamiltonian $H(t)$ takes the form of a tridiagonal matrix:

$$H(t) = 4\hbar\omega_r \begin{pmatrix} \delta_{-m} & \gamma(t) & 0 & \dots & \dots & \dots & 0 \\ \gamma(t)^* & \ddots & \ddots & \ddots & \ddots & \ddots & \vdots \\ 0 & \ddots & 0 & \ddots & \ddots & \ddots & \vdots \\ \vdots & \ddots & \ddots & \ddots & \ddots & \ddots & \vdots \\ \vdots & \ddots & \ddots & \ddots & \delta_n & \ddots & 0 \\ \vdots & \ddots & \ddots & \ddots & \ddots & \ddots & \gamma(t) \\ 0 & \dots & \dots & \dots & 0 & \gamma(t)^* & \delta_{n+m} \end{pmatrix}, \tag{2.3}$$

where ω_r is the one-photon recoil frequency, $\gamma(t) = \frac{\Omega(t)}{8\omega_r}$ corresponds to the adimensional two-photon Rabi frequency. The diagonal terms $\delta_l(t) = l^2 + l\tilde{v}/v_r$ depend on the kinetic energy in l^2 and the velocity $\tilde{v}(t)$ of the lattice relative to the free-falling atoms (in units of $v_r = \hbar k/m$):

$$\tilde{v}(t) = \frac{\delta\omega}{4\omega_r} + \frac{v_a(t)}{v_r} \tag{2.4}$$

v_a is the projection of the atomic velocity onto the lattice direction in the laboratory reference frame. When $\delta\omega = 4n\omega_r + 2kv_a$, the diagonal term δ_n cancels out, thus defining the Bragg condition at order n for a given velocity v_a. In chapter 3, the optical lattice is stationary ($\delta\omega = 0$) in the laboratory reference frame, and we consider atoms whose velocity $\vec{v}$ makes an angle θ with respect to the normal of the optical lattice (figure 2.4(b)). Bragg's condition is then rewritten

as $4n\omega_r + 2\vec{k} \cdot \vec{v} = 4n\omega_r - 2kv\sin\theta_B$, which gives the Bragg angle of order n associated with a wavelength $\lambda_{\mathrm{dB}} = h/mv$ and a grating period $\lambda/2$.

$$\sin\theta_B^{(n)} = n\frac{\lambda_{\mathrm{dB}}}{\lambda} \tag{2.5}$$

In the chapter 4, the optical lattice is vertical and the atoms are in free fall (figure 2.4(c)). Consequently, a time-dependent frequency ramp $\delta\omega(t) = 4n\omega_r + 2kv_0 - 2kgt$ is set to compensate for the acceleration due to gravity and to maintain the Bragg condition.

The corresponding Schrödinger equation gives rise to a system of differential equations for which approximate solutions exist, in particular for rectangular pulse shapes of the optical lattice amplitude. Two extreme cases are widely discussed in the literature [Champenois, 2001a]. The first case corresponds to interaction times short enough to neglect the dynamics of the motional states, i.e. for short interaction times compared to the oscillation period in the optical potential ($\tau < (8\omega_r\sqrt{\gamma})^{-1}$). This approximation corresponds to the Raman-Nath approximation [Raman, 1936], originally introduced for the diffraction of light by acoustic waves. In this approximation, the degeneracy of the momentum states leads to a multi-order diffraction phenomenon, which a priori reduces the interest of this diffraction mode for atomic beamsplitters.

The second case concerns atomic diffraction in the Bragg regime, which occurs for a weak potential $|\gamma| \ll 1$. In this perturbative regime, the population of non-resonant momentum states is negligible, leading to a truly effective two-level system and giving rise to Rabi oscillations characterized by an effective Rabi frequency Ω_{eff}. For the Bragg approximation, the spectral width of the two-photon $\sim \Omega$ transition must be small enough not to populate non-resonant momentum states (*i.e.* other than the two Bragg states) $\Omega \ll \delta_{n+1} = 4(n+1)\omega_r$. However, the duration of a pulse π of order n grows very rapidly at constant laser power. Consequently, the high-order Bragg regime requires very long pulse durations, which are of only limited practical interest. However, the Bragg regime of order $n = 1$ is very interesting, as we will see in the experiments described in chapter 3.

We are therefore interested in an intermediate regime known as the quasi-Bragg regime. This regime has shown high diffraction efficiency for high orders with experimentally accessible parameters [Keller, 1999 ; Jansen, 2007 ; Müller, 2008]. The quasi-Bragg regime occurs when the potential is adiabatically turned on and off. As in the Bragg regime, two momentum states are mainly populated at the end of the interaction. However, in contrast to Bragg diffraction, a complex dynamic between momentum states close to the two Bragg states occurs during the interaction.

We study this evolution by numerically solving the Schrödinger equation from the Hamiltonian (2.3). We use a Gaussian shape of lattice amplitude:

$$\gamma(t) = \gamma_{\mathrm{max}}\exp\left(-\frac{t^2}{2\sigma^2}\right) \tag{2.6}$$

where σ describes the duration of the Gaussian pulse (half duration at $1/\sqrt{e}$) and $\gamma_{\mathrm{max}} = \Omega_{\mathrm{max}}/(8\omega_r)$ where Ω_{max} is the maximum value of the 2-photon Rabi frequency. The numerical
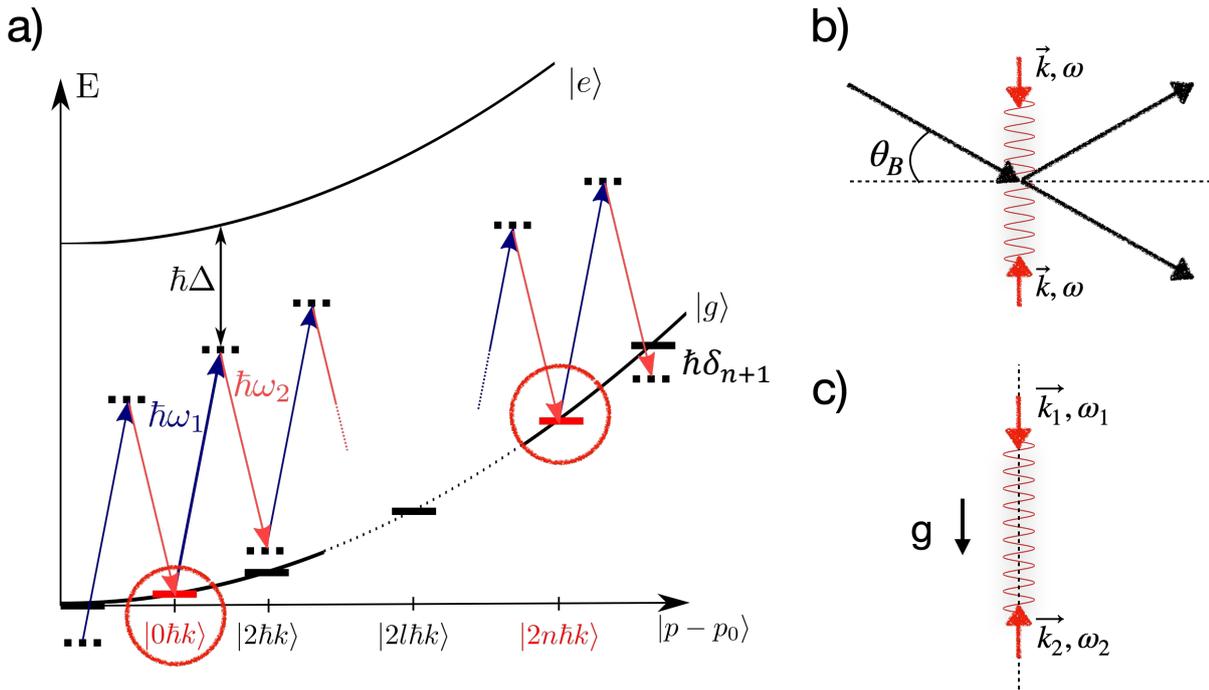
FIGURE 2.4 – a) Conservation of energy and momentum in the Bragg regime. Bragg diffraction of order n is a $2n$ photon process that couples two Bragg states. b) Diffraction of atoms by a stationary lattice in the laboratory reference frame. The resonance condition is tuned by adjusting the angle between the optical lattice and the incident velocity of the atoms. c) The vertical optical lattice is formed by two beams propagating in opposite directions. The resonance condition is adjusted during the free fall of the atoms by adjusting the frequency difference of the atoms $\delta\omega = \omega_1 - \omega_2$.

propagation is performed over a time window of 10σ centered on the laser pulse.

Figure 2.5 shows the evolution of the populations in the two resonant states (*Bragg states*), as well as in the neighboring momentum states, at the end of the Gaussian pulse. This figure also shows the evolution of the populations, assuming an effective two-level system. We have highlighted two interaction sub-regimes: i) the short pulse regime (SP), for which the population in the undesired states (non-adiabatic losses) is non-negligible, and ii) the long pulse regime (LP), for which the populations in the undesired states become negligible, allowing us to recover a regime in which, at the end of the pulse, the populations of the two Bragg states oscillate with opposite phase.

Quasi-Bragg diffraction led to extensive numerical and experimental studies, which I will present in chapter 4. We will see that in practice it is difficult to diffract atomic wave functions with good efficiency beyond the order of $n \sim 10$. To go beyond these limits, it is possible to combine quasi-Bragg diffraction and methods of coherent acceleration of the atom with an optical lattice accelerated either continuously in the manner of Bloch oscillations or sequentially. The study of interferometers based on these LMT (Large Momentum Transfer) beamsplitters is a line of research on which we are currently working, and the main results will be presented in the chapter 4.
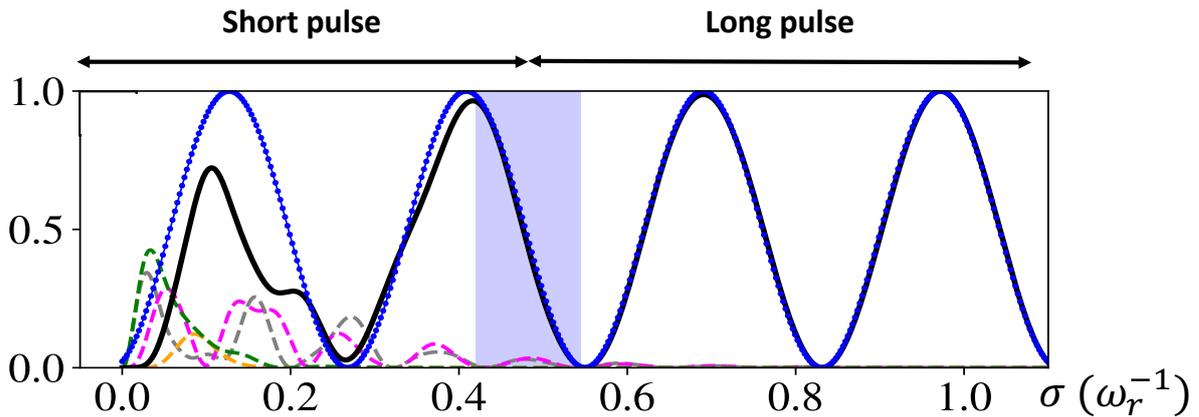
FIGURE 2.5 – Numerical simulation at order $n = 3$ in the quasi-Bragg regime for $\gamma_{\max}$. Evolution of the populations in the different momentum states at the end of a Gaussian pulse of duration σ. The black curve represents the population in the $|6\hbar k\rangle$ state, and the dashed curves represent the population in the *unwanted* states. This population is not negligible in the SP regime. On the other hand, for longer interaction times, i.e. in the LP regime, we find the dynamics of a two-level system, with the simulation results superimposed on a calculation of an effective two-level system (blue dots).

2 Atom Interferometers: Applications

2.1 A brief introduction

Atom interferometers have played a role in many precision measurements over the past two decades, including the development of inertial sensors, the measurement of the gravitational constant G, the fine structure constant α, and the test of the equivalence principle, to name a few.

Inertial sensors. The idea of inertial sensors using matter-wave interferometers was introduced by J.F. Clauser in 1988 [Clauser, 1988]. Atoms, isolated from environmental electromagnetic fields, serve as the inertial reference. Accelerations and rotations of the interferometer cause the laser wavefronts to move relative to the atoms. These displacements induce phase shifts $(\vec{k} \cdot \vec{r}(t))$ of the atomic wave function in the diffraction process, which manifest as a measurable phase shift at the output of the interferometer. These inertial phase shifts are given by $\vec{k} \cdot \vec{a} \, T^2$ for accelerations and $\vec{k}(\vec{v} \times \vec{\Omega} \, T^2)$ for rotations.

For more than two decades, there has been a strong effort to exploit this remarkable sensitivity to develop sensors with a wide range of applications in geophysics and inertial navigation. In absolute gravimetry, the best atom interferometers have demonstrated in laboratories a sensitivity [3] of 50 nm.s^{-2}.Hz$^{-1/2}$ and 0.7 nm.s^{-2} at 10^4s [Gillot, 2014b ; Freier, 2016] and are now competitive with conventional devices such as cube-corner optical interferometers [Nie-

---

3. It is necessary to distinguish between sensitivity, the smallest measurable value in a given time interval, and accuracy, which expresses the uncertainty associated with the measured quantity.

bauer, 1995]. The sensitivity of atom interferometers is not as good as that of the best relative gravimeters, such as superconducting gravimeters (about 0.1nm.s^{-2} at 200 s) [Merlet, 2021]. However, the latter have a time-varying bias and require regular calibration with absolute gravimeters [Merlet, 2021]. The best atomic gravimeters achieve accuracies on the order of 20 nm.s^{-2} [Karcher, 2018]. The maturity of this technology has now reached a stage where commercial products are available with a sensitivity of about 750 nm.s^{-2}.Hz$^{-1/2}$ and an accuracy of 100 nm.s^{-2} [Ménoret, 2018]. The sensitivity limitation of these measurements is mainly due to vibrations.

Differential phase-shift measurements of atom interferometers, spatially separated but sharing common laser beams, offer the possibility of making gravitational gradient measurements with a sensitivity that exceeds the limits imposed by the vibrational noise of each interferometer, thanks to the rejection of common-mode noise in differential measurements. Atom gradiometers have been studied in both horizontal and vertical configurations, with dimensions of the order of a meter, to measure local variations in the gravitational potential [Fixler, 2007 ; Sorrentino, 2014 ; Duan, 2014 ; Biedermann, 2015]. The sensitivity of these instruments ($\propto \sigma_\phi/(kT^2)$) is limited by the quantum projection noise $\sigma_\phi = (V\sqrt{N})^{-1}$ (N is the number of detected atoms and V is the fringe visibility), which justifies the development of techniques to increase the scale factor kT^2 of interferometers, e.g. by using LMT beamsplitters (increasing k) or long interrogation times (increasing T), as well as the implementation of detection below quantum projection noise [4]. Much longer baselines are envisioned, either as part of space missions [Aguilera, 2014 ; Lévèque, 2022 ; Chiow, 2015] or as part of "large instrument" research infrastructures [Canuel, 2018 ; Badurina, 2020 ; Zhan, 2020 ; Schlippert, 2020 ; Abe, 2021]. Precise measurements of gravity gradients at these scales have applications in geodesy, hydrology, and fundamental physics.

Atom interferometers are also considered as gyroscopes. The sensitivity to rotation is derived from the Sagnac phase shift given by $\Delta\phi = \frac{2AE}{\hbar c^2}\Omega$ [Anandan, 1981 ; Bordé, 2002 ; Gauguet, 2014]. In this equation, A is the area of the interferometer, Ω is the rate of rotation relative to an inertial reference frame, and E is the total energy associated with one particle of the wave. For a matter wave propagating at speeds $v \ll c$, the energy is mainly given by $E \sim mc^2$, while for electromagnetic waves it is $E = \hbar\omega$. Consequently, the potential gain in sensitivity of a matter-wave gyroscope over an optical one, with equivalent area and comparable signal-to-noise ratio, is about 10^{11}. However, this statement must be tempered by the fact that the signal-to-noise ratio and area of atom interferometers remain significantly smaller than those of optical interferometers. Atomic gyroscopes have demonstrated short-term sensitivities of the order of a few nrad/s.Hz$^{-1/2}$ using atomic beams [Gustavson, 2000]. On the other hand, gyroscopes using cold atoms have achieved sensitivities of the order of 10^{-10}rad/s (evaluated with Allan's variance at 10^4 s), due to a very good control of the instrument drifts [Savoie, 2018]. However, their implementation is more complex than accelerometers and developments are still required for their use in navigation. Nevertheless, the accuracy of atomic gyroscopes obtained in the laboratory opens up new prospects in geophysics, in particular for the measurement of parameters that were previously inaccessible to experiment, such as variations in the direction of the Earth's axis of rotation on relatively short timescales (a few hours).

---

4. The interested reader will find references in the recent review [Szigeti, 2021]

Determination of fundamental constants. Atom interferometers are also used to measure the gravitational constant, G, and the fine structure constant, α.

The gravitational constant G is determined by measuring the changes in the gravitational gradient induced by the displacements of heavy masses along the lines of two atom interferometers forming a gradiometer [Fixler, 2007]. The best measurements made with this method allowed the gravitational constant G to be determined with a relative uncertainty of 10^{-4} [Rosi, 2014], which is comparable to classical methods using torsion balances [Quinn, 2000]. The gravitational constant G is the most inaccurate fundamental constant, and different series of measurements have led to contradictory results [Quinn, 2013]. In metrology it is always very interesting to benefit from different measurement methods for the same quantity. This is why measurements with atom interferometry, with systematic effects different from other experiments, are essential.

The measurement of the fine structure constant α by atom interferometry is based on the atomic recoil velocity ($v_r = \hbar k/m$) [Wicht, 2002]. This measurement yields the ratio h/m, and hence α, using the relation :

$$\alpha^2 = 2\frac{R_\infty}{c}\frac{m}{m_e}\frac{h}{m} \tag{2.7}$$

The Rydberg constant R_∞ is determined with a relative uncertainty of 1.9×10^{-12} from hydrogen spectroscopy [Mohr, 2016]. The ratio between the mass m of a rubidium atom and that of the electron m_e is known with an uncertainty of $\sim 7\times10^{-11}$ [Mount, 2010]. The measurement of h/m is performed with a Ramsey-Bordé interferometer whose phase shift depends on a contribution to the additional kinetic energy associated with the photon recoils exchanged with the atoms. Recent measurements of h/m allow the fine structure constant α to be determined with a relative uncertainty on the order of 10^{-10} [Parker, 2016 ; Morel, 2020], which is comparable to the best existing results from the measurement of the anomalous magnetic moment of the electron [Aoyama, 2012 ; Fan, 2023]. Atom interferometry measurements now contribute to the determination of the α value of the CODATA [Tiesinga, 2021]. Furthermore, the comparison of these two results can be seen as a check on QED calculations and, more generally, as a test of the Standard Model of particle physics [Parker, 2016 ; Morel, 2020].

Gravitation tests. Among the fundamental tests planned with atom interferometers, tests of gravitation play an essential role and contribute to a better understanding of the connections between gravitation and quantum theory. The investigation of the validity of Einstein's weak equivalence principle using atom interferometry has led to a number of experimental [Fray, 2004 ; Bonnin, 2013 ; Schlippert, 2014 ; Tarallo, 2014 ; Asenbaum, 2020 ; Zhou, 2021 ; Barrett, 2022] and theoretical [Göklü, 2008 ; Kostelecký, 2011 ; Damour, 2012 ; Altschul, 2015 ; Battelier, 2021] developments. These experiments compare measurements of local gravity using an atomic gravimeter, either with two isotopes of the same atomic species, or with two different atomic species. The most constraining limit obtained by atom interferometry corresponds to an Eötvös parameter [5] $\eta < 10^{-12}$. It was obtained by comparing the free fall of the two stable rubidium isotopes. Experiments currently under development propose to surpass the best classical tests

---

5. Weak equivalence principle tests are characterized by the Eötvös η parameter, which is the relative acceleration of the test masses divided by the mean acceleration between the masses in the gravitational field.

based on devices such as the torsion balance experiments [Schlamminger, 2008] ($\eta < 10^{-13}$) or the Microscope space mission using classical accelerometers in free fall [Touboul, 2017] ($\eta < 10^{-14}$).

In parallel with the experiments to test the universality of free fall, theoretical studies have demonstrated the feasibility of measuring general relativity effects in the laboratory, such as the Lense-Thirring effect [Jentsch, 2004], or the measurement of PPN parameters [Dimopoulos, 2008]. Despite their small amplitude, some of these effects seem to be accessible to the very large interferometers currently under development [Dimopoulos, 2007], which reach several meters in height. These apparatuses are also being considered to study the effects of time dilation, with quantum superpositions exploring different gravitational potentials on each of the interferometer arms [Zych, 2011 ; Greenberger, 2012]. In addition, major efforts are underway to assess the ability of atom interferometers to detect gravitational waves [Dimopoulos, 2008 ; Canuel, 2018 ; Badurina, 2020 ; Zhan, 2020 ; Schlippert, 2020 ; Abe, 2021] or manifestations of dark matter [Geraci, 2016 ; Arvanitaki, 2018 ; Du, 2022].

2.2 Separate-arm atom interferometers

One of the special features of the interferometers discussed in this manuscript is the large distance between the interferometer arms. This feature allows controlled perturbations to be applied to one arm of the interferometer. In the following, we will refer to experiments that directly exploit this feature as "separated-arm interferometers".

Matter-wave interferometers can produce large distances between the arms. This distance, denoted Δz, is given by the following relation:

$$\Delta z \propto \frac{n\hbar k_G}{m} T \tag{2.8}$$

In this equation, k_G is the reciprocal lattice vector, m is the particle mass, and T is the free propagation time between the beamsplitter and the mirror. To increase the separation between the interferometer arms, it may be advantageous to use light particles (e.g. neutrons, helium, lithium), to increase the momentum transfer between the lattice and the particles ($n\hbar k_G$), and/or to increase the free propagation time.

Neutron interferometers benefit from the low mass of neutrons and the possibility of highly efficient diffraction processes on material gratings [Rauch, 2015]. Typical separations of these interferometers are several centimeters, allowing the experimental verification of many fundamental effects in quantum physics [Danner, 2023]. However, these devices are limited by neutron time-of-flight (typical neutron velocity is $\sim 10^3 \mathrm{m.s}^{-1}$) and signal-to-noise ratio (the detected signal is a few neutrons per second).

The first separated-arm atom interferometer experiment was performed in 1991 by the team of D. Pritchard [Keith, 1991]. This interferometer used a thermal beam of sodium atoms diffracted by three material gratings. This configuration was used to measure the electrical polarizability of the sodium atom [Ekstrom, 1995], as well as the refractive index of gases for sodium waves [Schmiedmayer, 1995]. In addition, this team carried out several studies on laser excitation induced decoherence [Chapman, 1995 ; Kokorowski, 2001]. The interferometer was

subsequently transferred to the University of Arizona, where A. Cronin performed measurements of atom-surface interaction in the van der Waals regime [Perreault, 2005], dynamic polarizability of different atoms [Trubko, 2017], and studies of collision-induced decoherence [Uys, 2005].

The use of ultracold atom sources paves the way for larger separations between the interferometer arms, aided by longer times of flight and the introduction of very large momentum transfer beamsplitters, known as LMT beamsplitters. In 2008, the team led by C. Sackett at the University of Virginia developed an interferometer using a rubidium Bose-Einstein condensate, allowing a separation of several millimeters [Burke, 2008]. This configuration was used to measure the dynamic polarizability of rubidium by illuminating a single arm with a laser beam [Deissler, 2008 ; Leonard, 2017]. More recently, the team led by M. Kasevich at Stanford University has demonstrated interferometers with separations of up to several tens of centimeters [Kovachy, 2015a], using a 10-meter atomic fountain and LMT beamsplitter techniques. This approach has been used to demonstrate the gravitational equivalent of the scalar Aharonov-Bohm effect [Overstreet, 2022].

This manuscript presents two atom interferometers characterized by a large spatial separation between the interferometer arms. The chapter 3 presents results obtained with a lithium beam interferometer. This apparatus has allowed the measurement of non-inertial effects with applications to the study of atomic structure, matter-wave engineering, and the demonstration of new phases in the Aharonov-Bohm family. The second setup (chapter 4), currently under construction, is based on the use of a rubidium condensate and LMT beamsplitters. It will allow interferometers with separations of tens of centimeters. Interferometers with such spatial separations open the way to new experiments with applications in fundamental physics, which will be discussed in chapter 4.

Chapitre 3

Separated-arm lithium interferometer

J'aime passionnément le mystère, parce
que j'ai toujours l'espoir de le débrouiller.

C. Baudelaire

Objectifs

This chapter is a description of the lithium interferometer research from 2010 to
2015. This experiment has been developed since the late 1990s by J. Vigué (DR-
CNRS), M. Büchner (CR-CNRS), G. Trénec (IR-CNRS) and seven PhD students:
C. Champenois (1999), R. Delhuille (2002), A. Miffre (2005), M. Jacquey (2006),
S. Lepoutre (2011), J. Gillot (2013), B. Décamps (2016). When I joined the team
in 2010, the experimental setup was operational. After a presentation of the main
features of this atom interferometer, I describe the studies we have carried out with
this experiment between 2010 and 2015.

1   Description de l'interféromètre lithium

The design of the experiment and comprehensive analyses of the device are documented in the thesis [Champenois, 1999 ; Delhuille, 2002 ; Miffre, 2005 ; Jacquey, 2006 ; Lepoutre, 2011 ; Gillot, 2013b ; Decamps, 2016]. The atom interferometer is shown in figure 3.1, and is based on a supersonic beam of a lithium-rare gas mixture. Lithium atoms are diffracted in the Bragg regime by three horizontal standing light waves separated by a distance L. The interferometer has a geometry analogous to the Mach-Zehnder interferometer in optics, with a length of $2L = 1,2$ m. The average velocity of the atomic beam can be adjusted between 700 and 3400 m·s^{-1}, depending on the choice of rare gas used. The special feature of this experiment is the sufficiently large separation between the two arms of the interferometer (~ 100 µm) to introduce a controlled perturbation on just one arm of the interferometer.
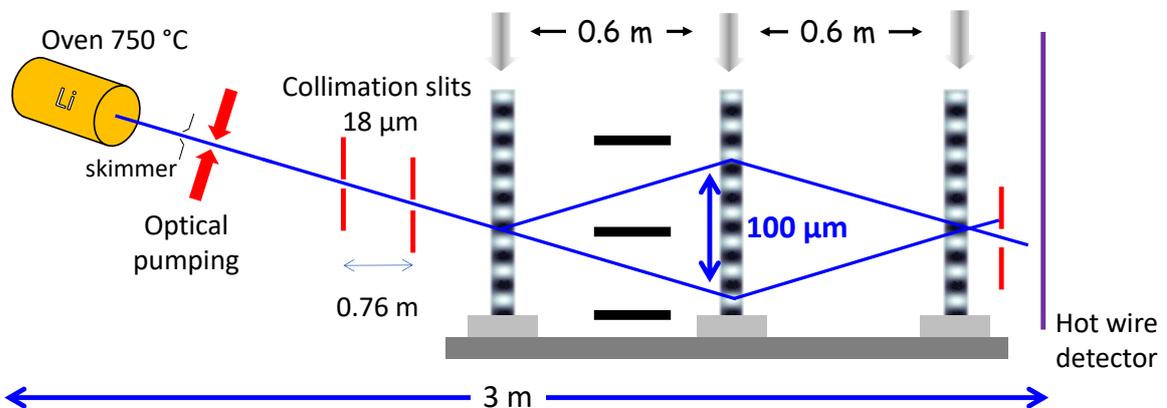

FIGURE 3.1 – We distinguish four zones: the lithium source, the beam collimation, the interferometer and the detection. The interferometer has a Mach-Zehnder geometry with a spatial separation of the order of 100 µm.

1.1   The atomic source

The choice of the lithium atom is based on its low mass, resulting in a substantial recoil velocity $v_r = \frac{\hbar k}{m} = 8,5$ cm·s^{-1}, which in turn facilitates the spatial separation of the interferometer's output beams. In addition, lithium has intense optical transitions near $\lambda_L = 671$ nm, which are accessible with single-frequency lasers. Finally, lithium can be detected very efficiently by ionization on a hot wire.

The atomic beam is produced by supersonic expansion of a carrier gas mixed with a small amount of lithium. In most cases, the carrier gas is argon, and the mixture is produced in an oven heated to 1073 K with an argon pressure of 330 mbar. Under these conditions, the average velocity of the lithium beam is $v_l = 1060$ m·s^{-1}, corresponding to a wavelength of $\lambda_{\mathrm{dB}} = 56$pm and a Bragg angle of $\theta \approx 2v_r/v_l = 160$ µrad. The beam then passes through a skimmer, which selects the most intense part of the beam and reduces the gas load. After the skimmer, the beam is polarized by optical pumping in a Zeeman sublevel. It is then collimated by two vertically

aligned slits, 780 mm apart and 18 mm wide. The beam divergence is $\sim 25\,\mu$rad[1]. This value is smaller than the first-order diffraction angle and allows the spatial separation of the two exit ports. The flux of detected atoms is about 3×10^4 at.s^{-1}, resulting in a brightness of about $\mathcal{B} = 2 \times 10^{20}$ at.s^{-1}.m^{-2}.sr^{-1}.

1.2   Atom optics

Lithium atoms interact sequentially with three optical lattices that diffract the atoms in the Bragg regime. The Bragg regime is characterized by the fact that only two diffraction orders can be coupled, allowing two-wave interferometers without parasitic interferometers. Although it is possible to perform Bragg diffraction at high diffraction orders, in practice only the 1st order can strictly satisfy the Bragg conditions. For this reason, the experiments presented in this chapter were all performed at 1st order diffraction.

Standing light waves are generated with a frequency-stabilized continuous dye laser at 2 GHz on the blue side of the $^2S_{1/2}-^2P_{3/2}$ transition of ^{7}Li. The laser beam is directed into the vacuum chamber. The beam waist of the standing waves is $W = 5$ mm, and the power is divided among the three standing waves to obtain atom beamsplitters for the first and third standing waves, and an atom mirror for the second standing wave. The three retroreflecting mirrors used to create the standing waves are placed under vacuum on a rigid bench to limit relative displacements between the mirrors. Mirror orientation is finely controlled using piezoelectric actuators to adjust the parallelism of the three optical lattices.

1.3   Atomic signal

A slit of about $50\,\mu$m is placed at a distance $d = 400$ mm after the third standing wave to select only one of the interferometer output paths. The two interferometer output ports differ only in the atomic momentum direction. A very good separation is essential because the interference signals on these two outputs are complementary. Selected atoms are counted by a surface ionization detector (Langmuir-Taylor detector or hot-wire detector) with an efficiency of about 30%.

The atomic interference fringes are scanned by moving the third mirror parallel to itself with a piezoelectric actuator. To overcome the nonlinear response of the actuator and the thermal deformation of the mirror mount, the mirror displacements are measured with an optical Michelson interferometer. Figure 3.2 shows a typical interference signal obtained with our atom interferometer. The fringe visibility is about 80%, which is mainly limited by mirror vibrations that induce interferometric phase noise. The phase sensitivity is on the order of $20\,$mrad$/\sqrt{\text{Hz}}$, limited by shot noise during atom counting and vibration noise.

The experiments I will present address phase drift by implementing differential measurements. In this way we achieve a statistical uncertainty of the order of a mrad after several minutes of measurement.

---

1. Transverse collimation is associated with a velocity dispersion $\sigma_v \sim 0.3 v_{rec}$.
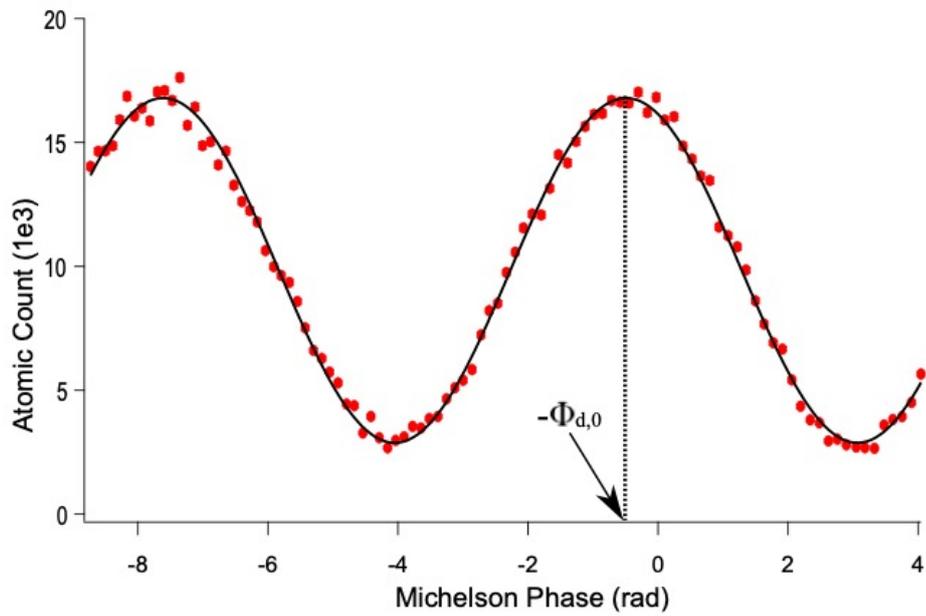
(a) Interferometric signal

FIGURE 3.2 – Phase-dependent interference fringes from the Michelson interferometer (at 633 nm) measuring the displacement of the mirror forming the third standing wave. Each data point corresponds to the detected signal integrated over 1 s. The fringes have a visibility of 71% and the average flux of detected atoms is a few 10^4 atoms/s.

Lithium Interferometer		
Function	Attribute	Value ($\sim$)
Atomic source	longitudinal velocity	1000 $m.s^{-1}$
	longitudinal velocity dispersion	150 $m.s^{-1}$
	atom flux	$5 - 10 \times 10^4 s^{-1}$
Beamsplitter	diffraction angle	$\theta = n\frac{\lambda_{dB}}{\lambda_L} = 160$ μrad
	Diffraction order	n = 1
	Recoil velocity transfer	$2v_r = 17$ cm/s
Interferometer	size	2L = 1.2 m
	duration	$2T \sim 1$ ms
	area	$A = 0.6cm^2$
	Inertial Scale factors $2nkT^2$	$2nkT^2 \sim 2s^2.m^{-1}$
	Max separation	d $\sim$ 100 μm
Detection	efficiency	30 %
	Signal-to-Noise detection at 1 s	100
	phase sensitivity	20 mrad $Hz^{-1/2}$

TABLE 3.1 – Summary of the characteristics of the lithium interferometer. The interferometer has a Mach-Zehnder type geometry, spatial in the horizontal plane.

This apparatus has been used to perform studies of metrological interest, such as the electrical polarizability of lithium [Miffre, 2006b] or the tune-out wavelength [Décamps, 2020]. Studies of collisional properties have been conducted via refractive index measurements of matter waves [Jacquey, 2007] or atom-surface measurements [Lepoutre, 2009], or more fundamentally in quantum physics, such as the first measurement of the He-McKellar-Wilkens (HMW) geometric phase [Lepoutre, 2012 ; Gillot, 2013a]. In the following sections I describe the measurements I participated in between 2010 and 2015.

2   Measurement of HMW and AC phase shifts

The study of He-McKellar-Wilkens and Aharonov-Casher phase shifts has been the main focus of research on this experiment between 2010 and 2013. These geometric phases belong to the family of the vector Aharonov-Bohm phase.

2.1   The Aharonov-Bohm effect

What is the Aharonov-Bohm Effect?   In classical physics, the dynamics of a charged particle is affected by a magnetic field only when it enters a region where the magnetic field strength is not zero. In quantum physics, the Aharonov-Bohm effect occurs when an interferometer is made with a charged particle in the presence of a magnetic flux Φ_0 confined to the region between the arms of the interferometer [2]. This effect leads to a phase shift ϕ_{AB}, observable in the interferometer signal, proportional to the magnetic field flux and the electric charge q, without

---
2. Y. Aharonov and D. Bohm also propose an electric potential effect, which we discuss in chapter 4.
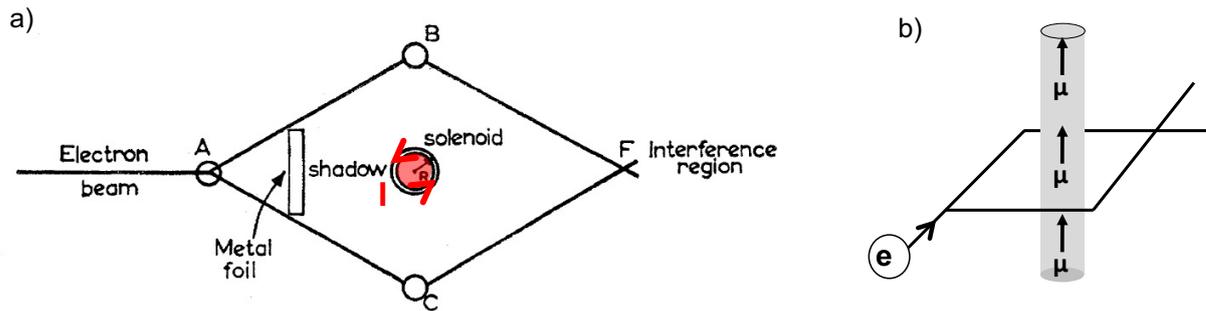
FIGURE 3.3 – Principle of the vector Aharonov-Bohm effect.

necessarily having a magnetic field on the semiclassical trajectory of the particle.

$$\phi_{\text{AB}} = \frac{q}{\hbar} \oint \vec{A}(\vec{r}) \cdot d\vec{r} = \frac{q}{\hbar} \Phi_0 \tag{3.1}$$

This effect was anticipated in 1949 by Ehrenberg and Siday [Ehrenberg, 1949], as part of theoretical work on the development of magnetic lenses for free electrons. However, the deeper meaning of this effect became clear only after Aharonov and Bohm's detailed discussion of quantum effects in 1959 [Aharonov, 1959]. They showed that the theoretical predictions were observable with existing experimental techniques and, more importantly, outlined the remarkable conceptual implications [Aharonov, 1961]. The effect, now known as the Aharonov-Bohm effect, has been the subject of considerable controversy and extensive study in the literature. Peshkin and Tonomura have carefully documented the major historical and experimental advances in the field up to 1988. [Peshkin, 2014]. Since the remarkable measurements of the A-B effect by electron holography [Tonomura, 1986], its existence is no longer disputed, even if discussions of interpretation remain.

Questions raised by the A-B effect. Part of the discussion concerns the "significance of electromagnetic potentials in quantum theory", initiated by Yakir Aharonov and David Bohm in their seminal paper [Aharonov, 1959]. Indeed, although they are optional in classical electromagnetism, potentials appear naturally in the Schrödinger equation, and it seems complicated to replace them only by the $\vec{B}$ and $\vec{E}$ fields [Aharonov, 2016]. Y. Aharonov and D. Bohm attribute a more fundamental meaning to vector and scalar potentials than to electromagnetic fields. This position is obviously unsatisfactory, since the vector potential $\vec{A}$ can be changed by a gauge transformation, and thus has no direct physical meaning, giving rise to several controversies [Peshkin, 2014; Olariu, 1985].

What is the minimum information needed to describe the coupling between a charged particle and an electromagnetic field? The most widely accepted answer was given by Wu and Yang [Wu, 1975], who introduced the concept of the *non-integrable* phase factor (i.e., this phase factor depends on the path when the integral is not performed on a closed contour):

$$\exp\left(\frac{iq}{\hbar c} \oint \vec{A}(\vec{r}) d\vec{r}\right) \tag{3.2}$$

23

The *non-integrable* phase factor is a gauge invariant (adding a gradient of a scalar field only adds multiples of 2π to the phase when integrated over a closed path) and therefore represents a physical quantity. This formalism thus provides a complete, non-redundant description of electromagnetism. [Wu, 1975] extended the concept to non-abelian gauge fields and proposed a geometric interpretation by generalizing the concept of parallel transport (see also [Tourrenc, 1977]). In 1984, M. Berry introduced the concept of geometric phase [Berry, 1984], generalizing the idea of parallel transport of quantum states and showing that the A-B effect is a special case of geometric phase.

Recently, theoretical studies have taken a closer look at the nature of the A-B effect, following theoretical work published by VAIDMAN [Vaidman, 2012] and KANG [Kang, 2015]. This research proposes an interpretation of the A-B effect using *local forces* acting between the charged particle of the interferometer and the charges responsible for the magnetic field, i.e. the electrons moving in the solenoid. Although this proposal has some inaccuracies [Aharonov, 2015 ; Aharonov, 2016], it has led to explanations of the A-B effect with the concept of entanglement [Marletto, 2020]. However, despite the profusion of theoretical work, there is still no consensus on a detailed microscopic description of the A-B effect [Boyer, 2002 ; Earman, 2019 ; Pearle, 2017 ; Marletto, 2020 ; Li, 2022]. The lack of consensus leaves fundamental elements of the A-B effect without definitive explanations, such as the possibility of a gauge invariant description based on electromagnetic fields, the role of entanglement, and non-locality [Aharonov, 2015 ; Aharonov, 2016].

From a phenomenological point of view, an essential feature of the A-B effect is its non-dispersive character (the phase shift is independent of the electron velocity), which can be understood as the absence of forces [Zeilinger, 1986 ; Peshkin, 1999 ; Batelaan, 2015 ; McKellar, 2016]. Time-of-flight and electron diffraction experiments have ruled out the presence of forces in this context [Caprez, 2007 ; Becker, 2019]. However, the non-dispersive nature of the A-B effect has yet to be experimentally proven, leaving loopholes in the conventional geometric interpretation. Another approach to study these effects is to generalize the A-B effect to other phases with similar geometric properties [Zeilinger, 1986 ; McKellar, 2014 ; McKellar, 2016 ; Marletto, 2020]. These phases are related to the propagation of neutral particles carrying a magnetic or electric dipole and evolving in an electromagnetic field. In the following paragraphs, I will present our contribution to the study of Aharonov-Casher and He-McKellar-Wilkens geometric phases with our separated-arms atom interferometer.

2.2   The Aharonov-Casher and He-McKellar-Wilkens phases

The Aharonov-Casher phase.   In 1984, AHARONOV et al. [Aharonov, 1984] described the Aharonov-Bohm effect as resulting from the relative motion between a charged particle q and a line of neutral particles with magnetic moment $\vec{\mu}$ modeled by a permanent current loop (see figure 3.4(a)). They show that the Lagrangian of the charged particle interacting with the potential vector $\vec{A}$, induced by the magnetic moment $\vec{\mu}$ is:

$$L = \frac{mv^2}{2} + \frac{MV^2}{2} + q\vec{A}(\vec{r} - \vec{R}) \cdot (\vec{v} - \vec{V}) \tag{3.3}$$

$(\vec{r},\,m,\,\vec{v})$ and $(\vec{R},\,M,\,\vec{V})$ correspond to the position, mass and velocity of the charged particle q and the neutral magnetic moment particle $\vec{\mu}$, respectively.

We find that the interaction term depends only on relative positions and velocities. Aharonov and Casher thus predict the existence of a geometrical phase by exchanging the role of the charge q and the magnetic moment $\vec{\mu}$ in the A-B effect. The Lagrangian for the magnetic moment $\vec{\mu}$ at position $\vec{R}$ and a charged particle in $\vec{r}$ (stationary in the laboratory reference frame) is rewritten as $L = \frac{MV^2}{2} - q\vec{A}(\vec{r}-\vec{R})\cdot\vec{V}$. The classical formalism of electromagnetism allows to calculate the potential vector $\vec{A}(\vec{r}-\vec{R})$ due to a classical magnetic moment $\vec{\mu}$ at the position $\vec{R}$ [Jackson, 1999] :

$$\vec{A}(\vec{r}-\vec{R}) = \frac{1}{4\pi\epsilon_0 c^2}\frac{\vec{\mu}\times(\vec{r}-\vec{R})}{\left|\vec{r}-\vec{R}\right|^3} = -\frac{\vec{\mu}\times\vec{E}(\vec{r}-\vec{R})}{qc^2} \tag{3.4}$$

where $\vec{E}$ is the electrostatic field at position $\vec{R}$ created by a charged particle at $\vec{r}$, ϵ_0 is the permeability of the vacuum, and c is the speed of light. The Lagrangian is rewritten as:

$$L = \frac{MV^2}{2} + \frac{\vec{\mu}\times\vec{E}(\vec{r}-\vec{R})\cdot\vec{V}}{c^2} \tag{3.5}$$

The Hamiltonian of the neutral particle $H = \frac{1}{2M}(\vec{P}-\frac{1}{c^2}\vec{\mu}\times\vec{E})^2$ is obtained using the canonical transformations of analytical mechanics $\vec{P} = \frac{\partial L}{\partial\vec{V}} = m\vec{V} + \frac{1}{c^2}\vec{\mu}\times\vec{E}$. Similar to the A-B effect, it is possible to define a vector potential for the neutral particle:

$$\vec{\tilde{A}} = \frac{1}{c^2}\vec{\mu}\times\vec{E} \tag{3.6}$$

Consequently, a geometric phase shift analogous to the A-B effect occurs when a neutral particle with a magnetic dipole $\vec{\mu}$ propagates in an interferometer whose arms enclose a line of charged particles (figure 3.4(b)). The Aharonov-Casher phase shift (A-C) is given by:

$$\phi_{AC} = \frac{1}{\hbar}\oint\vec{\tilde{A}}\cdot d\vec{R} = \frac{\mu\lambda_E}{\hbar\epsilon_0 c^2} \tag{3.7}$$

In this equation, λ_E is the linear charge density. HAGEN [Hagen, 1990] has shown that the A-C effect, like the A-B effect, does not depend on the particle velocity and is therefore not associated with any classical force. Moreover, KLEIN [Klein, 1986] gives a simple physical interpretation of the A-C phase: in the reference frame of the particle translating with velocity $\vec{v} = d\vec{r}/dt$, a magnetic field $\vec{B}_m = -\frac{\vec{v}\times\vec{E}}{c^2}$ arises from the Lorentz transformation of the electric field $\vec{E}$. In the particle's rest frame, the A-C phase is the result of the magnetic interaction between $\vec{\mu}$ and the "motional" magnetic field:

$$\phi_{AC} = \frac{1}{\hbar c^2}\oint\vec{E}(\vec{r})\times\vec{\mu}\cdot d\vec{r} = \frac{1}{\hbar}\oint\vec{\mu}\cdot\vec{B_m}dt \tag{3.8}$$

The A-C phase was detected in 1989 by A. CIMMINO et al. [Cimmino, 1989] using a neutron interferometer. Several months of integration and a clever design of the experiment allowed to measure a phase shift of $\phi_{exp} = 2.19 \pm 0.52$ mrad, to be compared with the theoretical value
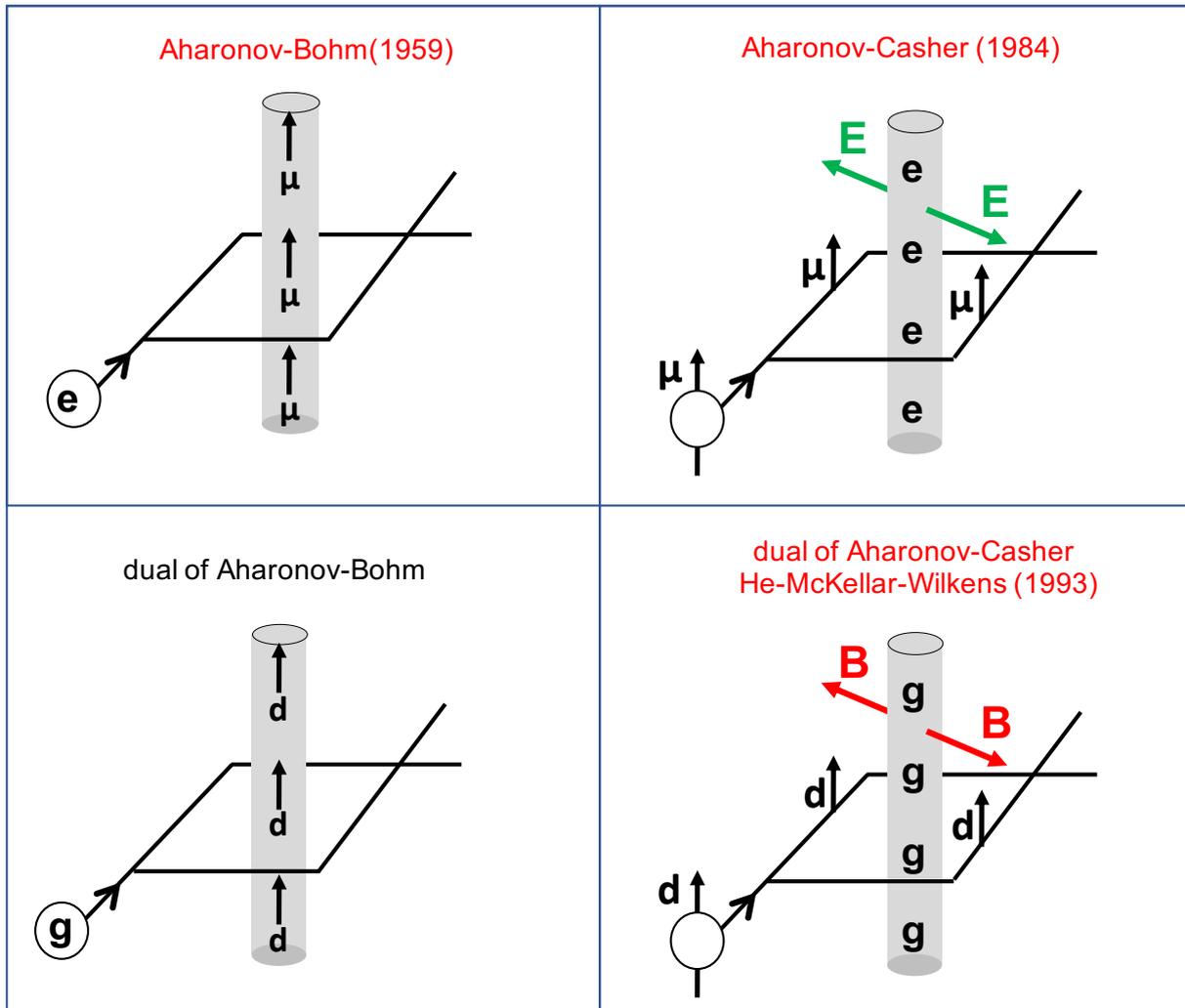
FIGURE 3.4 – Inspired by [Dowling, 1999]. Summary of geometric phases for four types of topological effects. e and g are electric and magnetic charges, d and μ are electric and magnetic dipoles. The A-C phase is obtained from the A-B phase by transforming $e \leftrightarrow \mu$. The HMW phase corresponds to the dual effect of the A-C effect.

of $\phi_{theo} = 1.5$ mrad.

In 1993, SANGSTER et al. [Sangster, 1993] measured the A-C effect with a setup similar to a Ramsey interferometer, using molecular magnetic moments. Instead of spatially separating the magnetic moments, the first $\pi/2$ pulse of the Ramsey interferometer prepares the particle in a coherent superposition of two states with opposite magnetic moment. After propagating in an electric field, these two states are phase-shifted by the A-C effect. This phase shift is measured after the second $\pi/2$ pulse. This experiment allowed to measure an A-C phase shift with a relative uncertainty of 4%, confirming its non-dispersive nature. Other measurements using a similar configuration achieved an accuracy comparable to that of SANGSTER et al. [Sangster, 1993] using atoms [Görlitz, 1995 ; Zeiske, 1995 ; Yanagimachi, 2002].

The dual effect of the A-C phase: the He-McKellar-Wilkens phase. Phases analogous to the A-B and A-C effects can be identified by introducing the magnetic charge and current density ρ_m and $\vec{J}_m$ in addition to the electric charge and current density ρ_e and $\vec{J}_e$. Maxwell's equations are then written:

$$
\begin{aligned}
\vec{\nabla} \cdot \vec{\mathcal{D}} &= \rho_e, & \vec{\nabla} \times \vec{\mathcal{H}} &= \frac{\partial \vec{\mathcal{D}}}{\partial t} + \vec{J}_e \\
\vec{\nabla} \cdot \vec{\mathcal{B}} &= \rho_m, & -\vec{\nabla} \times \vec{\mathcal{E}} &= \frac{\partial \vec{\mathcal{B}}}{\partial t} + \vec{J}_m,
\end{aligned}
\tag{3.9}
$$

These equations are invariant under the action of the following transformations (3.10), called the electromagnetic duality [Jackson, 1999] :

$$
\begin{aligned}
\vec{E} &= \vec{E}' \cos\xi + Z_0 \vec{H}' \sin\xi & Z_0 \vec{D} &= Z_0 \vec{D}' \cos\xi + \vec{B}' \sin\xi \\
\vec{B} &= -Z_0 \vec{D}' \sin\xi + \vec{B}' \cos\xi & Z_0 \vec{H} &= -Z_0 \vec{E}' \sin\xi + \vec{B}' \cos\xi
\end{aligned}
$$

$$
q_m = -Z_0 q_e' \sin\xi + q_m' \cos\xi \qquad Z_0 q_e = Z_0 q_e' \cos\xi + q_m' \sin\xi
\tag{3.10}
$$

In particular, for $\xi = \pi/2$, the duality of electromagnetism exchanges the roles of magnetic and electric fields, charges (magnetic monopole), and dipoles.

Applying Maxwell's duality to the Aharonov-Casher phase transforms it into a dual phase for an interferometer in which a particle carrying an electric dipole encloses a line of magnetic monopoles 3.4(d), producing a radial magnetic field. The existence of this effect was predicted in 1993 by HE et al. [He, 1993]. Since magnetic monopoles have a hypothetical existence, this prediction remained pure speculation until WILKENS [Wilkens, 1994] proposed a possible test with an electrically polarized atom interacting with a realistic magnetic field configuration. However, Wilkens' proposal seems to be particularly complex to implement with paramagnetic atoms due to the use of an inhomogeneous magnetic field.

In addition, Wilkens [Wilkens, 1994] gives a complementary interpretation of the HMW phase by considering the motion of a polarizable particle in a magnetic field. In the rest frame of
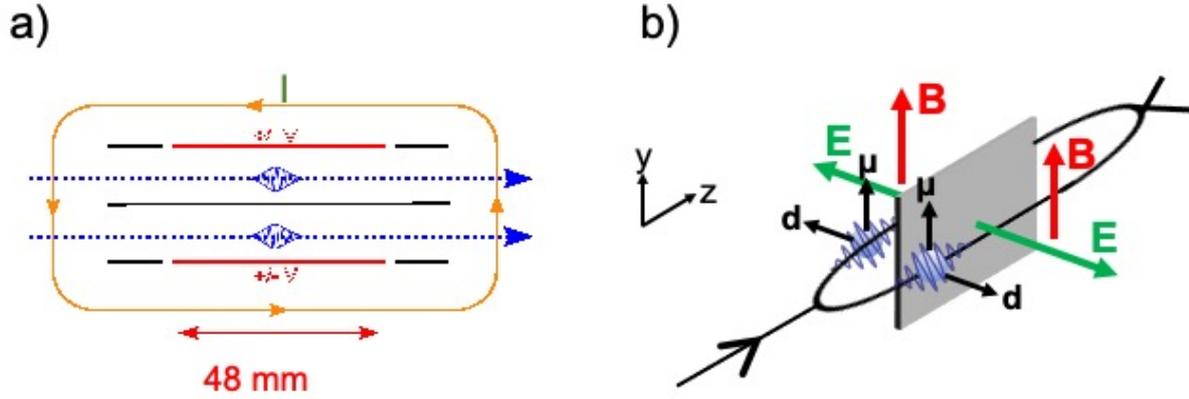
FIGURE 3.5 – a) Diagram of the double capacitor. The two high voltage electrodes are labeled $\pm V$, followed by grounded electrodes to limit field gradients at the edges. The septum is placed between the two arms of the interferometer (blue dotted line). b) In this configuration, an electric (or magnetic) dipole propagates in a magnetic (or electric) field, giving rise to the HMW (or -AC) phase.

the particle, a motional electric field $\vec{E}_m = \vec{v} \times \vec{B}$ appears and interacts with the electric dipole. The HMW phase is calculated by integrating the interaction energy $\vec{E}_m \cdot \vec{d}$ over the duration of the interferometer:

$$\phi_{HMW} = -\frac{1}{\hbar} \oint (\vec{B} \times \vec{d}) \cdot d\vec{r} = \frac{1}{\hbar} \oint \vec{d} \cdot \vec{E}_m dt \tag{3.11}$$

The so-called He-McKellar-Wilkens (HMW) phase is probably the last geometric phase in the Aharonov-Bohm family to be detected by free particle propagation[3].

2.3 Experimental results

To measure the HMW effect, our setup is inspired by the proposal of WEI et al. [Wei, 1995]. In this setup, electric dipoles are induced in opposite directions on each of the interferometer arms and propagate in a uniform magnetic field. Our setup is shown in Figure 3.5, where the electric dipoles are induced by two capacitors separated by a septum between the two arms of the interferometer, generating opposite electric fields. The device can apply a maximum field of about 800 kV/m, corresponding to voltages of the order of $V = \pm 800$ V[4]. In this configuration, the electric fields are in the horizontal plane, while a vertical magnetic field generates an HMW effect. The magnetic field is produced by circulating a current I in two coils surrounding the capacitor assembly. The B field is given by $B \approx 0.56 \times I$ mT, and is limited by the heating of the wires to a current $I = 40$A. The expected value of the HMW phase shift is $\phi_{HMW}/VI = -(1.28 \pm 0.03) \times 10^{-6}$ rad/VA for the value of lithium-7 polarizability. This corresponds to an HMW phase shift of around 40 mrad, for the maximum values of V and I.

The accurate measurement of such small phase shifts in the presence of such intense electro-

---

3. The dual phase of the Aharonov-Bohm effect 3.4(c) would require a source of magnetic monopoles.

4. The geometry we use is equivalent to that of WEI et al. [Wei, 1995] by contracting the septum into a wire.

magnetic fields is unusual in atom interferometry. The magnetic and electric phases accumulated on each arm are on the order of 10^5 rad and 300 rad, respectively. Controlling the homogeneity of the electric and magnetic fields is therefore crucial for this measurement. In our setup, the relative inhomogeneity of the magnetic field is of the order of 10^{-4} and the deviation from electrode parallelism is less than one mrad. The residual Zeeman and electrical polarizability phase shifts are on the order of 10 rad and 0.1 rad, respectively. To measure the HMW phase, it is therefore necessary to use differential measurements, combining measurements in the absence of fields, in the presence of the electric (or magnetic) field only, and in the presence of both magnetic and electric fields. The field configurations are alternated during a single fringe scan to avoid phase drift in the interferometer.

He-McKellar-Wilkens and Aharonov-Casher phase measurements. A measurement campaign allowed the first detection of the HMW phase [Lepoutre, 2012] with a relative uncertainty of 30% dominated by imperfect subtraction of systematic effects during differential measurements in electric and magnetic fields. These limitations are due to correlations induced by averaging over the different velocities, positions and Zeeman $|F, m_F\rangle$ sublevels of atoms in the atomic beam. The detailed study of these effects is an important part of Steven Lepoutre's PhD thesis [Lepoutre, 2011 ; Lepoutre, 2013a ; Lepoutre, 2013b].

To improve the accuracy and sensitivity of the measurements, we set up an optical pumping stage to prepare atoms in the states $|F = 2, m_F = \pm 2\rangle$ [Gillot, 2013c] . Atoms in $|F = 2, m_F = \pm 2\rangle$ have a magnetic moment $\vec{\mu} = \pm \mu_B \vec{e}_B$ aligned along the direction of the magnetic field $\vec{e}_B$ with a magnitude equal to the Bohr magneton μ_B. In this configuration, the atoms are sensitive to the A-C and HMW phase[5]. However, the A-C phase changes sign with the direction of the magnetic moment $\vec{\mu}$, so it is possible to distinguish these two contributions with measurements for opposite values of $m_F = \pm 2$. Figure 3.6(a) shows the HMW phase measurements, the discrepancy with the theoretical value is less than 5% [Gillot, 2013a]. The improvement in accuracy is due to the absence of averaging over the $\{|F, m_F\rangle\}$ as well as to the fact that in the states $|F = 2, m_F = \pm 2\rangle$ the Zeeman effect is linear with $|B|$, thus reducing correlations. In addition, we have performed these measurements for different carrier gases and verified the non-dispersive nature of the HMW phase (Figure 3.6(b)), thus demonstrating the geometric nature of this phase shift.

Figure 3.7(a) shows the A-C phase measurements derived from the same experiments. We obtain a measurement in good agreement with the expected value (theory-experiment difference $\sim 3\%$). The accuracy is similar to that obtained with Ramsey type configurations. We have also verified the independence of the AC effect from the atomic velocity [Gillot, 2014a].

Following these experimental results, He and McKellar carried out a more detailed analysis of the topological properties of the A-C and HMW effects [McKellar, 2014 ; McKellar, 2016 ; He, 2017]. They have shown that there is a mapping between the A-B effect and the A-C and HMW effects when the dipoles propagate in a plane and exhibit invariance along the charge line. The

---

5. Note that the A-C and HMW phases are induced by the vector product of the electric and magnetic fields $\vec{B} \times \vec{E}$, illustrating the dual nature of these two geometric phases
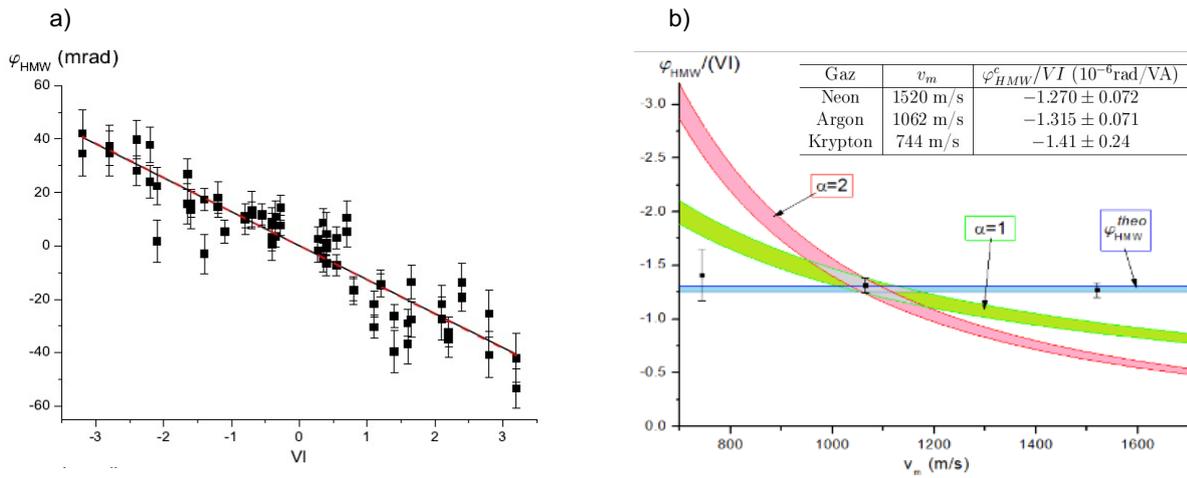
FIGURE 3.6 – a) Measurement of the He-McKellar-Wilkens phase shift as a function of the amplitude of the fields E and B measured by the product V I. b) Verification of the non-dispersive nature of the HMW phase. The colored areas represent the variations expected for a $\phi(v) \propto v^{-\alpha}$ phase, where $\alpha = 1$ corresponds to a perturbation by a potential and $\alpha = 2$ corresponds to a phase induced by a constant force.

problem is then reduced to (2+1) dimensions. Experimentally, it is essential that the magnetic (or electric) moment is orthogonal to the plane defined by the electric (or magnetic) field and the direction of motion, and that the magnetic moment remains constant. Our measurement of the A-C phase is the first (and, to my knowledge, the only) demonstration that satisfies all the conditions necessary to prove the topological nature of the A-C phase. [6].

2.4 Conclusions and prospects

Conclusions.   There are three geometric phases of the Aharonov-Bohm family that can be observed in electromagnetism: the A-B phase, the A-C phase, and the HMW phase. With our atom interferometer, we have developed a unique device that allows precise control of the magnetic and electric fields applied to each arm of the interferometer. This capability has allowed us to experimentally demonstrate the existence of the HMW phase, the last unobserved geometric phase in the A-B family. In addition, we measured the A-C phase to a level of accuracy comparable to the state of the art. In contrast to previous measurements, our experimental setup revealed the topological character of the A-C phase.

Prospects.   I am convinced that the results of this study will contribute to a better understanding of geometric phases in quantum physics. The study of A-C and HMW effects by atom interferometry offers the possibility to precisely study the geometric properties of A-B type phases, taking advantage of the very high accuracy of atom interferometers. More accurate measurements of geometrical phases would pave the way for experimental studies of the role played

---

6. The experimental configuration used in the neutron interferometer [Cimmino, 1989] has all the characteristics, but this work does not show the independence of the A-C phase with velocity.
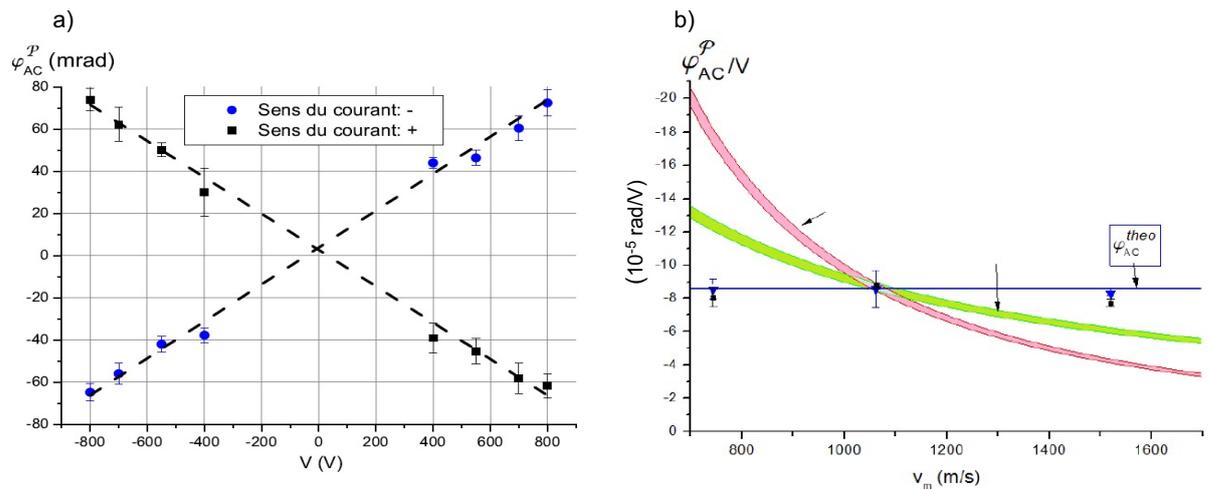
FIGURE 3.7 – a) Measurement of the Aharonov-Casher phase shift as a function of the amplitude of the E and B fields. b) Verification of the non-dispersive nature of the Aharonov-Casher phase. The colored areas represent the variations expected for a phase $\phi(v) \propto v^{-\alpha}$, where $\alpha = 1$ corresponds to a perturbation by a potential and $\alpha = 2$ corresponds to a phase induced by a constant force.

by quantum entanglement and non-locality in the context of A-B type effects [Marletto, 2020], and provide a better understanding of "quantum force" phenomena [Becker, 2019 ; Berry, 1999].

Another interesting perspective concerns the experimental study of the A-B effect extended to non-Abelian gauge fields. These effects were introduced by WU et al. [Wu, 1975] as part of their very thorough theoretical study of topological phases. In this paper they propose a thought experiment that highlights the effect of a non-Abelian field induced by moving neutrons. This proposal is based on a modification of the AB effect configuration in which the electron interferometer is replaced by a neutron interferometer, and the electron flow in the solenoid is replaced by a massive rotating cylinder made of a neutron-rich material (^{238}U). Such an experiment was attempted by ZEILINGER et al. [Zeilinger, 1983] without positive results.

In addition, improving the accuracy of Aharonov-Bohm phase measurements would enable new fundamental physics tests in atom interferometry. For example, A-B phase measurements impose a limit on the possible photon mass $m_\gamma < 2 \times 10^{-11}$ eV [Boulware, 1989]. Although this limit is not competitive with tests based on astrophysical observations ($m_\gamma < 2 \times 10^{-18}$ eV) [7] [Ryutov, 2007], it paves the way for laboratory tests. SPAVIERI et al. [Spavieri, 2007] suggest that measurements of A-B, A-C, and HMW phases could provide limits comparable to astrophysical observations. Another example, given by KOBAKHIDZE et al. [Kobakhidze, 2007], shows that A-B interferometers provide a competitive new method for testing Lorentz invariance [Wolf, 2004]. Extending this theoretical study to experimental A-C and HMW configurations would allow to assess the relevance of testing Lorentz invariance using separate-arm atom interferometers. In addition, the possibility of measuring a gravitational analog of the A-B effect has stimulated a considerable number of papers [Dowker, 1967 ; Ford, 1981 ; Bezerra, 1991 ; Audretsch, 1983 ;

---

7. Value taken by the Particle Data Group.

Zeilinger, 1986 ; B Ho, 1994 ; Hohensee, 2012]. Recently, OVERSTREET et al. [Overstreet, 2022] detected a gravitational scalar A-B effect, opening up new prospects for precise measurements of the gravitational constant G. Such experiments also shed new light on the connections between gravity and quantum physics [Overstreet, 2023]. Finally, the scalar Aharonov-Bohm effect can be exploited to perform new tests of the neutrality of matter [Greenberger, 1981]. This novel approach was first proposed in atom interferometry by our group in 2001 [Champenois, 2001b] and then developed in the context of interferometers with ultracold atoms by the team led by the M. Kasevich group at Stanford [Arvanitaki, 2008]. This proposal will be further developed in the next chapter.

These perspectives open new horizons for deepening our understanding of quantum physics and offer new explorations in the fields of quantum technologies and fundamental physics. The implementation of these experiments with ultracold atom interferometers is at the heart of my research project, which is described in detail in the next chapter.

3   Phase modulation of matter waves

Using the same setup as for the HMW and AC phase measurements, we have implemented a phase modulator for matter waves by applying a time-dependent perturbation on each of the interferometer arms [Décamps, 2016 ; Décamps, 2017]. As the atom propagates in a time-modulated potential at the frequency ω, it exchanges energy quanta $\hbar\omega$, thus changing its kinetic energy. For an incident plane wave of amplitude A_i, momentum p_i and energy $\hbar\Omega_i$, the transmitted wave function $|\Psi_t\rangle$ is written as a superposition of kinetic energy states separated by $\hbar\omega$: $|\Psi_t\rangle = \sum_l A_l |p_l, \Omega_i + l\omega\rangle$ [8]. We have developed an exact theory of matter wave propagation in an oscillating potential based on Floquet's formalism [Décamps, 2017]. This theory allows us to justify the use of a semi-classical model in which the perturbation $U(z,t)$ manifests itself as a phase shift of the incident wave :

$$\phi(t) = -\frac{1}{\hbar}\int_\Gamma U(s(t'))dt' = -\frac{U_0 L}{\hbar v} + \phi_{\max}\cos{(\omega t)} \tag{3.12}$$

In this equation, $s(\cdot)$ is the curvilinear abscissa along the (unperturbed) classical trajectory of the atoms Γ and v is the group velocity of the wave. In the case of a harmonic modulation of the potential $U(z,t) = U_0 + U_M \cos{(\omega t)}$, a phase term $U_0 L/(mv)$ appears, corresponding to the time-averaged perturbation, and a harmonic phase modulation of amplitude $\phi_{\max}$:

$$\phi_{\max} = -\frac{2U_M}{\hbar\omega}\sin{(\frac{\omega L}{2v})} \tag{3.13}$$

The complex phase factor $e^{i\phi(t)}$ can be expanded on a plane wave basis weighted by Bessel functions of the first kind $J_l(\cdot)$, $e^{i\phi(t)} = \sum_l i^l J_l(\phi_{\max})e^{il\omega t}$. The transmitted wave function then

---

8. These sidebands can be interpreted as the temporal analog of matter wave diffraction [Moshinsky, 1952].
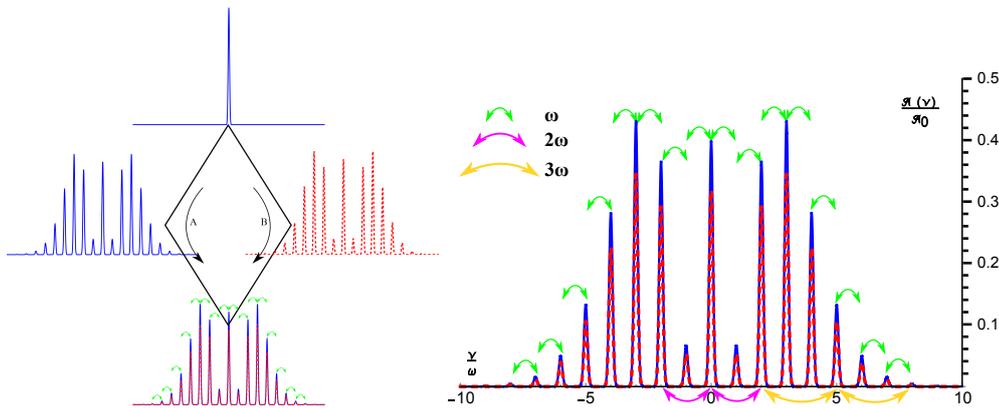
FIGURE 3.8 – (a) Phase modulation of the wave function creates a frequency comb on each arm. The interfering signal is shown in figure (b).

forms a matter wave *frequency comb*:

$$|\Psi_t\rangle = A_i \sum_l i^l J_l(\phi_{\max}) e^{il\omega t} |k_l, \Omega_i\rangle \tag{3.14}$$

Measurement of matter wave beats. In our experiments, the bandwidth of the hot-wire detector (≈ 1 ms) limits the maximum observable modulation frequency. In practice, we modulate perturbations between $10 - 100$ Hz. Since these frequencies are well below the spectral width of the atomic source (≈ 2 THz), it is not possible to resolve the comb components by direct spectroscopy. However, we can perform a homodyne detection of the different components by modulating the perturbations $U_A(t)$ and $U_B(t)$ on each arm of the atom interferometer (see figure 3.8). The perturbations are generated by the Stark effect by applying variable electric fields with voltages on each arm of the form $V_A = V_0 + \cos(\omega t)$ and $V_B = -V_0 + \cos(\omega t)$.

The measured interference signal oscillates as a function of the phase shifts $\phi_{A,B}$ induced on each of the arms:

$$\mathcal{S}(z_d, t_d) = I_0[1 + \mathcal{V}_0 \cos(\phi_r + \phi_A(t) - \phi_B(t))] \tag{3.15}$$

where I_0 and $\mathcal{V}_0$ correspond to the flux of detected atoms and the visibility of the interferometer, respectively. Figure 3.9a shows the interferometric signal obtained for a low-frequency modulation of the potential, $\omega/(2\pi) =21$ Hz, with the beat phenomenon between the first two harmonics clearly visible on the signal. Spectral analysis can be used to determine the amplitudes A_l of the components at the modulation frequency and its harmonics. Figure 3.9a shows an example of a spectrum where the first four harmonics are resolved.

We measured the amplitude of each harmonic for several modulation amplitudes $\phi_{\max}$ at 11 Hz and 21 Hz (see figure 3.9b), in very good agreement with a theoretical model that takes into account the detector response time, the propagation, and the velocity distribution of the atomic beam.

We have also performed heterodyne measurements of Stark perturbations by modulating the perturbations at two different frequencies, ω_A and ω_B, on the interferometer arms. We then detect a signal at the difference in frequencies, so the frequencies ω_A and ω_B can be significantly
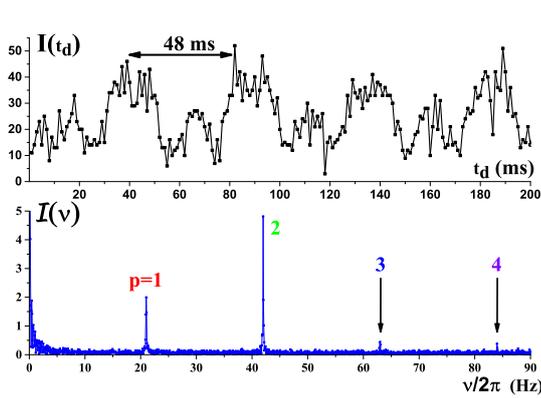
(a) Phase modulation at 21 Hz, beat signal and spectrum.
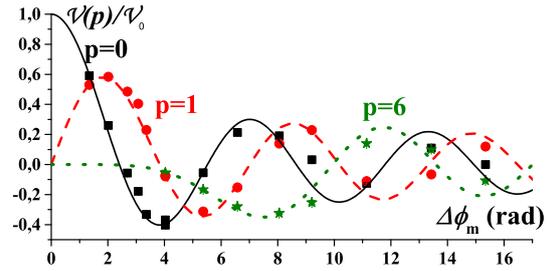
(b) Amplitude of the different components of the atomic frequency comb, $p = 0$ (black squares), $p = 1$ (red circles) and $p = 6$ (green stars) for different values of ϕ_{max}. The solid lines correspond to our theoretical model without adjustable parameters.

FIGURE 3.9 – Measurement of phase modulation phenomena by homodyne beating of matter waves.

larger (30 kHz) than the bandwidth of the detector.

Prospects. Homodyne and heterodyne detection techniques are widely used in electromagnetic signal processing, with applications in radar, telecommunications, high resolution spectroscopy, frequency metrology, and more. Our study of the phase modulation of matter waves using electric fields has paved the way for heterodyne (or homodyne) measurements in atom interferometry. For example, the sensitivity of He-McKellar-Wilkens and Aharonov-Casher geometric phase measurements (see section 2) could be improved by modulating electric and magnetic fields at different frequencies. The spectral components of the signal resulting from the sum and difference of the modulation frequencies then provide a signature of the He-McKellar-Wilkens and Aharonov-Casher phases.

However, a fundamental difference between classical optics and atom optics is the dispersion of matter waves in vacuum, which results in a dispersion of the propagation times between the modulator and the detector. This time dispersion limits the visibility of the beating phenomenon. The use of continuous sources of ultracold atoms would attenuate this effect. On the other hand, conventional atomic detectors (based on ionization, fluorescence, etc.) have typical response times in the microsecond range, which limits the bandwidth of atomic heterodyne detection. An attractive prospect arising from this research would be to apply these modulation methods to electronic interferometers, paving the way for time-resolved electronic interferometers [Décamps, 2017].

4 Electrical polarizability: tune-out wavelength

The interaction of an atom with a non-resonant optical field results in a "light shift" of energy levels proportional to the intensity of the light and the dynamical polarizability of the atom $\alpha(\omega)$. The most sophisticated calculations of dynamical polarizability include quantum electrodynamics effects [Flambaum, 2005], the Breit interaction [Dzuba, 2006], and electronic

Atomes	$\lambda_T O$	Methods	rel. uncertainties	References
He	413 nm	OMMT	$3,6 \times 10^{-7}$	[Henson, 2022]
Li	671 nm	AI	$1,64 \times 10^{-8}$	[Décamps, 2020]
Li	671 nm	AI	$1,0 \times 10^{-8}$	[Copenhaver, 2019]
K	769 nm	AI	$5,2 \times 10^{-7}$	[Trubko, 2017]
Rb	790 nm	AI	$4,05 \times 10^{-8}$	[Leonard, 2017]
Rb	790 nm	AD	$5,2 \times 10^{-7}$	[Schmidt, 2016]
Rb	421 nm	AD	x	[Herold, 2012]
Cs	880 nm	AD	$4,6 \times 10^{-7}$	[Ratkata, 2021]
Dy	741 nm	AD	x	[Kao, 2017]
Sr	689 nm	PH	$2,3 \times 10^{-8}$	[Heinz, 2020]
NaK	866 nm	PH	$2,3 \times 10^{-7}$	[Bause, 2020]

TABLE 3.2 – Tune-out wavelength measurements for different species and for different methods: optical modulation in magnetic traps (OMMT), atom interferometry (IA), atom diffraction (AD), parametric heating in optical traps (PH).

correlation effects [Arora, 2011]. Uncertainties in these calculations are difficult to estimate, so benchmark polarizability measurements are needed to verify these calculations or to experimentally determine the parameters used in them.

Precise measurements of polarizability in the optical frequency range are difficult to make because they require accurate knowledge of the light intensity seen by the atoms. However, it is possible to precisely measure a wavelength at which the polarizability cancels out. These wavelengths λ_0 are known as "tune-out" wavelengths [9]. If the wavelength is chosen between two atomic transitions, their contributions cancel and the dynamical polarizability vanishes. This phenomenon has been introduced in the context of ultracold atomic mixtures to manipulate specific species in optical traps [LeBlanc, 2007]. Exact measurements of tune-out wavelengths allow to test fundamental atomic properties such as dipolar transition matrix elements or excited state lifetimes. These parameters are essential for the determination of the black-body radiation shift of atoms [Safronova, 2012 ; Nicholson, 2015], which is a limit of the accuracy of atomic clocks, or for the interpretation of atomic parity violation and electron dipole moment experiments [Dzuba, 2012].

The tune-out wavelengths were measured by parametric heating in optical traps (PH), by atomic diffraction experiments on optical lattices (AD), and by atom interferometer experiments (AI). These experiments measured the tune-out wavelengths for different alkalis Li [Copenhaver, 2019 ; Décamps, 2020], K [Trubko, 2017], Rb [Herold, 2012 ; Schmidt, 2016 ; Leonard, 2017], and Cs [Ratkata, 2021], as well as for other atomic species, including He [Henson, 2022], Sr [Heinz, 2020], and Dy [Kao, 2017], and for NaK [Bause, 2020] molecules. Published relative uncertainties for these species are given in the table 3.2.

We have measured the lithium tune-out wavelength [Décamps, 2020] with our separated-arm interferometer. The principle of the measurement is to focus a laser beam of intensity I on one

9. To be distinguished from the "magic wavelengths" used in optical clocks, which correspond to identical light shifts for the two clock states.

arm of the interferometer and to measure the phase shift induced by the light shift $\frac{U}{\hbar}$ as a function of the laser frequency $\omega/(2\pi)$:

$$\phi = \frac{1}{\hbar} \int U(\omega) dt = -\frac{\alpha(\omega)}{2\epsilon_0 c \hbar} \int I(t) dt \tag{3.16}$$

For an alkali in the $|i\rangle$ state, the dynamical polarizability is the sum of a contribution from the core electrons $\alpha_{\text{core}} = 2.04$ a.u., which is almost independent of frequency, and contributions corresponding to the excited $|e\rangle$ states of the valence electron:

$$\alpha_i(\omega) = \alpha_c + \frac{1}{\hbar} \sum_e \frac{2\omega_{ie}}{\omega_{ie}^2 \pm \omega^2} |d_{ie}|^2 \tag{3.17}$$

In this equation, the transition frequency between the $|i\rangle$ and $|e\rangle$ states is denoted by ω_{ie}, $d_{ie} = \langle f | \vec{d} \cdot \vec{\epsilon} | i \rangle$ is the dipole matrix element, and $\vec{\epsilon}$ is the polarization of the Stark beam. For an atom with total angular momentum F and projection m_F, the general form of the polarizability can be decomposed into a scalar part $\alpha_i^{(0)}$, a vector part $\alpha_i^{(1)}$, and a tensor part $\alpha_i^{(2)}$:

$$\alpha_i(\omega) = \alpha_c + \alpha_i^{(0)} - V \vec{e}_B \cdot \vec{k} \frac{m_F}{2F} \alpha_i^{(1)} + \left(\frac{3(\vec{\epsilon} \cdot \vec{e}_B)^2 - 1}{2} \right) \frac{3m_F^2 - F(F+1)}{F(2F-1)} \alpha_i^{(2)} \tag{3.18}$$

where V is the Stokes parameter representing the degree of circular polarization of the laser beam, $\vec{e}_B$ is a unit vector in the direction of the quantization axis, and $\vec{k}$ is the unit vector in the direction of the wave vector.

We want to find the wavelength at which the scalar part of the polarizability vanishes. To get rid of the vector component, the Stark beam is linearly polarized ($V = 0$) and a magnetic field is directed orthogonal to the laser wavevector. The experimental setup for this measurement is shown in figure 3.10. In this configuration, the dynamical polarizability is expressed as :

$$\alpha_{F=2,m_F} = \alpha_c + \alpha_{g,F=2}^{(0)} + \frac{3(\vec{\epsilon} \cdot \vec{e}_B)^2 - 1}{2} \frac{m_F^2 - 2}{2} \alpha_{g,F=2}^{(2)} \tag{3.19}$$

In practice, the tune-out wavelength is determined by measuring the phase shifts ϕ_S as a function of the Stark laser frequency. This frequency is measured using a laser beatnote with a reference laser locked to the $S_{1/2}, F = 1 \longleftrightarrow P_{1/2}, F = 2$ transition. An example of a signal is shown in Figure 3.11(a), where the measured Stark phase shift is $\phi_S = 213$ mrad. The phase shifts ϕ_S are measured as a function of the frequency difference in the region of the tune-out frequency, and a linear fit is used to estimate the frequency at which ϕ_S cancels. *In-fine*, we have determined the contribution of the scalar part of the tune-out wavelength [Décamps, 2020] with an uncertainty of 11fm dominated by the optical pumping instability in $\left| 2S_{1/2}, F = 2, m_F = \pm 2 \right\rangle$, which corresponds to:

$$\omega_0/(2\pi) \quad = \quad 446803175(8)\text{MHz} \tag{3.20}$$

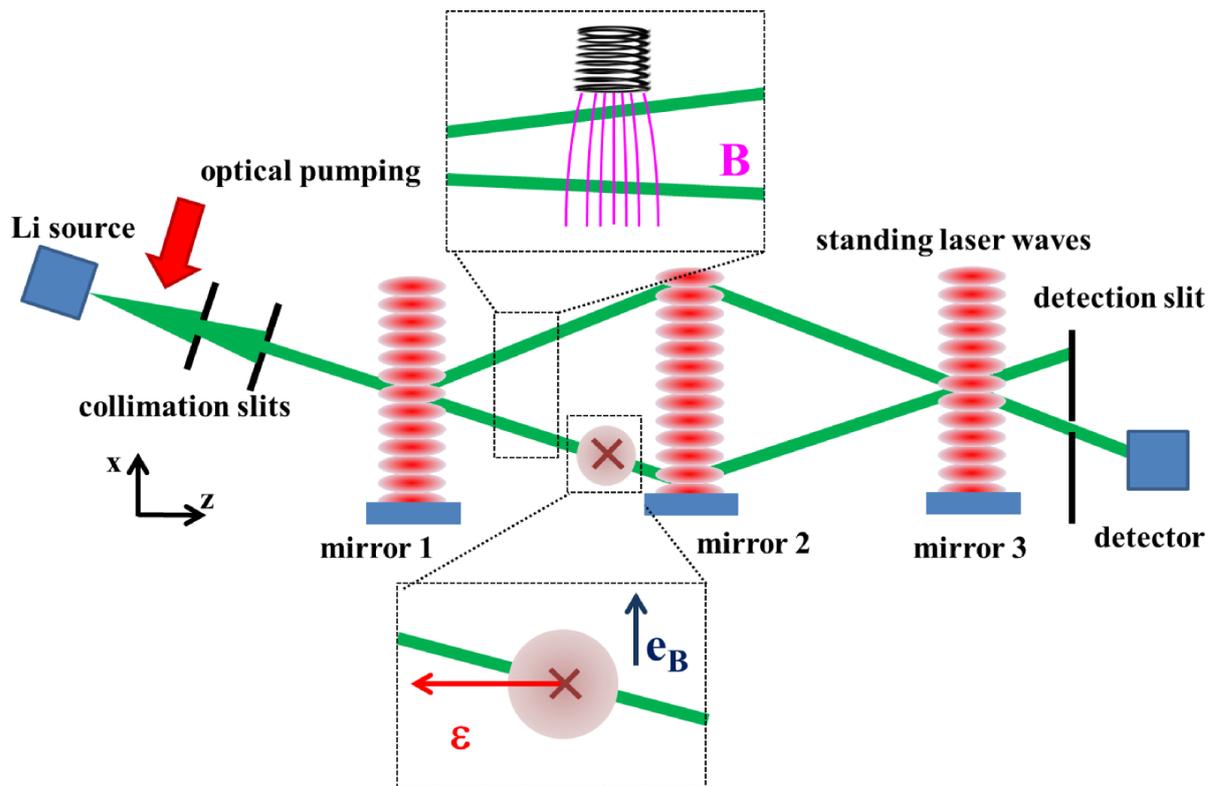$$\lambda_0 \quad = \quad 670972085(11)\text{fm} \tag{3.21}$$

FIGURE 3.10 – Experimental setup for Tune-Out wavelength. A laser beam is focused on one of the interferometer's arms, inducing a phase shift due to light shift. The diagram shows the beam polarization and quantization axis.
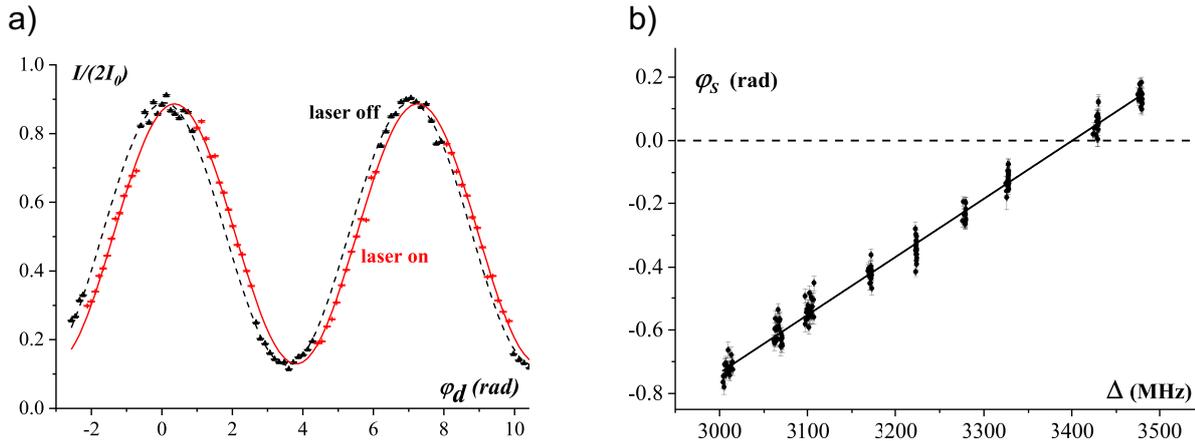
a)

b)

FIGURE 3.11 – (a) The phase shift induced by illuminating one arm of the interferometer with a laser beam is measured. (b) By changing the laser wavelength, it is possible to determine the Tune-Out wavelength when the phase shift cancels.

This measurement is in agreement with COPENHAVER et al. [Copenhaver, 2019]. Furthermore, the tune-out wavelength depends critically on the ratio $R = d_{3/2}^2/d_{1/2}^2$ between the oscillator strengths of the alkali D_1 and D_2 transitions. Our measurement of λ_0 gives an experimental value for the ratio of $R = 1.999(7)$, a value in agreement with TANG et al. [Tang, 2013]'s calculations of $R - 2 = 0.000024107$[10].

Our results add to a series of recently completed measurements of tune-out wavelengths for different atomic species (see table 3.2). The most accurate measurements in oscillator strength ratio, made using an atom interferometer with a rubidium-87 condensate [Leonard, 2017], have achieved relative uncertainties on the order of 10^{-5}, while with a helium condensate the uncertainty obtained is on the order of 6×10^{-6} [Henson, 2022]. Measurements of the tune-out wavelengths for different atomic species have contributed to a better understanding of the theoretical predictions and have confirmed the validity of the methods used to evaluate computational uncertainties.

In this context, lithium is of particular interest for polarizability measurements because its electronic structure is simple enough to allow explicit consideration of electronic correlations in ab initio calculations. In addition, measurements on more massive atomic species (such as rubidium and cesium) are more sensitive to relativistic effects. Therefore, it seems appropriate to have several references to tune-out wavelengths for different atomic species in order to test theoretical models.

5   Pancharatnam phase shifter

As part of his work on light propagation in anisotropic media, S. Pancharatnam studied the problem of determining the phase of a light wave when its polarization is changed. When the

---

10. In the case of a 1-electron atom $R = 2$ in the non-relativistic approximation.
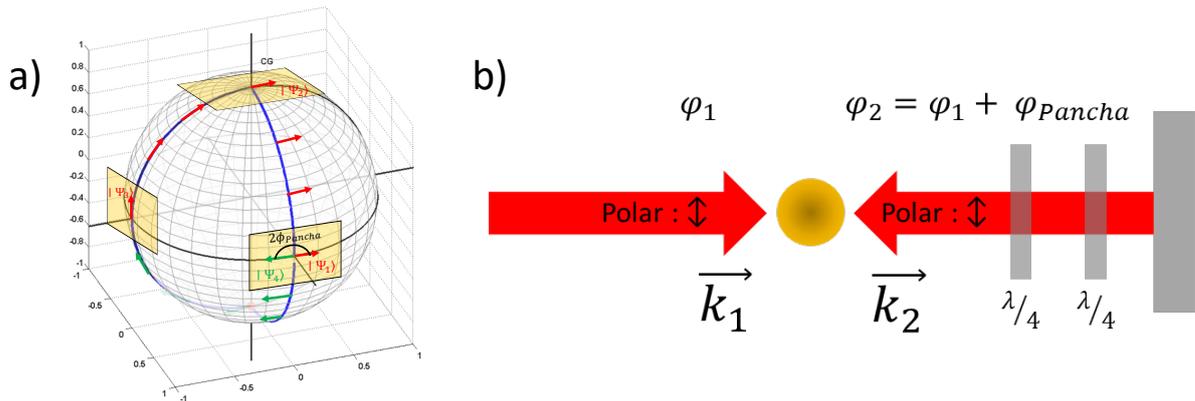
FIGURE 3.12 – The polarization state of light is represented on the Poincaré sphere, with the poles representing circular polarization and the equator representing linear polarization. The orientation of the vector on the tangent plane represents the phase of the light wave. When a vector travels a closed path on the sphere, it returns with a different orientation equal to the solid angle enclosed by the surface. The initial polarization of the standing wave is linear $|Psi_1\rangle$. The ray passes through two quarter-wave plates. The first is fixed with a fast axis at 45° with respect to the incident polarization. The second is at an angle θ to the initial polarization direction. The corresponding trajectory is shown on the Poincaré sphere (a). The polarization state changes from straight to right circular. Then, depending on the angle θ, it returns to linear polarization. After being reflected by the mirror, it changes from linear to left circular polarization and finally returns to its original state.

polarization of the wave is changed and returns to its initial state of polarization, he demonstrated a phase shift between the initial and the final wave that depends solely on the path traveled in the space of polarization states. These results were published in 1956 [Pancharatnam, 1956], anticipating the concept of geometric phase. A few decades later, M. Berry demonstrated the underlying geometrical nature of these phases and generalized the concept beyond electromagnetic waves [Berry, 1984; Berry, 1987]. The polarization state of the light field is represented on the Poincaré sphere; more generally, the state of the light field is represented by a vector tangent to the Poincaré sphere, whose orientation measures the phase. If a vector is parallel transported on a sphere along a closed path, it returns with a different orientation, and the angle between the two vectors is proportional to the solid angle subtended by the path traveled [11]. We used this phase shift induced by a change in polarization to modify the phase of the standing wave diffracting the atoms, and thus to control the output phase of the atom interferometer.

In practice, the laser beam with linear polarization is retroreflected by two quarterwave plates (Fig. 3.12(b)). The axis of the first quarterwave plate is fixed at 45° to the incident polarization, and the second quarterwave plate can be rotated continuously. The angle between the initial polarization direction and the waveplate axis is called θ. The polarization state changes from horizontal polarization (H on the Poincaré sphere) to right-handed circular polarization (RH) after the first quarterwave plate. After passing the second quarterwave plate, the polarization

---

11. Note that the rules of parallel transport are not specific to wave phenomena; they also explain mechanical effects such as the precession of Foucault's pendulum
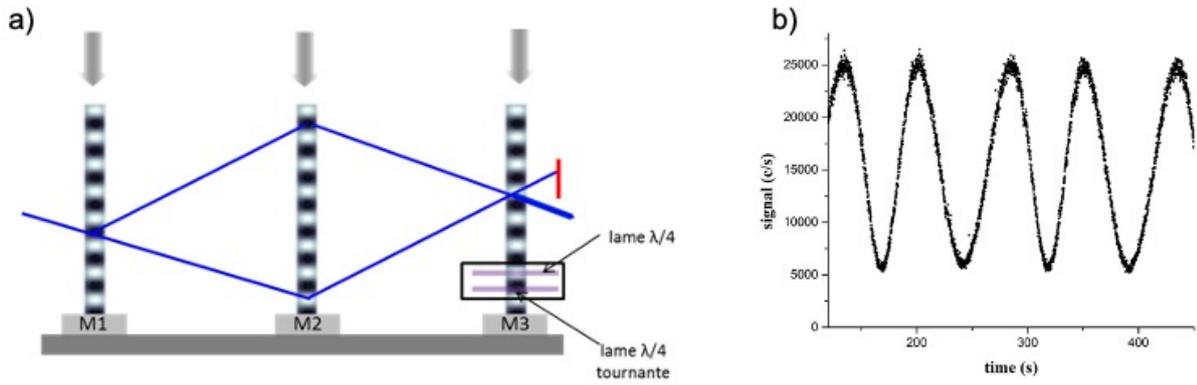
FIGURE 3.13 – a) The Pancharatnam phase shifter is located in front of the M3 retroreflecting mirror. b) Atomic interference fringes scanned with the Pancharatnam phase shifter.

state returns to linear polarization (P) with an orientation that depends on θ. After retrore-flection on the mirror, the linear polarization (P) is transformed into the left-handed circular polarization (LH) and finally returns to its original polarization state (H), but phase-shifted by $\phi_{Pancha} = 2\theta$. To change Pancharatnam's phase, we simply rotate the second quarter wave plate.

The main result of this study is the demonstration of a new technique, based on the Pancharatnam phase, for controlling the phase of an atom interferometer using a retroreflected optical lattice. Figure 3.13(b) shows interference fringes scanned with the Pancharatnam phase. This first result confirms the principle of the Pacharatnam phase shifter. Indeed, the visibility is not degraded by this device and we did not observe any additional phase noise. In addition, we identified its limitations using optical interference devices. The main limitation relates to the li-nearity between the induced phase shift and the angle of rotation of the quarter wave plate. This is due to the imperfect alignment of the quarterwave plates, which could be greatly improved by appropriate mechanical design.

In conclusion, the Pancharatnam phase shifter is of interest for the engineering of atom inter-ferometers, especially for space missions. This method allows precise control of the interferometer phase without the need to move the retro-reflecting mirror, thus simplifying the implementation of other controls such as mirror rotations, which are essential to compensate for the rotations of an on-board sensor. Furthermore, by exploiting the geometric nature of the Pancharatnam phase, it is possible to effectively control the phase shift of atomic species diffracted by laser beams of different wavelengths. This property is of particular interest in space experiments designed to test the equivalence principle using two-species interferometers.

6   Conclusion and prospects

In this chapter, I have presented my research activities carried out between 2010 and 2015 in the atom interferometer team at LCAR. The work I presented is based on the operation of an atom interferometer, which uses a continuous source of lithium atoms diffracted by stan-

ding light waves. What distinguishes our device from most other atom interferometers is the spatial separation between the arms of the interferometer, which allows to control the different perturbations on each of the two arms. This feature has paved the way for the exploration of non-inertial measurements that are uncommon with atom interferometers.

Continuous sources of atoms are less frequently used in atom interferometry than "pulsed" sources of laser-cooled atoms (e.g. optical molasses). In our experiment, the choice of a supersonic atomic beam was made with the aim of observing refractive index effects during the propagation of matter waves in a dilute medium. However, beyond the study of these collisional properties, continuous sources offer advantages that could be exploited in the field of inertial sensors. Interferometers using thermal beams have a considerable flux of atoms, which translates into excellent performance in terms of signal-to-noise ratio. In addition, continuous measurements allow for a wider measurement bandwidth, which also reduces spectral aliasing effects that can limit the sensitivity of these instruments. These features are extremely useful for atomic gyroscopes, whose scaling factor is proportional to atomic velocity (unlike accelerometers) [Durfee, 2006 ; Gustavson, 2000]. However, thermal beam interferometers have a high longitudinal atomic velocity, which poses a problem in terms of device compactness. Research is underway to develop high-brightness, continuous sources of cold atoms [Phillips, 1982] for use in inertial sensors and atomic clocks [Xue, 2015 ; Manicchia, 2023] or for short-range force measurements with material nano gratings [Garcion, 2021]. Furthermore, recent developments have highlighted the possibility of cold atom sources without the need for laser cooling [Huntington, 2023]. This approach, successfully demonstrated on lithium, could be generalized to other paramagnetic atoms or molecules, paving the way for metastable hydrogen or helium cold atom beams. In addition, the slowing and rovibrational cooling of more massive paramagnetic molecules, such as YbF, would have significant implications for parity violation measurements, as well as for the study of collisions and chemistry at ultracold temperatures.

The work carried out by our team using the Lithium Interferometer has demonstrated the possibility of making new measurements using the spatial separation of the interferometer arms. This approach has allowed us to explore the special features of quantum physics, in particular geometric phases of the Aharonov-Bohm type. Furthermore, recent developments in interferometers using ultracold atoms have highlighted the possibility of manipulating quantum coherences at macroscopic scales, with dimensions up to several tens of centimeters [Kovachy, 2015a]. The prospect of interferometers with macroscopic spatial separations and better control of systematic effects opens up new possibilities for fundamental tests. In the next chapter, some promising aspects of these prospects will be discussed in more detail, highlighting their novel character in the context of atom interferometry.

Chapitre 4

Ongoing research and prospects

> The most exciting phrase to hear in science, the one that heralds new discoveries, is not "Eureka!" but "That's funny..."
>
> I. Asimov

Objectifs

Since 2016, I have oriented our efforts on the study of atom interferometers using Bose-Einstein condensates (BECs) with large spatial separation. These interferometers have led to many proposals, both in the field of quantum sensors and in the implementation of fundamental physics tests. Our research focuses on the development of new methods in atom optics, such as atom beamsplitters with very high momentum transfer, the study of ultracold atom sources at high rates, and new physics tests exploiting geometric phase shifts.

Sommaire

1 Atom interferometry with macroscopic separation

The experimental setup we are developing is designed to make atom interferometers with separations between the arms of the interferometer ranging from centimeters to a meter. It is based on Bose-Einstein condensates manipulated by an optical lattice. Recently, ultracold atoms have demonstrated their ability to achieve large momentum transfers using optical lattices, while allowing interferometer durations (T) significantly longer than those obtained with atomic beams. These devices therefore allow a significant enhancement of the scaling factors of inertial sensors, as well as h/M measurements used to determine the fine structure constant. In addition, the large spatial quantum superpositions generated in these interferometers create singular situations in quantum physics, paving the way for tests of the macroscopicity of quantum physics. The macroscopic separation between the interferometer arms also provides opportunities to tailor the interaction potentials at these arms. This allows detailed studies of phenomena such as geometric phase shifts and their applications in metrology, as well as gravitational measurements, including the determination of the universal gravitational constant G.

In this section I will briefly present the preliminary results we have obtained in the field of Large Momentum Transfer (LMT) with an interferometer using rubidium Bose-Einstein condensates. I will then describe the main features of a new apparatus that is currently under development. Finally, I will discuss some of the measurements we plan to achieve with this device, focusing on a new method for measuring the neutrality of matter based on the scalar Aharonov-Bohm effect.

1.1 Preliminary results

1.1.1 Interferometer with ultra-cold atom sources

Between 2016 and 2022, we developed a new atom interferometer based on rubidium-87 Bose-Einstein condensates (BECs) (figure 4.1 (a)). Atoms are launched upward through an optical lattice at 1064 nm and then diffracted by a vertical lattice at 780 nm to create the interferometer (Figure 4.1 (b)). The atoms are detected by fluorescence imaging on a CMOS camera after a time-of-flight of 15 ms, a time that allows the different pulse states to be clearly distinguished at the output of the interferometer (figure 4.1 (c)). The design and assembly details of the vacuum system and the laser cooling system are documented in the thesis of Boris Décamps [Decamps, 2016].

Bose Einstein condensate source. The atomic source consists of an ensemble of Rubidium-87 atoms evaporatively cooled in an all-optical trap. The configuration of this dipole trap is based on two horizontally crossing beams at 1070 nm (*crossed trap*), plus a third beam at 1560 nm at an angle of 45^{circ} to the vertical, with a smaller waist (*dimple trap*) (see figure 4.2). This configuration, inspired by the work of CLÉMENT et al. [Clément, 2009], allows the confinement frequencies and trapping depth to be tuned independently with the power of the *cross-trap*, and the runaway regime to be reached during evaporative cooling. In addition, a horizontal magnetic field gradient is applied during the evaporative cooling process to prepare
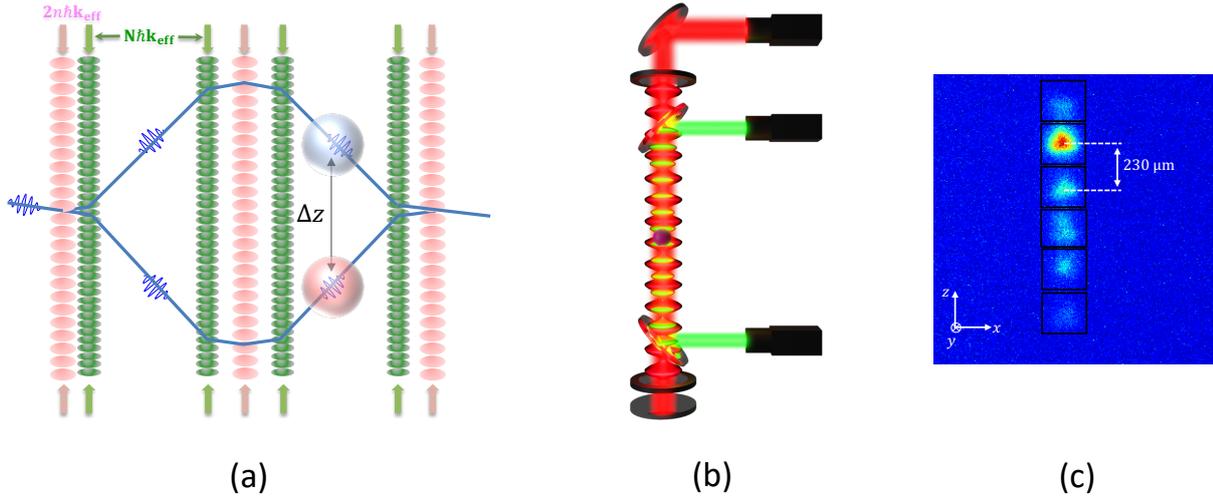
FIGURE 4.1 – (a) In the experiment we are building, ultracold atoms are manipulated with optical lattices to create an interferometer with arms separated by several centimeters. Such a separation Δz allows to apply different potentials on each of the interferometer arms. (b) The condensate is manipulated with a 780 nm retro-reflected optical lattice (in red). A 1064 nm optical lattice, superimposed on the previous one, is used to launch the atoms upwards. (c) The atoms are detected by fluorescence. The exit ports correspond to momentum states separated by $2\hbar k$, with populations that can be measured after a time of flight. The image shows that the spots corresponding to these different states are well separated.

the condensate in the pure $|F = 1, m_F = 0\rangle$ [Cennini, 2003] state. In 6 seconds we create a Bose-Einstein condensate (BEC) of $N = 6 \times 10^4$ atoms. The trap frequencies at the end of the evaporation reach about $(60 \times 900 \times 1100)\text{Hz}^3$. By transferring the BEC to a less confining trap, characterized by frequencies around $(10 \times 80 \times 80)\text{Hz}^3$, we achieve a significant reduction in the velocity dispersion. This allows us to obtain atomic ensembles of $3 times 10^4$ atoms with a velocity dispersion of about 0.3v_r (corresponding to an effective temperature of 30 nK). Details of the experimental setup and methods for characterizing the optical trap can be found in the thesis of Julien Alibert [Alibert, 2017] and Maxime Bordoux [Bordoux, 2019].

Launching and collimation. To increase the free fall time of the interferometer, the condensate is launched vertically with Bloch oscillations into a 1070 nm optical lattice with a waist of 80 μm. This optical lattice is formed by a pair of vertically aligned, counter-propagating laser beams that are independently controlled in frequency and amplitude by acousto-optic modulators (AOMs)[1]. We adjust the relative frequency difference of the lattice beams to accelerate the atoms. We have recently obtained the first results for vertical atom acceleration, launching up to $40\text{v}_\text{r} \approx 160$ mm/s without observing any atom loss or increase in velocity dispersion. The launch velocity is currently limited by transverse confinement, which produces center-of-mass oscillations and leads to heating of the atomic cloud. This limitation results from a compromise

---

1. This optical lattice is not retroreflected, which avoids the problems associated with interference induced by dual lattices at zero velocity, unlike the Bragg optical lattice.
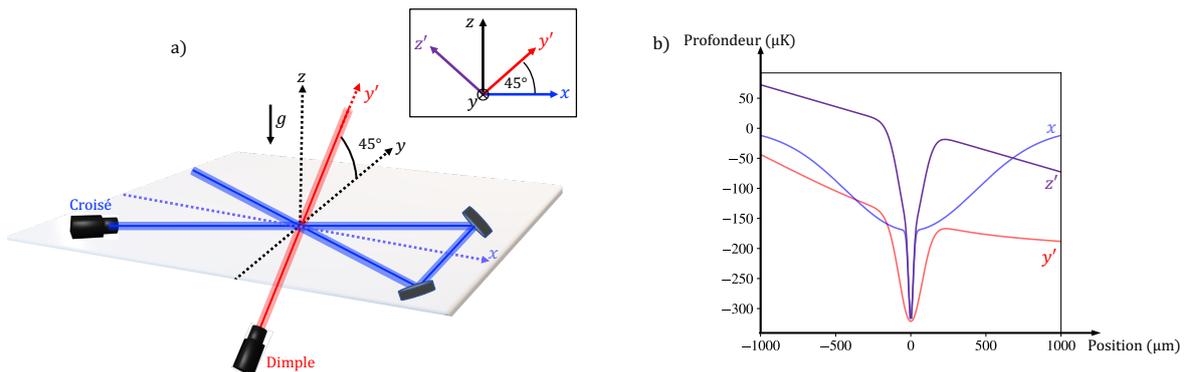
FIGURE 4.2 – a) Diagram of the *crossed* (blue) and *dimple* (red) traps used to realize the conservative dipole trap during evaporative cooling. b) Trapping potential plots of the dipole trap used at the beginning of evaporation. This geometry allows to decouple the frequencies (dominated by ω_x and ω_z^{prime}) and the trap depth (dominated by the depth of the trap *crossed* along the y^{prime} axis) during evaporation.

in the size of the beam used for both the launch and the optical trap. A modification of the optical setup of the beams at 1070 nm will increase the waist of the optical lattice and overcome this limitation.

Measurements planned with the separated-arm interferometer experiments require a subnanokelvin atom source. To achieve this goal, we have implemented a phase-space manipulation technique, also known as delta-kick collimation (DKC) [Chu, 1986 ; Ammann, 1997 ; Morinaga, 1999 ; McDonald, 2013 ; Kovachy, 2015b ; Corgier, 2020 ; Deppner, 2021]. This technique consists of applying a velocity dependent force field that opposes the atomic motion, leaving the cloud with almost zero velocity dispersion. In practice, the atoms are allowed to spread out for a sufficiently long free-fall time so that the position distribution of the atoms reflects the initial velocity dispersion. We then apply a harmonic optical potential to collimate the spatial expansion of the source to reduce its velocity dispersion. The DKC sequence is shown in figure 4.3(a). After being released from the dipole trap, the atoms are in free fall. They are then accelerated upward at a velocity of $40v_r$ so that the apogee of their trajectory coincides with the center of the optical trap (a similar implementation with ytterbium atoms is described in [Gochnauer, 2021]). After an expansion period of t_{exp}, the DKC pulse is realized by reflashing the optical trap. For a velocity of $40v_r$, expansion times of 16.5 ms can be achieved. Under these conditions, the DKC technique allows us to obtain a source of atoms with an effective temperature of about 2 nK (Figure 4.3(b)), in agreement with our numerical simulations. These simulations also indicate that, despite the nonlinearities of the trap, temperatures of the order of 500 pK can be achieved for longer expansion times. However, increasing the expansion time requires higher launch velocities, which leads to a heating of the atomic cloud with the current lattice, compensating for the advantages of DKC.

The details of the experimental setup and the characterization of the launching and DKC collimation are described in Ashley Béguin's thesis [Beguin, 2023].
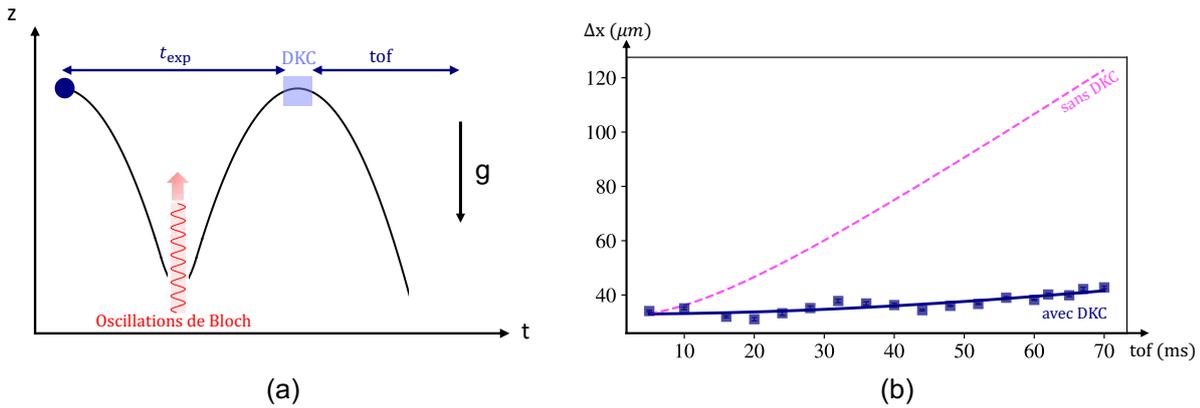
FIGURE 4.3 – a) Schematic diagram of the atom trajectory for the DKC experiment. The collimation pulse is applied at the top of the atom trajectory to minimize displacements during the laser pulse. b) Experimental study of the cloud size evolution after time of flights: without DKC (pink), corresponding to an effective temperature of 30 nK, and with DKC (blue). The DKC parameters are: duration $\tau = 150 \mu s$, power P = 6 W, waist $w_0 = 145$ μm and expansion time before DKC of 16.5 ms. We obtain an effective temperature of 1.78 ± 0.25 nK.

1.1.2 Diffraction in the quasi-Bragg regime

To achieve a spatial separation of several centimeters with free fall times limited to a few hundred milliseconds, the use of atomic beam splitters capable of inducing large momentum transfers ($> 80\hbar k$) is essential. In addition, we will see that for some applications it is important that the atoms propagate through the interferometer in the same internal state. To satisfy these constraints, the interferometers we use employ an optical lattice operating in the quasi-Bragg diffraction regime.

We have performed a comprehensive numerical and experimental study of the diffraction of ultracold atoms in the quasi-Bragg regime. Although diffraction by an optical lattice has been the subject of numerous theoretical and experimental investigations, our study has provided insight into the convergence of numerical models, the phase shifts inherent in the quasi-Bragg regime, and the optimal conditions for diffraction. Details of this study have been published in [Béguin, 2022 ; Beguin, 2023], and I present the main results here.

The theoretical model we use to describe diffraction in the quasi-Bragg regime is presented in chapter 2. The n-order diffraction process results from resonant coupling between the $|p_0\rangle$ and $|p_0 + 2n\hbar k\rangle$ momentum states. We study the dynamics by numerically solving the Schrödinger equation using the Hamiltonian 2.2 (page 10). In this study, the time envelope of the interaction with the optical lattice is a Gaussian defined numerically over an interval $\pm 5\sigma$:

$$\gamma(t) = \gamma_{\max} \exp\left[\frac{-t^2}{2\sigma^2}\right].$$ (4.1)

We distinguish two interaction subregimes: Short Pulse ("SP"), dominated by non-adiabatic transitions populating unwanted pulse states, and Long Pulse ("LP"), where oscillations between

the two Bragg states are found.

We have numerically investigated the interaction time and lattice depth that optimize the diffraction efficiency to order n for a given atomic cloud temperature. The temperature T is defined by the standard deviation σ_v of a Gaussian velocity distribution $\sigma_v^2 = k_B/mT$. The right side of the figure shows the evolution of the population in the Bragg state $|6\hbar k\rangle$ as a function of lattice duration and amplitude $\sigma - \gamma_{mathrmmax}$. We observe a series of local maxima corresponding to odd multiples of π of the Rabi phase θ_R. The left side of the figure shows the evolution of the transferred population along the lines of the local maxima (dashed lines in the right side of the figure). Each curve corresponds to a particular Rabi phase $(pi, 3pi, 5pi, \dots)$. All odd Rabi phases in the LP regime reach a similar maximum transfer efficiency for a pair $\sigma - \gamma_{mathrmmax}\}_{mathrmopt}$. We have demonstrated an interesting compromise that minimizes the maximum amplitude of the optical lattice at the boundary between the SP regime, characterized by non-adiabatic

FIGURE 4.4 – Population P_3 of the diffracted state $|6\hbar k\rangle$ in the quasi-Bragg regime. The simulation considers a velocity dispersion of 1.8 mm/s (i.e. T = 30 nK). Right panel: population P_3 as a function of $(\sigma, \gamma_{mathrmmax})$. Dashed lines indicate local maxima associated with Rabi phases $\pi[2\pi]$. The blue line corresponds to the Rabi oscillation of figure 4.5 for $\gamma_{\max} = 3.3$. Left panel: Population P_3 as a function of σ along the lines of the local maximum. For this temperature, the optimal diffraction efficiency is reached for a pair $(\sigma, \gamma_{\max})$ such that $\theta_R \geq 3\pi$.

losses, and the LP regime, dominated by velocity selectivity. Considering a higher Rabi phase would have the effect of reducing non-adiabatic losses and the associated diffraction phases. However, this approach has the disadvantage of accentuating other effects, such as spontaneous emission and light shifts, which increase in proportion to the product $\sigma \times \gamma_{\max}$. The trade-off between the SP and LP regimes is illustrated in figure 4.4, where maximum efficiency is observed for values of $\theta_R \geq 3\pi$. An important feature of this study is the very good agreement between our experimental data and our numerical simulations. High-order Bragg diffraction in the quasi-Bragg regime is illustrated in the figure 4.5. In this example, we measure the populations in the different pulse states at the end of the laser pulse, adjusted to a transition of $n = 3$. The pulse duration σ is scanned between $0.05\omega_r^{-1}$ and $1.1\omega_r-1$. We distinguish between SP ($\sigma \lesssim 0.5\omega_r^{-1}$) and LP ($\sigma \gtrsim 0.5\omega_r^{-1}$) regimes. We obtain very good agreement between our experiment and our numerical model, with the populations of the different momentum states being very well reproduced by the numerical simulation without adjustable parameters.

We have also studied three-pulse Mach-Zehnder interferometers. In a two-level model adapted to Raman pulses or the Bragg regime, the beam splitters are realized with a $\theta_R = \pi/2$ pulse, while the mirror is obtained with a $\theta_R = \pi$ pulse. However, in the quasi-Bragg regime, these Rabi phases correspond to the SP regime, leading to significant non-adiabatic losses. For these

FIGURE 4.5 – The figure shows the evolution of P_n populations in each of the $2n\hbar k$ momentum states as a function of σ for a Gaussian envelope of the lattice. The coupling is chosen to be resonant for 3rd-order diffraction with a two-photon Rabi frequency $\gamma_{\max} = 3.3$. The initial state is the $n = 0$ momentum state. (a) Evolution of the two Bragg states $n = 3$ and $n = 0$, (b) and (c) population in the non-resonant momentum states. The solid lines are the results of numerical simulation for a velocity dispersion $\sigma_v \approx 1.8$mm/s (≈ 30 nK) without adjustable parameters.
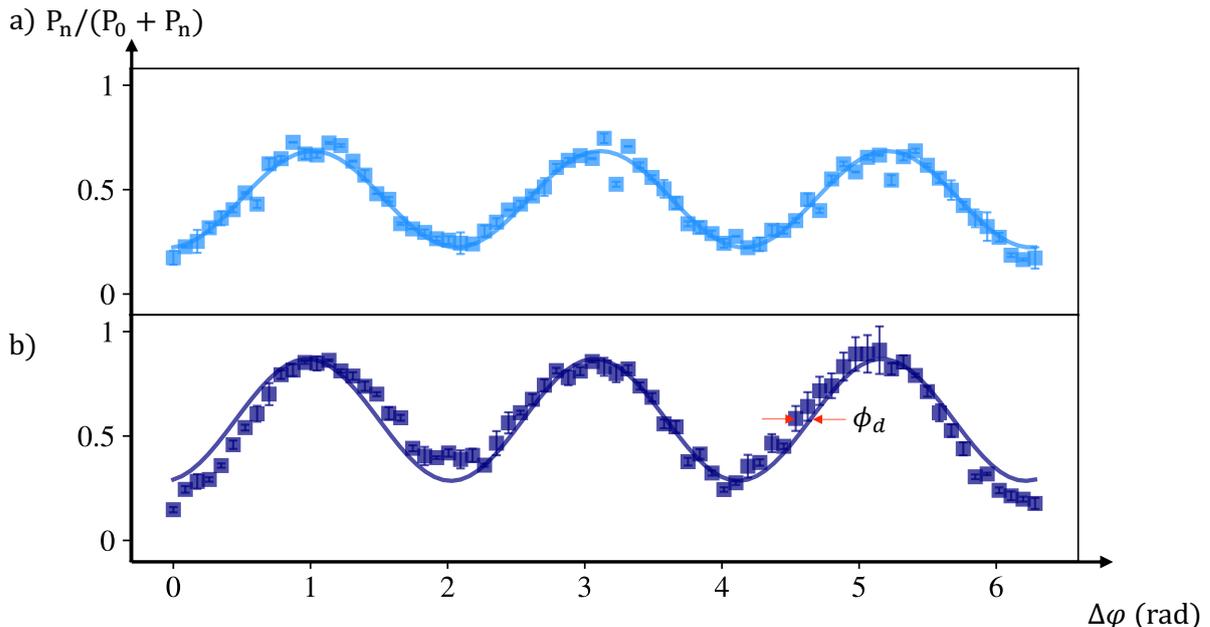
FIGURE 4.6 – Interference fringes obtained for a mirror pulse in the LP (a) and SP (b) regime for $n = 3$. The solid lines are the result of a sinusoidal fit. Each experimental data is the average of 5 measurements. The LP regime allows for a two-wave interferometer that produces sinusoidal fringes, while the SP regime induces multiple interferometers that distort the interference fringes. The distortion of the fringes is interpreted as an additional phase ϕ_d.

experiments, atomic beam splitters with longer pulses $\theta_R = 3\pi/2$ are used. This corresponds to a pulse at the boundary between the SP and LP regimes. The mirror pulse is chosen either in the SP regime $\theta_R = \pi$ or in the LP regime $\theta_R = 3\pi$. In particular, we have studied the effect of non-adiabatic losses up to $n = 5$ on the visibility and deformation of interference fringes. For example, the figure 4.6 shows fringes for $n = 3$. Unlike previous studies [Altin, 2013 ; Parker, 2016], we directly measure the interference fringes in all output channels of the interferometer. This feature opens the way to quantitative studies of the systematic effects associated with diffraction phases [Kirsten-Siemß, 2023].

Conclusion. We have studied atomic diffraction and interferometry with a BEC diffracted by an optical lattice in the quasi-Bragg regime up to the sixth order of diffraction. We have presented simulations performed without adjustable parameters, which are in excellent agreement with experimental data. This work provides a quantitative understanding of the diffraction phases associated with the multiport nature of interferometers based on quasi-Bragg diffraction. We have numerically confirmed the relationship between diffraction phases and non-adiabatic losses, explaining diffraction phase shifts up to tens of milliradians.

These characterization elements contribute to our understanding of atom interferometers using high order diffraction. Laser power limitations reduce the interest in diffraction orders beyond $n = 10$. However, interferometers using Bragg beam splitters $\lesssim 20\hbar k$ remain relevant in the context of inertial sensors where sensitivity is the main limitation. These beamsplitters

also have applications in space missions, where long interferometry durations in small volumes and thus moderate pulse separation are required [2]. However, their use for metrological purposes requires a better understanding of the multipath phases. A detailed study of these phase shifts and of methods to attenuate them is currently being pursued in collaboration with the group of N. Gaaloul in Hannover [Kirsten-Siemß, 2023]. Last but not least, these studies have given us a deep understanding of the quasi-Bragg regime, both experimentally and numerically. These insights have been crucial for the design and development of the large momentum transfer interferometers we are planning.

1.1.3 Beam splitters with large momentum transfer

Recently, there have been many efforts in the community to increase the number of photon momentum ($\hbar k$) transferred to atoms, with the goal of creating Large Momentum Transfer (LMT) atomic beam splitters. Various solutions have been demonstrated, most of them beginning with the creation of a superposition of two momentum states using a quasi-Bragg diffraction. One of the two states is then accelerated, either continuously using Bloch oscillations [Cladé, 2009], or discretely using π pulse sequences [McGuirk, 2000; Gupta, 2002].

The first method, based on Bloch oscillations and Bragg diffraction, was implemented by the group of E. Rasel [Gebbe, 2021] for the demonstration of an interferometer that allowed a transfer of 408 $\hbar k$ in the horizontal direction. A similar approach proposed by Malinovsky et al. [Malinovsky, 2003], based on the use of two optical lattices accelerated in opposite directions, was used by Pagel et al. [Pagel, 2020] to construct 240 $\hbar k$ interferometers. M. Kasevich's group demonstrated interferometers with a momentum separation of $102\hbar k$ using successive Bragg transitions ($n = 3$) [Chiow, 2011]. More recently, in the group of S. Gupta, a $112\hbar k$ interferometer was realized also using sequences of Bragg pulses, but with ytterbium atoms [Plotkin-Swing, 2018]. Sequential acceleration methods have also been implemented with single-photon transitions on strontium atoms using a sequence of π pulses [Rudolph, 2020; Wilkason, 2022]. These achievements have led to the demonstration of interferometers with beam splitters of $400\hbar k$. Our team has recently demonstrated an interferometer with a beamsplitter of $200\hbar k$. A non-exhaustive list of LMT interferometers is given in the table 4.1.

LMT Type	Atoms	References	Transfer
Bragg CEBS	Rb	[Béguin, 2023]	200 $\hbar k$
Bragg	Yb	[Plotkin-Swing, 2018]	112 $\hbar k$
Bragg	Rb	[Chiow, 2011]	102 $\hbar k$
Bloch	Cs	[Pagel, 2020]	240 $\hbar k$
Bragg + Bloch	Rb	[Gebbe, 2021]	408 $\hbar k$
1 photon	Sr	[Rudolph, 2020]	141 $\hbar k$
1 photon (Floquet)	Sr	[Wilkason, 2022]	400 $\hbar k$

TABLE 4.1 – Non-exhaustive list of LMT interferometers achieved in recent years.

---

2. As an example, the STE-QUEST project considers an interferometer duration of $2T = 25$ seconds, which would result in a separation of almost 1 m for $6\hbar k$ beamsplitters with rubidium atoms

Coherent Enhancement of Bragg Sequences. Large momentum transfer interferometers require very high transfer efficiencies due to the cumulative losses associated with each transition. Using $1000\hbar k$ as a reference for the next generation of LMT interferometers, an efficiency greater than 99.88% per $\hbar k$ (or 99.97%) is required to detect 10% (or 50%) of useful atoms at the output of a Mach-Zehnder-type interferometer.

The previous approach to achieve efficient transfers relies on optimizing each Bragg transition individually. [Chiow, 2011 ; Plotkin-Swing, 2018]. However, achieving efficiencies greater than 99.5% in the quasi-Bragg regime is a real challenge. To meet this challenge, it is necessary to combine the use of long pulses to minimize non-adiabatic losses with the use of highly collimated atomic sources (temperature below 500 pK) to limit losses due to velocity selectivity. Typically, the time interval between each pulse is in the millisecond range, resulting in interferometer durations of several hundred milliseconds or even a few seconds, limiting the practical interest of these techniques to $\gtrsim 100\hbar k$ interferometers. We have demonstrated the possibility of circumventing this limitation by exploiting destructive interference between non-adiabatic losses. This approach has been named Coherent Enhancement of Bragg pulse Sequence (CEBS) [Béguin, 2023].

Before studying the effects of this sequential transfer on a complete interferometer, we analyze a single acceleration sequence. The evolution of the number of atoms in the accelerated state ($|2N\hbar k\rangle$) is shown in figure 4.7(a). The sequence consists of N π pulses at $n = 1$, of duration τ and separated by a time t_c. We have set the lattice parameters to favor non-adiabatic losses, which, unlike those associated with velocity selectivity, are coherent and thus allow interference between losses. This setting leads to an efficiency of 0.6 for a single pulse ($N = 1$ in figure 4.7(a)). If we were to consider independent processes for each acceleration pulse, this would lead to dramatic cumulative losses, since the remaining fraction of 0.6^N would be undetectable after only $N = 10$ pulses. However, we find that more than 30% of the initial atoms are detected in the fully accelerated trajectory after $N = 37$ pulses. This corresponds to an efficiency of over 99% per $\hbar k$.

This efficiency results from destructive interference between the loss channels. To illustrate this process, we examine the losses in the $|2(N-2)\hbar k\rangle$ state at the Nth pulse (Figure 4.7(b)). We consider two paths, the first corresponding to the atoms not diffracted at the (N-1)-th pulse, whose amplitude is calculated to be equal to ϵ (path a in Figure 4.7(b)), the second path corresponds to the non-resonant coupling at the Nth pulse with an amplitude of $\epsilon \exp[i(\pi - 4\omega_r t_c)]$ (path b in figure 4.7(b)). If the coherence length $\xi = \hbar/(m\sigma_v)$ is larger than the distance between the two paths $\Lambda = 2v_r t_c$, they interfere, and the population in this loss channel oscillates according to:

$$P_{|N-2\rangle} \approx 2\epsilon^2 \left[1 + \cos(\pi + 4\omega_r t_c) \right]. \tag{4.2}$$

When the time between pulses is short enough, $t_c \ll (4\omega_r)^{-1}$, the loss channels interfere destructively. This phenomenon also occurs in all other loss channels, leading to a significant reduction in non-adiabatic losses. To study these dynamics in more detail, we have performed simulations including higher order paths, finite temperature, and lattice amplitude fluctuations between each
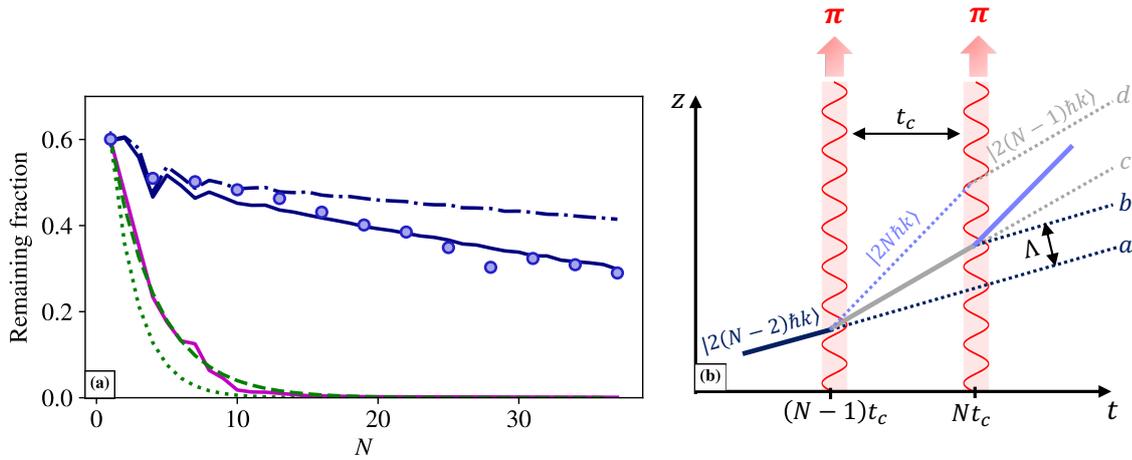
FIGURE 4.7 – (a) Blue circles: Population measured in the accelerated state after a sequence of N π pulses. The dark blue (respectively magenta) solid line is a model including interference phenomena between loss channels and lattice amplitude fluctuations (respectively without interference). The dashed line is a simulation without fluctuations. The dotted (respectively dashed) lines represent the power law corresponding to an independent process for each acceleration pulse for $\sigma_v = 2.2$ mm.s^{-1} (respectively $\sigma_v = 0$ mm.s^{-1}). (b) Diagram of the space-time trajectories around the (N-1)th and Nth π acceleration pulses. The accelerated trajectory corresponds to the solid lines, and the dotted lines are the loss channels. After the second pulse, several trajectories (e.g., a and b, c and d, etc.) have the same momentum state. These trajectories interfere destructively if the distance between them Λ is smaller than the coherence length and if $t_c \ll \omega_r^{-1}$.
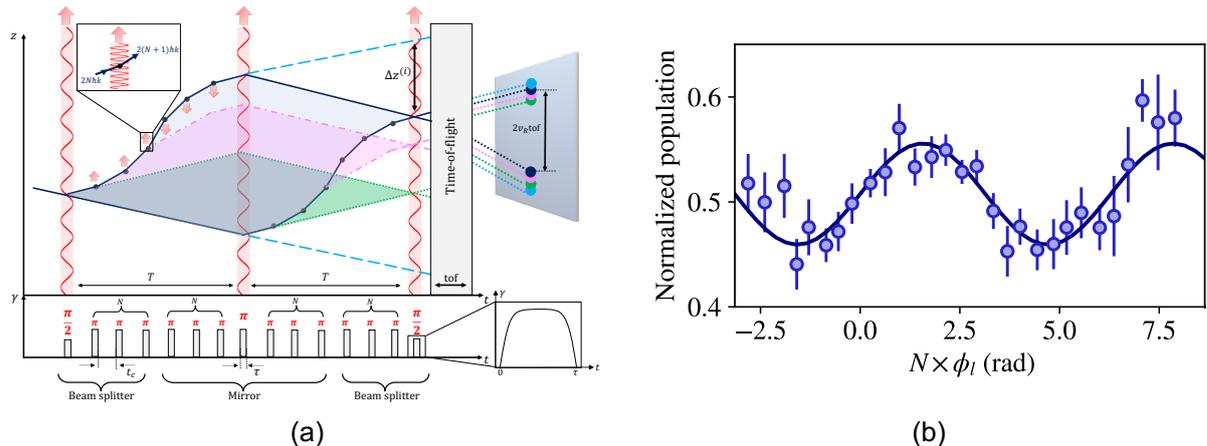
FIGURE 4.8 – (a) Paths corresponding to an 8 $\bar{k}$ interferometer in the free-fall frame of reference. The red lattices represent the $\pi/2 - \pi - \pi/2$ diffraction pulses of a standard atom interferometer. The separation between the arms is increased by sequences of N π pulses separated by a time t_c acting on only one arm (red arrow). Due to imperfections in the π pulses, loss channels (dashed and dotted lines) can induce spurious interferometers. The bottom panel shows the optical lattice pulse train and the hyperbolic tangent amplitude profile used for each pulse. (b) Interference fringes for a 200 $\hbar k$ beamsplitter.

pulse. The results of these simulations agree remarkably well with the experimental data (see figure 4.7(a)), confirming the favorable effect of interference between the different loss channels. The efficiency is limited by the power fluctuations of the optical lattice, which are of the order of 7%. By reducing these fluctuations to less than 1% and using a 50 nK source like the one we used, our simulations predict an efficiency per $\hbar k$ greater than 99.5% (dotted line in Figure 4.7(a)). This efficiency could be further improved by using a sub-nK source, reaching an efficiency of 99.9%.

We have implemented these LMT beamsplitters in Mach-Zehnder LMT interferometers, realized by a sequence of Bragg pulses (see figure 4.8(a)). The interferometer is one dimensional according to gravity $\vec{g} = -g\vec{z}$. The first beam splitter consists of a $\pi/2$ pulse, which creates a coherent superposition between two momentum states $2\hbar k$. Next, the upper path in the figure 4.8 undergoes a CEBS acceleration sequence of N π pulses, which do not act on the lower arm. After a time T' of free propagation, the upper path is decelerated by a CEBS sequence. A π pulse then acts as a mirror for both arms. The lower path then undergoes identical sequences of CEBS acceleration (N pulses π), free propagation T', CEBS deceleration (N pulses π). Finally, a $\pi/2$ pulse forms the second beamsplitter that closes the interferometer. We detect populations in the two main output ports with states $|0\rangle$ and $|2\hbar k\rangle$. Due to imperfect π pulses, visibility measurements may be biased by unwanted interferometric paths; these effects are studied in detail in [Beguin, 2023].

Figure 4.8(b) shows fringes from an interferometer made with 399 pulses[3] to produce a maximum momentum separation between the arms of $200\hbar k$. To scan the fringes, we add a laser

---

3. $4N + 3$ pulses where N is the number of CEBS acceleration pulses

phase jump (ϕ_l) during the first N acceleration pulses, generating an oscillating signal at $N \times \phi_l$. The frequency of these oscillations with N is a signature of the interferometer $2(N+1)\hbar k$. We measure a visibility of $9 \pm 1\%$ up to $200\hbar k$ (Figure 4.8 (b)). The limitation at $200\hbar k$ is related to the time of flight available in our apparatus, which limits the number of Bragg pulses.

Conclusion The CEBS method allows very high transfer efficiencies, paving the way for very large momentum transfer interferometers. To demonstrate the potential of CEBS beam splitters, we have performed numerical simulations which suggest that efficiencies in excess of 99.95% per $\hbar k$ are achievable. This allows the design of interferometers with beam splitters in excess of $1000\hbar k$. In addition, this method relaxes the usual trade-off between velocity selection and non-adiabatic losses. In addition, the CEBS technique achieves shorter pulse trains than many other acceleration methods. For example, our simulations show that a transfer of $1000\hbar k$ is achievable in less than 5 ms with an overall efficiency of $> 10\%$. This technique is therefore well suited for the compact LMT interferometers being developed for quantum sensors. In addition, fast LMTs can increase the spatio-temporal range and the spatial separation between the arms for a given interferometric duration. We have performed a quantitative study of the effect of the finite duration of pulse sequences by extending the sensitivity function formalism to LMT interferometers [Décamps, 2019].

The increase in efficiency and speed of momentum transfer associated with destructive interference between loss channels is also the basis of "shortcut to adiabaticity" methods [Guéry-Odelin, 2019]. In addition, the acceleration regime we have studied is closely related to quantum resonance phenomena in the delta-kick rotor [Moore, 1995 ; Daszuta, 2012 ; Fekete, 2017], to the temporal Talbot effect [Deng, 1999], and more recently to multiple interference phenomena during continuous acceleration in an optical lattice [Rahman, 2023].

We are currently investigating the limits of the CEBS beamsplitter, particularly in terms of pulse transfer rate, efficiency and robustness. To this end, we plan to implement optimal control protocols and to use atom sources at temperatures below 500 picoKelvin. The metrological characterization of LMT interferometers using these CEBS beamsplitters will be an important outcome of this project. To achieve these goals, we are developing an improved version of the device, the main features of which are outlined in the next section.

1.2 A new experimental setup

We are currently developing a new vacuum chamber. The principle of the apparatus is illustrated in the figure 4.9. The new experimental setup will allow us to isolate and independently access the chambers dedicated to the BEC source and interferometry. This advance will provide greater flexibility to integrate different interaction potentials within the interferometry chamber.

The current design of the cold atom source was originally specified for integration with an atom chip [Alibert, 2017]. This specification has imposed significant limitations on optical access that will be overcome in the new device under development. Several approaches are possible for the production of rubidium condensates. In the context of a laboratory experiment, particular attention will be paid to the reliability of the method, the atom flux and the integration with the

overall experimental setup, including aspects related to optical access and magnetic shielding. All-optical methods provide high confinement and optimized optical access while significantly reducing magnetic field complications. These approaches can be implemented in a variety of configurations combining multiple laser beams. All-optical methods often allow fast and efficient evaporation, leading to high frequency BEC production. Among the various possible implementations, the use of "time-averaged optical potentials" seems to be a promising solution. This technique simplifies the configuration of the optical setups and optimizes the use of the available laser power by adapting it to the different steps of the evaporative cooling. These methods have already demonstrated their ability to generate BEC of $\sim 10^5$ atoms in a few seconds, with a flux of the order of 1 to 5×10^4 atoms per second [Roy, 2016; Condon, 2019; Albers, 2022]. Mode matching between optical molasses and optical traps is a significant limitation on atomic flux. To overcome this limitation, a promising strategy is to use sub-recoil laser cooling techniques in the optical traps during the loading process. By applying a double cross trap configuration combined with laser cooling methods in optical lattices, YAMASHITA et al. [Yamashita, 2017] obtained a condensate of 10^6 atoms in 4 seconds (2.5×10^5 at./s). Condensation in magnetic traps can perform highly efficient, though relatively slow, evaporation cooling, allowing up to 10^7 rubidium atoms to be condensed in a few tens of seconds [Streed, 2006]. However, these magnetic traps often have limited optical access and require the use of large electrical currents, limiting their applicability in the context of quantum sensing. However, their robustness makes them attractive candidates for laboratory experiments. The so-called TOP ("Time Orbiting Averaged Potential") and "Plug" configurations have successfully generated condensates containing between 1 and 2×10^6 atoms within a time window of 10 to 20 seconds (about $\sim 2 \times 10^5$ at./s). This type of trap is used in particular in the rubidium interferometer of M. Kasevich's team at Stanford. On the other hand, Ioffe-Pritchard type configurations on atom chips have demonstrated the realization of condensates containing about 2×10^5 atoms in 1 second [Rudolph, 2015]. These sources are used in the 0-g interferometers in Hannover or in the CAL project on the International Space Station and are being considered for future space missions. It should be noted, however, that atom chips impose significant constraints on optical access. A hybrid approach, first proposed by COMPARAT et al. [Comparat, 2006] and implemented by LIN et al. [Lin, 2009], consists in using a quadrupole trap as a reservoir to feed a dipole trap. This method has allowed the creation of robust BEC sources with production rates of about $5 - 10 \times 10^4$ at./s and is currently used by several research groups. The configuration planned for the new experiment is based on an adaptation of the all-optical approach currently used. These adaptations are aimed at integrating time-averaged optical potential techniques (or "painted potentials") to simplify the configuration of our dipole trap. In addition, we plan to integrate sub-recoil laser cooling methods [Wolf, 2000; Kinoshita, 2005; Hu, 2017a; Schreck, 2021] to improve the loading efficiency of the optical trap.

The visibility and the number of atoms detected in our LMT interferometers are mainly limited by spatio-temporal fluctuations in the phase and amplitude of the optical lattice, as well as by spontaneous emission and the limited efficiency of the LMT pulse sequences. To overcome these problems, we are building a new laser system for the optical lattice that is capable of pro-
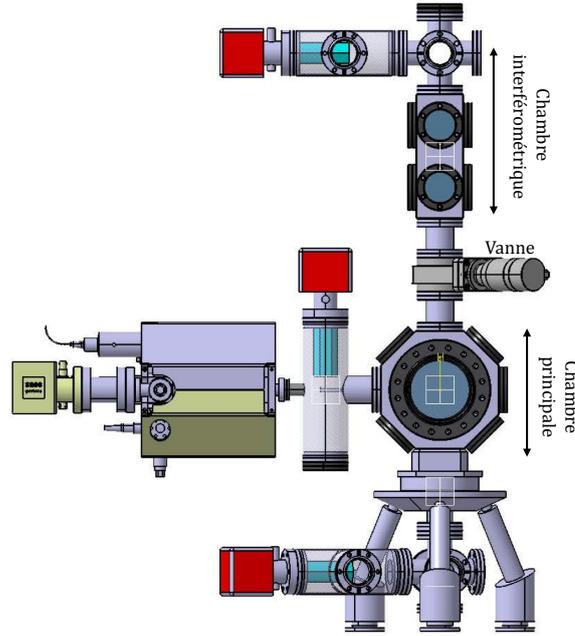
FIGURE 4.9 – New vacuum chamber in development.

viding higher optical power (> 10 W) [Kim, 2020]. This will allow higher detuning (> 300 GHz), making spontaneous emission negligible. In addition, the new system will benefit from improved servo control, which will significantly reduce phase and amplitude fluctuations. Furthermore, the divergence of the optical lattice introduces different light shifts on the interferometer arms, which can cause decoherence problems and systematic phase shifts. To eliminate these effects, we plan to use a beam from the same optical fiber as the optical lattice, but with an opposite one-photon detuning to compensate for the light shifts. This additional beam contains only a single frequency and therefore does not induce Bragg transitions [Kovachy, 2015a].

To improve the efficiency and robustness of LMT beam splitters, we investigate the implementation of optimal control methods to identify the most efficient optical lattice amplitude and phase profile. Several control methods inspired by nuclear magnetic resonance techniques have already been implemented with Raman transition interferometers [Luo, 2016], Adiabatic Rapid Passage (ARP) [Kovachy, 2015a], as well as numerical optimal control methods [Saywell, 2020]. For Bragg diffraction, numerical studies have been performed [Goerz, 2023 ; Louie, 2023], and [Saywell, 2023] have implemented these protocols with $6\hbar k$ interferometers, but without demonstrating any significant gain. Unlike methods that aim to optimize the robustness or efficiency of a single laser pulse, our approach aims to optimize the entire LMT sequence, i.e. the diffraction process that favors destructive interference conditions between non-adiabatic losses. Our goal is to make the CEBS acceleration sequence as fast as possible, while at the same time making it robust to amplitude and frequency fluctuations. Robustness with respect to the initial velocity of the atoms may prove useful in mitigating the constraints associated with source temperature and fluctuations in the velocity of the condensate center of mass.

1.3 Applications in fundamental physics

With the lithium interferometer, our team has developed expertise in measuring non-inertial effects and geometrical phase shifts using separated-arm interferometers. The experiment we are currently building is a continuation of this work. The new apparatus will allow a much larger macroscopic separation of the arms, opening new perspectives for the study of geometrical phase shifts induced, for example, by electromagnetic fields [Anandan, 1995], gravitational fields [Anandan, 1995; Hohensee, 2012; Overstreet, 2022], or artificial gauge fields [Bouchiat, 2011; Zygelman, 2015]. In this chapter I focus mainly on a proposed test for the electrical neutrality of the atom.

1.3.1 Measuring matter neutrality

All experiments to date [Unnikrishnan, 2004; Bressi, 2011] indicate that atoms are electrically neutral, i.e. there is an exact correspondence between the electron (q_e) and proton (q_p) charges, and the neutron charge (q_n) is zero. The best existing upper bounds for the electron-proton charge asymmetry $| q_p + q_e | / q_e$ and the residual neutron charge $| q_n | / q_e$ are close to 10^{-21}. Despite the remarkable accuracy of these measurements, a tiny residual atomic charge would have major implications for particle physics [Foot, 1993; Lammerzahl, 2007; Arvanitaki, 2008], astrophysics and cosmology [Caprini, 2005]. Our new device will allow the implementation of a new method based on the measurement of the scalar Aharonov-Bohm phase [Champenois, 2001b; Arvanitaki, 2008]. We are confident that this approach could significantly improve the current limits, possibly by several orders of magnitude.

State-of-the-Art Atomic Neutrality Measurements. It seems that one of the first proposals that triggered tests of the neutrality of matter came from A. Einstein [Einstein, 1924]. In 1924, he proposed to explain the origin of the magnetic fields of astronomical bodies in terms of a slight charge asymmetry leading to a non-zero charge density and, consequently, to the emergence of a magnetic field comparable to that generated by a magnetic dipole when a body is rotating. According to this model, a value of the order of $10^{-19}q_e$ would explain the Earth's magnetic field. This proposal stimulated the first accurate matter-neutrality experiment, [Piccard, 1925], which ruled out this explanation.[4].

Since these first experiments, many measurements of the electrical neutrality of matter have been made with various atomic and molecular species. In the table below we summarize the most important experiments. We distinguish between those that establish independent limits for the electron-proton charge asymmetry ($q_p + q_e$) and the neutron charge (q_n), and those that do not distinguish between these two contributions ($q = \frac{q_{At}}{A}$), where A is the number of nucleons in the atomic species (or sample in the case of macroscopic bodies). These methods fall into four categories:

1. Gas flow methods measure the electrostatic potential of a chamber (with electrical filters

---

4. We now know that the Earth's magnetic field is due to a self-sustaining dynamo mechanism in the outer core.

to prevent the passage of charged particles) through which a gas flows [Piccard, 1925 ; HILLAS, 1959 ; King, 1960] [5].

2. The electroacoustic method consists in the detection of the acoustic wave excited in a gas by an alternating electric field inside an acoustic resonator [Bressi, 2011].

3. Levitation methods: An electrostatic force is applied to small magnetically levitated masses. Analysis of the displacements induced by this force is used to define constraints on the neutrality of matter [Marinelli, 1984]. This modern version of Millikan's experiment was originally designed to detect the presence of free quarks in matter.

4. Beam deflection methods [6]: it consists of measuring the deflection of a molecular or neutron beam under the influence of an electric field [Hughes, 1988 ; Baumann, 1988].

Methods (1-3) are based on the use of macroscopic bodies for which it is difficult to model the systematic effects associated with the presence of free charges or inhomogeneous electric fields. Significantly improving the accuracy of the first two methods seems to be a considerable challenge [Bressi, 2011]. Thanks to advances in optical trapping techniques for nanoparticles, the levitation method (3) is currently attracting renewed interest [Moore, 2021]. The proposed accuracies, of the order of $10^{-24}q_e$, are close to what we are aiming for. It should be noted, however, that this method does not distinguish between contributions from neutrons and those from the electron-proton charge asymmetry. Experiments based on atomic beams (method 4) look for an anomalous deviation in the trajectory of atoms in the presence of an electric field induced by a Lorentz force. This method requires very good knowledge of the beam profile and the electric field. YOUNG et al. [Young, 1997] have suggested using the remarkable sensitivity of atom interferometers to acceleration with cold atoms to measure these electric forces. However, effects related to the polarizability of atoms limit the practical interest of this method CHAMPENOIS et al. [Champenois, 2001b]. Finally, DURSTBERGER-RENNHOFER et al. [Durstberger-Rennhofer, 2011] have proposed a new method using spectroscopy of ultracold neutron quantum states in the gravitational potential above a vertical mirror. However, as with the other methods, this experiment requires a very good knowledge of the spatial homogeneity of the electric field.

Method	Ref.	q/q_e	$(q_p + q_e)/q_e$	q_n/q_e
1	[Piccard, 1925]	5×10^{-21}	x	x
1	[HILLAS, 1959]	1×10^{-21}	3×10^{-20}	3×10^{-20}
2	[Bressi, 2011]	1.1×10^{-21}	x	x
3	[Marinelli, 1984]	0.8×10^{-21}	x	x
4 Atoms	[Hughes, 1988]	3×10^{-21}	1.2×10^{-19}	9×10^{-20}
4 Neutrons	[Baumann, 1988]	x	x	1.1×10^{-20}

TABLE 4.2 – Summary of the limits of matter neutrality from laboratory experiments.

The Aharonov-Bohm effect is an interesting phase shift for testing the matter neutrality using matter wave interferometers. This phase shift is proportional to the charge of the particle,

---

5. Inconsistencies in these measurements are reported in [Stover, 1967]

6. This method, first implemented by HUGHES et al., is said to have been suggested to V.W. Hughes in 1947 by I.I. Rabi after a discussion with A. Einstein [Hughes, 1988].
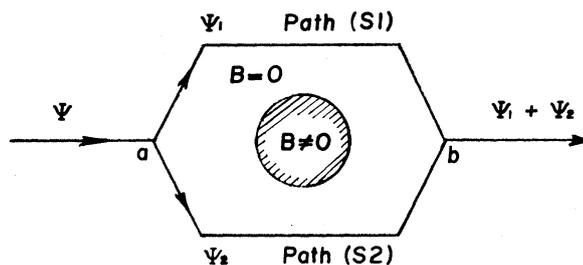
FIGURE 4.10 – Testing the Aharonov-Bohm effect with neutrons allows neutron neutrality to be tested. This experiment was performed by GREENBERGER et al. [Greenberger, 1981] by constraining the neutron charge to $10^{-12}q_e$.

in a configuration where the electromagnetic field is zero on both arms of the interferometer, thus minimizing polarizability effects. Proofs of principle for this method have been established by GREENBERGER et al. [Greenberger, 1981] with neutrons (see figure 4.10). However, due to the low flux of neutron interferometers, the measurements performed did not allow to constrain neutron neutrality with an uncertainty better than $10^{-12}q_e$. We propose to test atom neutrality using the scalar Aharonov-Bohm effect in atom interferometers.

Measurement principle. This approach was first proposed by our group [Champenois, 2001b] using a thermal atom beam. It was then adapted by M. Kasevich's group for cold atoms launched in a fountain [Arvanitaki, 2008], thus approaching the solution we wish to implement. The principle consists in applying opposite electrostatic potentials $\pm V$ to each arm of the interferometer for a time interval τ. The electrodes are not turned on until both wave packets are completely inside the electrodes. If the atom has a non-zero electric charge δq_{At}, then a phase shift proportional to δq_{At} is measured:

$$\Delta\phi = \frac{2\delta q_{At}V\tau}{\hbar} \tag{4.3}$$

From the uncertainty of this phase shift we obtain the limit on neutrality of the rubidium atom and the charge per nucleon $\delta q_{At}/A$:

$$\frac{\sigma_q}{q_e} = \sigma_\phi \frac{\hbar}{2V\tau} \frac{1}{Aq_e} \tag{4.4}$$

This measurement has important conceptual advantages. First, it is a single-particle interference effect, which eliminates the free charge bias often observed in macroscopic experiments. In addition, in the Aharonov-Bohm configuration, the atoms do not experience an electric field, reducing polarizability phenomena. Furthermore, the small number of particles involved in the measurement is compensated for by the fast oscillation with the charge of the Aharonov-Bohm phase ($\Delta\phi \propto \hbar^{-1}$).

Furthermore, measurements on the two rubidium isotopes ^{85}Rb and ^{87}Rb allow to independently constrain the neutron charge q_n and the electron-proton charge asymmetry $q_e + q_p$. The
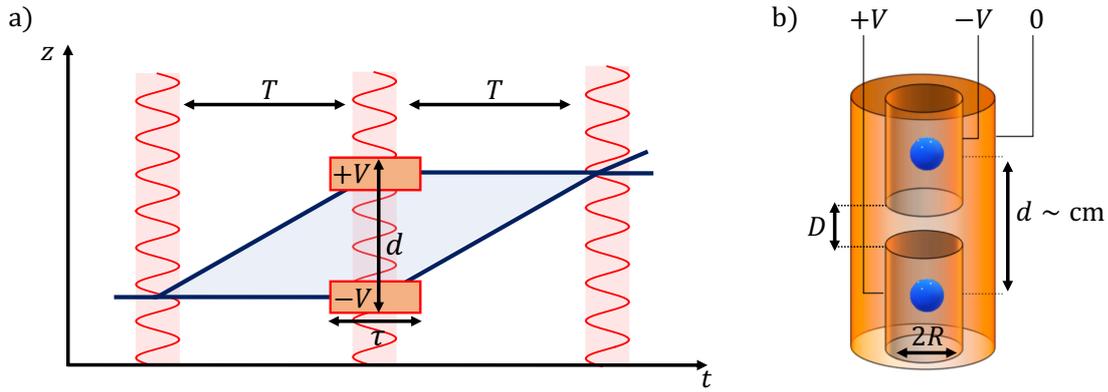
FIGURE 4.11 – (a) The arms of the interferometer are separated by a centimeter distance d to accommodate the electrodes. The electrodes are turned on for a period of time. (b) The electrodes are rotationally symmetric, of length L, radius R, and separated by a distance D.

charge conservation in β decay ($n \rightarrow p + e^- + \overline{\nu}_e$) then allows to derive a constraint on the neutrino electric charge ($\overline{\nu}_e$) with the same accuracy as on the $q_p + q_e$ and q_n charges.

The principle of the experiment is illustrated in the figure 4.11. The rubidium BEC is launched vertically and then interacts with a vertical optical lattice to create two coherent paths via LMT beam splitters. At the top of the trajectory, the distance d between the two arms is centimetric, allowing the electrodes to be placed around the arms. We consider cylindrical electrodes of length $L = 2$ cm and radius $R = 5$ mm (figure 4.11(b)) and potentials up to $V = 20$ kV.

To demonstrate the applicability of our approach, we have theoretically studied the propagation of atoms along the interferometer arms, taking into account the electrostatic potential generated by the electrodes. The analyzed interferometers have a total duration of $2T =$120 ms and are based on atomic beamsplitters transferring momentum in the range of $80\hbar k$ to $200\hbar k$, with the interaction duration within the electrodes fixed at $\tau =$20 ms. Our analysis accounts for sources of phase noise caused by laboratory vibrations, trajectory fluctuations correlated with inhomogeneities in the electrostatic potential, and quantum projection noise [Beguin, 2023].

The uncertainty in matter neutrality targeted by this device is of the order of $10^{-24}q_e$. We assume that the neutrality measurements are averaged over a period of 72 hours, which is approximately 2.5×10^4 measurements, with a phase shift measurement every 5 seconds. The main factors limiting the statistical uncertainty are summarized in the table below 4.2.

	$80\hbar k$ configuration	$164\hbar k$ configuration
Separation	2 cm	4 cm
Vibrations	2×10^{-23}	4×10^{-23}
QPN	6×10^{-24}	6×10^{-24}
$E(\delta z)$	1×10^{-23}	7×10^{-27}

TABLE 4.3 – Sensitivity on neutrality measurement for $80\hbar k$ and $164\hbar k$ configurations.

The first limitation is likely to be the phase noise induced by the vibrations of the optical lat-

tice. To quantify this phase noise, we have performed vibration measurements in our laboratory using a seismometer *Nanometrics Trillium Compact*™installed on a passive vibration isolation platform *Minus-K*™. The vibration noise is weighted by the response function of the interferometer [Décamps, 2020] and averaged over the duration of the measurement, allowing us to estimate a vibration-induced phase noise of about $\sigma_\phi \sim 1$ mrad, giving a neutrality uncertainty of about $\sigma_q \sim 2 \times 10^{-23} q_e$.

The effect of vibration noise can be significantly reduced by using two interferometers that share the same optical lattice (gradiometer), with only one of the two interferometers interacting with the electrodes. In this configuration, the measured phase can reach the quantum projection noise (QPN), $\sigma_{QPN}\phi = (V\sqrt{N_d})^{-1}$. With $N_d = 10^4$ detected atoms and a visibility of $V = 50\%$, after an integration of 2.5×10^4 measurements, the quantum projection noise limits the phase measurements to 300 μrad, corresponding to an uncertainty on neutrality of about $3 \times 10^{-24} q_e$.

The evaluation of the accuracy of a new measurement method is a complex task. However, it is worth noting that unlike inertial or h/M measurements, the scalar Aharonov-Bohm effect used for neutrality measurements depends on the voltage applied to the electrodes. Therefore, differential measurements can be made by switching voltages to distinguish the Aharanov-Bohm effect from other systematic effects typically encountered in atom interferometry. We anticipate two systematic effects that could potentially bias the measurements.

The first systematic effect arises from the residual electric field in the electrodes, which induces a Stark phase shift. This electric field is mainly due to the curvature of the electric field near the edges of the two electrodes. Using finite element simulation and preliminary electrode design, we map the electric field. From this, we calculate the Stark phase shift:

$$\Delta\Phi_E = \frac{-2\pi\epsilon_0\alpha_0}{\hbar} \in_0^\tau \left[E^2(z_B(t) - E^2(z_A(t))) \right] dt, \qquad (4.5)$$

where α_0 is the static polarizability, ϵ_0 is the vacuum permittivity, and $z_{A,B}(t)$ is the trajectory of the atoms as they propagate through the electrodes. Our estimate is that this effect could bias the measurement by as much as $10^{-27} q_e$. However, real metal conductors are not perfectly equipotential due to "patch potentials" [Camp, 1991], which may introduce an additional contribution. Nevertheless, it is important to emphasize that these polarizability effects do not have the same voltage dependence in V as the Aharonov-Bohm effect. Finally, in-situ electric field measurements using Rydberg state spectroscopy are envisioned [Osterwalder, 1999; Thiele, 2015; Mohapatra, 2008].

Another systematic effect comes from the transient current that occurs when the voltage is turned on and off. With our electrode geometry, we estimate the presence of a transient magnetic field of about 300 μG for each electrode. This magnetic field can potentially affect the measurement via the quadratic Zeeman effect, since the measurement is made on a $m_F = 0$ state[7]. In the worst case, where the fields of each electrode are uncorrelated, this phase shift remains less than $1\mu rad$ ($< 10^{-27} q_e$). In addition, it is possible to measure the magnetic field

---

7. As both stable rubidium isotopes are bosons with $|F, m_F = 0\rangle$ in the ground state, it is possible to use this strategy

using $m_F = \pm 1$ states, thus minimizing this systematic effect.

The actual design of the electrodes and high-voltage electronics is currently being studied in detail, with the goal of maximizing the applied voltage and achieving the most uniform electrostatic potential possible. Although the full design of the experiment is not yet finalized, an uncertainty of about $10^{-24} q_e$ seems to be within reach. So what can we learn from this? First, it is important to emphasize that the proposed neutrality test uses a method that is fundamentally different from previous approaches, which is essential from a metrological point of view.

In addition, improved laboratory experiments will allow comparisons with constraints obtained from astrophysical observations: [Sengupta, 1996 ; Raffelt, 1999 ; Sengupta, 2000 ; Caprini, 2005]. To my knowledge, the tightest limits have been obtained by analyzing the anisotropy of the cosmic microwave background [Caprini, 2005]. These limits vary from $q \leq 10^{-22} q_e$ to $q \leq 10^{-38} q_e$, depending on the charge distribution. It would be interesting to study the possibility of refining these models using new laboratory measurements.

The search for a deviation from the neutrality of the atom is also an important test of the Standard Model (SM), and offers the possibility of exploring theories "beyond the Standard Model". In fact, the origin of the neutrality of matter is related to electric charge quantization ("ECQ"), i.e. the fact that all electric charges appear as multiples of a fundamental charge. P.A.M. Dirac tried to solve the problem of ECQ by introducing magnetic monopoles [Dirac, 1948]. On the other hand, the Minimal Standard Model (MSM) [8] is unable to explain the quantization of electric charge [Foot, 1993 ; Foot, 1994], and the extremely precise agreement between the charges of the fundamental particles is a free parameter of the model. Consequently, a slight deviation of the electric charge of neutrons or atoms from zero is allowed in this theoretical context. In the context of extensions to the Standard Model that incorporate the non-zero mass of neutrinos, the possibility of an Electric Charge Quantization (ECQ) violation depends on whether the neutrinos are Majorana or Dirac particles. If the neutrinos are Dirac particles, this allows for the existence of an unquantized charge defined as $\delta q = \epsilon(B - L)$, where B is the baryonic number and L is the leptonic number. In other words, this suggests that neutrons and neutrinos may have a non-zero ϵ charge. In addition, tests of atomic neutrality are seen as a means of probing models of physics described as "beyond the Standard Model" [Witten, 1979 ; Foot, 1993 ; Lammerzahl, 2007 ; Arvanitaki, 2008]. Finally, atomic neutrality measurements combined with fractional charge detection experiments [Moore, 2021 ; Afek, 2021] are used to test for the existence of new charged particles envisaged in dark matter models [Jaeckel, 2010 ; Essig, 2013].

1.4 Conclusion

The new interferometer will offer the possibility of obtaining spatial separations ranging from a few centimeters to a meter, allowing the creation of controlled gravitational and electromagnetic potentials on the interferometer arms. The use of electromagnetic potentials offers the possibility of studying geometric phases, and I have presented a particular application for

---

8. In this context *minimal* means that neutrinos have zero mass.

testing atomic neutrality. Other geometric phases can be studied using artificial gauge fields [Zygelman, 2015]. In addition, cavity electrodynamics experiments have been proposed using cavities around the arms of the interferometer [Qureshi, 2023]. In addition, by positioning masses close to the interferometer arms, we could study gravitational effects [Anandan, 1995 ; Hohensee, 2012 ; Overstreet, 2022] and make measurements of the gravitational constant G [Fixler, 2007 ; Rosi, 2014]. Finally, we can imagine the use of horizontal optical lattices to create non-zero area interferometers [Gautier, 2022 ; Schubert, 2021]. The latter configuration would offer the possibility to study more precisely certain properties of geometric phases of the Aharonov-Bohm vector type (HMW, AC, etc.) [McKellar, 2014 ; Marletto, 2020], as well as generalizations of the Sagnac effect applied to the total angular momentum of the atom [Oliveira, 1962 ; Mashhoon, 1988 ; Demirel, 2015].

Due to its versatility, our device is ideally suited to implement recent advances in atom optics and their metrological evaluation. We plan to use Bloch oscillations to trap atoms in the vertical optical lattice [Ferrari, 2006 ; Kovachy, 2010 ; Charrière, 2012 ; Zhang, 2016 ; Alauze, 2018 ; Xu, 2019], which could extend the duration of the interferometer without requiring the use of large atomic fountains. In addition, the application of squeezing techniques could potentially benefit our experiment with measurements below quantum projection noise ("QPN") [Hosten, 2016 ; Salvi, 2018 ; Corgier, 2020 ; Anders, 2021 ; Greve, 2022].

2 New atom sources for interferometry

We are also interested in the development of atom inertial sensors. Our work on LMT beamsplitters and atom interferometer metrology directly contributes to the improvement of these quantum sensors. In addition, we are developing on-chip sources of ultracold atoms suitable for on-board applications. I will briefly present these activities in this section.

2.1 Context

Atom interferometry is of great interest for the development of high-precision accelerometers and gyroscopes with applications in inertial navigation and geodesy. Most of the accurate measurements made so far with atom interferometers use thermally cold atom sources, producing about 10^7 atoms cooled to a few microkelvins, at a rate of more than 1 Hz. Typical interaction times for atom interferometers are on the order of $2T \sim 100$ ms. In gravimetric and geophysical applications, atom interferometers have proven to be as good as, if not better than, state-of-the-art commercial sensors, and are increasingly being investigated for their potential use in inertial navigation.

To improve the sensitivity of inertial sensors, it may be advantageous to increase the momentum separation between the two arms of the interferometer by using LMT beamsplitters, which requires the use of ultracold atoms to maintain a good visibility. It is also possible to increase the interaction time T, with durations of several seconds being envisaged in the context of space missions. However, the thermal expansion of the atomic clouds during the time of flight in the interferometer makes it difficult to control systematic effects. For example, if we consider
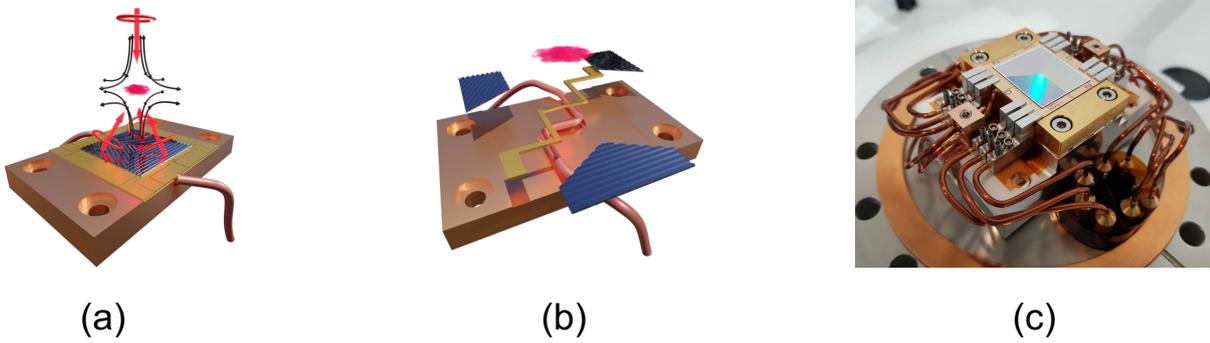
FIGURE 4.12 – (a) Magneto-optical trap created with diffraction gratings and (b) magnetic trap created with wires on the chip surface. (c) Photo of the optical and magnetic chip assembly.

rubidium atoms cooled to a few microKelvin, an interaction time of more than one second will result in an atomic cloud of a few centimeters in diameter.

To fully exploit the potential of atom interferometers under such conditions, it is essential to use cooling methods that allow to reach much lower temperatures < 100 nK, typically corresponding to Bose-Einstein condensates (BEC).

2.2 Atomic source on a chip

Bose-Einstein Condensation (BEC) sources used in the laboratory are generally limited in rate, with typical values of tens of seconds, and require high power consumption. The main goal of this study is to develop an ultracold atom source capable of producing BECs with high cycle rates, high atom flux, and low power consumption. Atom chips have the advantage of creating extremely confined atom traps, which allow for rapid production of ultracold atoms. In addition, they have already demonstrated their compatibility with on-board experiments in terms of reliability, power consumption and compactness. We have built an experimental device (see figure 4.12) that combines a magnetic chip and optical gratings to create a compact and robust device.

2.2.1 Laser cooling on a grating chip

The distribution of optical beams to the vacuum chamber is a potential source of instability for on-board cold atom sensors. To mitigate this problem, we have developed a magneto-optical trap consisting of multiple diffraction gratings arranged on a flat surface, which we refer to as an "optical chip". These gratings have been specially designed to generate all the beams required for the magneto-optical trap from a single incident laser beam, as shown in Figure 4.12. This feature greatly simplifies the optical device and increases its robustness during the laser cooling phase.

The optical chip consists of three one-dimensional (1D) diffraction gratings. The incident and diffracted beams, combined with the magnetic field generated by anti-Helmholtz coils aligned with the incident beam axis, form a magneto-optical trap in tetrahedral configuration, called

GMOT for Grating Magneto-Optical Trap [Nshii, 2013 ; McGilligan, 2015 ; McGilligan, 2017 ; Imhof, 2017]. The design of the GMOT was guided by several features, including the reduction of specular reflection (order 0), the quality of polarization of the diffracted beams, and the balance of radiation pressure forces at the atomic level.

Two-dimensional (2D) geometries are sometimes used to achieve GMOTs [McGilligan, 2015], but these require a 25 % distribution of optical power in each of the four diffracted beams to achieve a balance of radiation pressures, which corresponds to a perfect diffraction grating [9]. On the other hand, by choosing a 3x1D geometry, it is sufficient to produce 1D gratings with a diffraction efficiency of 33 % in the +1 order. This corresponds to a suboptimal diffraction grating in terms of diffraction efficiency, which makes it easier to implement experimentally.

The design of our one-dimensional gratings is based on an in-depth numerical analysis carried out by Romain Calviac with the expertise of our colleagues O. Gauthier Lafaye and A. Monmayrant at LAAS. Several grating configurations were studied with the aim of obtaining a radiation pressure balance to within 1%, a circular polarization of more than 90%, and a 0-order diffraction efficiency of less than 5%. We chose a simple Al/Si grating with a diffraction angle of 40 degrees, a robust option in terms of fabrication processes.
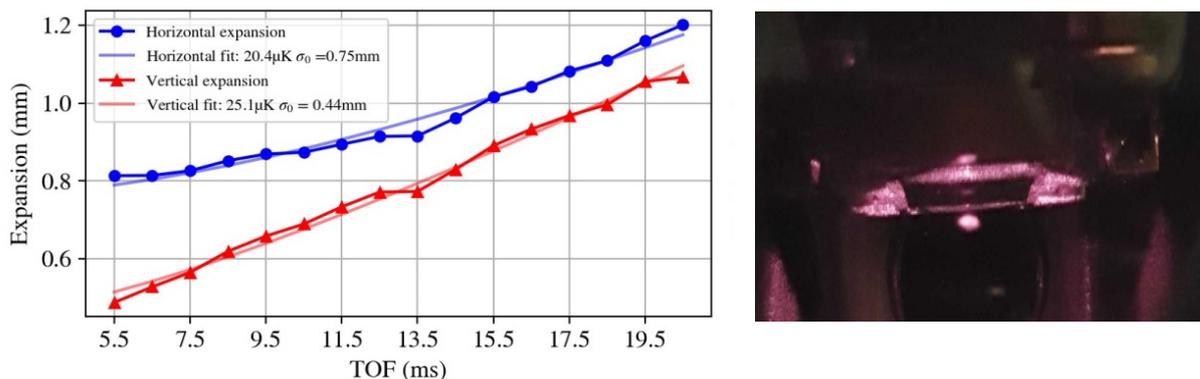
FIGURE 4.13 – (a) Image of a magneto-optical trap near the surface. (b) Temperature measurement of optical molasses.

The device is placed in a vacuum chamber where we manage to load about 7×10^7 atoms in just 1.5 seconds using 2D MOT. After a step of compressed MOT and optical molasses, the atoms are cooled down to a temperature of about 20 μK. These performances are similar to the best published results for GMOT. Table 4.4 shows the published performance of GMOT in terms of number of atoms, temperature, and phase space density (PSD). This table puts our results into perspective with the state of the art and underlines the validity of our approach.

The number of atoms is currently limited by the capture volume of the GMOT. We plan to use a flat-top incident laser beam to obtain a more uniform distribution of laser power over the atomic grating, thereby increasing the volume of the GMOT. In addition, sub-Doppler cooling

---

9. A perfect 2D square diffraction grating achieves 50 % diffraction in the +1 and -1 orders and 0 % in the other orders, in each of the grating's eigendirections. For a simple 1D grating, perfect diffraction efficiency corresponds to 50 % diffraction in the +1 order

Atom number	Temperature (μK)	PSD	Ref.
7×10^7	20	4.1×10^{-6}	LCAR
2.5×10^8	-	-	[Imhof, 2017]
3×10^6	3	-	[McGilligan, 2017]
3×10^7	46	3.7×10^{-6}	[McGilligan, 2015]

TABLE 4.4 – Performance oof ur GMOT and recently published.

in molasses is likely to be limited by the presence of stray magnetic fields near the chip resulting from eddy currents flowing in the copper baseplate. However, a temperature of a few tens of microkelvin is perfectly suited for efficient loading of the atomic assembly into the magnetic potentials of the atom chip.

2.2.2 Magnetic trapping on a chip

Atom chips allow atoms to be trapped and manipulated using magnetic potentials created by microfabricated conductive wires. This approach creates high-confinement traps that support efficient evaporative cooling. It also results in compact, robust, and energy-efficient devices. Our atomic chip design allows us to generate magnetic potentials similar to those used in the QUANTUS experiment, which succeeded in creating a Bose-Einstein condensate (BEC) of about 10^5 atoms in 1 second [Rudolph, 2015]. A peculiarity of our configuration is that the magnetic trap must be positioned at a sufficient distance from the wires to allow insertion of the optical chip, whose substrate is about 200 μm thick. This requires the use of currents on the order of 10 A, which is also higher than what is typically used on atom chips. Consequently, this implies the use of relatively large wires, measuring $50 \times 300 \mu m^2$.

The schematic of the magnetic chip we built is shown in figure 4.14. The chip is manufactured at the LAAS laboratory in Toulouse. The copper wires and the gold passivation layer are electroplated on an AlN substrate. The chip consists of three Z-shaped wires, 10 mm, 6 mm and 2 mm long, with a central cross section of $50 \times 300 \mu m^2$. The 6 mm and 2 mm Z wires are connected on both sides of the chip, which also allows the creation of H-shaped geometries. A central wire with a cross section of $100 \times 50 \mu m^2$ is used to create a dimple trap.

Details of the fabrication of the optical and magnetic chips, their hybridization, and the optical and thermal performance tests will be presented in Romain Calviac's thesis. The device we built allowed us to successfully demonstrate the first loading of an atom chip from a GMOT fused to the same chip (see figure 4.14). We were able to trap about 5×10^6 atoms in this trap, with a trap lifetime of 3 seconds.

These are the very first results and I think there is still a lot of room for improvement. For example, a better adaptation of the magnetic trap and the GMOT, the introduction of an optical pumping stage, or the use of a beam with a flat top profile are being considered. These results are promising and pave the way for the creation of robust ultracold atom sources suitable for on-board applications. Beyond atom source applications, Raman diffraction using the optical chip would allow acceleration measurements in all three spatial directions, exploiting different combinations of diffracted wave vectors. In collaboration with LP2N and the company
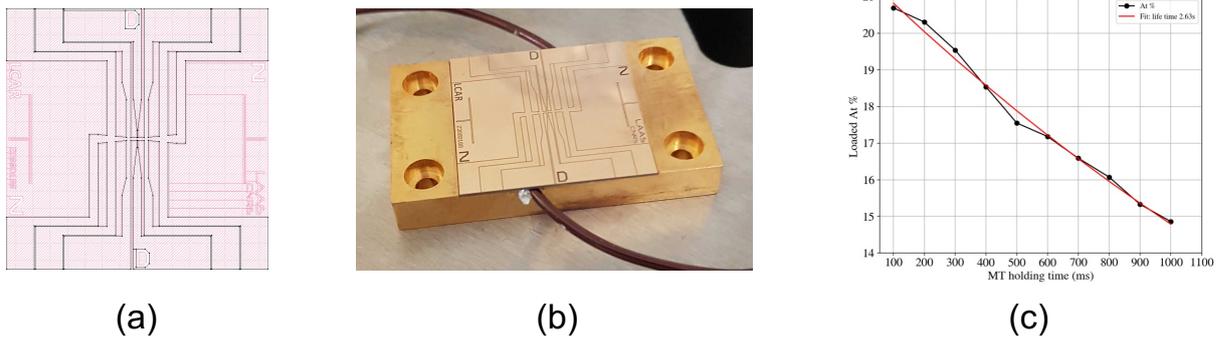
FIGURE 4.14 – (a) Mask of the magnetic chip wires. (b) Photo of the magnetic chip fabricated in the LAAS clean rooms. (c) Number of atoms in the trap as a function of time in the magnetic trap.

Exail, we are investigating the possibility of integrating this technique to create 3D inertial sensors with our system. More generally, this technology opens new perspectives in optical architecture for quantum technologies, whether for terrestrial or space applications. It allows the creation of optical gratings with a single beam, opening the way to explore different geometries and dimensions of optical gratings. This advance could contribute to the development of high-precision clocks, new inertial sensors, and quantum simulations.

3   Conclusion

The research project I have presented is a continuation of the separated-arm atom interferometry experiments initiated by Jacques Vigué. However, the apparatus we are implementing differs significantly from the interferometer originally used in Toulouse. We are developing new instruments based on the use of ultracold atoms, with applications in both fundamental physics and quantum technologies. These atom interferometers with separated arms will enable new tests in fundamental physics, such as tests of atom neutrality. Our developments in atom optics, such as the creation of high-rate Bose-Einstein condensate sources and the manipulation of ultracold sources using optical lattices, are in line with the development of inertial sensors and the large-scale instruments proposed for gravitational wave detectors and the exploration of physics beyond the Standard Model on Earth or in space.

Bibliographie

[Abe, 2021]   Mahiro Abe, Philip Adamson, Marcel Borcean, Daniela Bortoletto, Kieran Bridges, Samuel P Carman et al. « Matter-wave Atomic Gradiometer Interferometric Sensor (MAGIS-100) ». *Quantum Science and Technology* 6.4 (2021), p. 044003 (cf. p. 8, 14, 16).

[Afek, 2021]   Gadi Afek, Fernando Monteiro, Jiaxiang Wang, Benjamin Siegel, Sumita Ghosh et David C. Moore. « Limits on the abundance of millicharged particles bound to matter ». *Phys. Rev. D* 104 (2021), p. 012004 (cf. p. 62).

[Aguilera, 2014]   D N Aguilera, H Ahlers, B Battelier, A Bawamia, A Bertoldi, R Bondarescu et al. « STE-QUEST—test of the universality of free fall using cold atom interferometry ». *Classical and Quantum Gravity* 31.11 (2014), p. 115010 (cf. p. 14).

[Aharonov, 1959]   Y. Aharonov et D. Bohm. « Significance of Electromagnetic Potentials in the Quantum Theory ». *Phys. Rev.* 115 (1959), p. 485-491 (cf. p. 23).

[Aharonov, 1961]   Y. Aharonov et D. Bohm. « Further Considerations on Electromagnetic Potentials in the Quantum Theory ». *Phys. Rev.* 123 (1961), p. 1511-1524 (cf. p. 23).

[Aharonov, 1984]   Y. Aharonov et A. Casher. « Topological Quantum Effects for Neutral Particles ». *Phys. Rev. Lett.* 53 (1984), p. 319-321 (cf. p. 24).

[Aharonov, 2015]   Yakir Aharonov, Eliahu Cohen et Daniel Rohrlich. « Comment on "Role of potentials in the Aharonov-Bohm effect" ». *Phys. Rev. A* 92 (2015), p. 026101 (cf. p. 24).

[Aharonov, 2016]   Yakir Aharonov, Eliahu Cohen et Daniel Rohrlich. « Nonlocality of the Aharonov-Bohm effect ». *Phys. Rev. A* 93 (2016), p. 042110 (cf. p. 23, 24).

[Alauze, 2018]   X Alauze, A Bonnin, C Solaro et F Pereira Dos Santos. « A trapped ultracold atom force sensor with a μm-scale spatial resolution ». *New Journal of Physics* 20.8 (2018), p. 083014 (cf. p. 63).

[Albers, 2022]   Henning Albers, Robin Corgier, Alexander Herbst, Ashwin Rajagopalan, Christian Schubert, Christian Vogt et al. « All-optical matter-wave lens using time-averaged potentials ». *Communications Physics* 5.1 (2022), p. 60 (cf. p. 55).

[Alibert, 2017]   Julien Alibert. « Une nouvelle source pour l'interférométrie atomique avec un condensat de Bose-Einstein double espèce ». Theses. Université Paul Sabatier - Toulouse III, 2017 (cf. p. 44, 54).

[Altin, 2013]   P A Altin, M T Johnsson, V Negnevitsky, G R Dennis, R P Anderson, J E Debs et al. « Precision atomic gravimeter based on Bragg diffraction ». *New Journal of Physics* 15.2 (2013), p. 023009 (cf. p. 49).

[Altschul, 2015]   Brett Altschul, Quentin G. Bailey, Luc Blanchet, Kai Bongs, Philippe Bouyer, Luigi Cacciapuoti et al. « Quantum tests of the Einstein Equivalence Principle with the STE–QUEST space mission ». *Advances in Space Research* 55.1 (2015), p. 501-524 (cf. p. 15).

[Ammann, 1997]   Hubert Ammann et Nelson Christensen. « Delta Kick Cooling: A New Method for Cooling Atoms ». *Phys. Rev. Lett.* 78 (1997), p. 2088-2091 (cf. p. 45).

[Anandan, 1981]   J. Anandan. « Sagnac effect in relativistic and nonrelativistic physics ». *Phys. Rev. D* 24 (1981), p. 338-346 (cf. p. 14).

[Anandan, 1995]   Jeeva Anandan. *TOPOLOGICAL PHASES AND THEIR DUALITY IN ELECTROMAGNETIC AND GRAVITATIONAL FIELDS*. 1995. arXiv : `gr-qc/9504002 [gr-qc]` (cf. p. 57, 63).

[Anders, 2021]   F. Anders, A. Idel, P. Feldmann, D. Bondarenko, S. Loriani, K. Lange et al. « Momentum Entanglement for Atom Interferometry ». *Phys. Rev. Lett.* 127 (2021), p. 140402 (cf. p. 63).

[Antoine, 2006]   C. Antoine. « Matter wave beam splitters in gravito-inertial and trapping potentials: generalized ttt scheme for atom interferometry ». *Applied Physics B* 84.4 (2006), p. 585-597 (cf. p. 6).

[Antoine, 2003]   Ch. Antoine et Ch.J. Bordé. « Exact phase shifts for atom interferometry ». *Physics Letters A* 306.5 (2003), p. 277-284 (cf. p. 6).

[Aoyama, 2012]   Tatsumi Aoyama, Masashi Hayakawa, Toichiro Kinoshita et Makiko Nio. « Tenth-order QED contribution to the electron g- 2 and an improved value of the fine structure constant ». *Physical Review Letters* 109.11 (2012), p. 111807 (cf. p. 15).

[Arndt, 2014]   Markus Arndt et Klaus Hornberger. « Testing the limits of quantum mechanical superpositions ». *Nature Physics* 10.4 (2014), p. 271-277 (cf. p. 5).

[Arora, 2011]   Bindiya Arora, M. S. Safronova et Charles W. Clark. « Tune-out wavelengths of alkali-metal atoms and their applications ». *Phys. Rev. A* 84 (2011), p. 043401 (cf. p. 35).

[Arvanitaki, 2008]   Asimina Arvanitaki, Savas Dimopoulos, Andrew A. Geraci, Jason Hogan et Mark Kasevich. « How to Test Atom and Neutron Neutrality with Atom Interferometry ». *Phys. Rev. Lett.* 100 (2008), p. 120407 (cf. p. 32, 57, 59, 62).

[Arvanitaki, 2018]   Asimina Arvanitaki, Peter W. Graham, Jason M. Hogan, Surjeet Rajendran et Ken Van Tilburg. « Search for light scalar dark matter with atomic gravitational wave detectors ». *Phys. Rev. D* 97 (2018), p. 075020 (cf. p. 16).

[Asenbaum, 2020]   Peter Asenbaum, Chris Overstreet, Minjeong Kim, Joseph Curti et Mark A. Kasevich. « Atom-Interferometric Test of the Equivalence Principle at the 10^{-12} Level ». *Phys. Rev. Lett.* 125 (2020), p. 191101 (cf. p. 15).

[Audretsch, 1983]   J Audretsch et C Lammerzahl. « Neutron interference: general theory of the influence of gravity, inertia and space-time torsion ». *Journal of Physics A: Mathematical and General* 16.11 (1983), p. 2457 (cf. p. 31).

[B Ho, 1994]   Vu B Ho et Michael J Morgan. « An Experiment to Test the Gravitational Aharonov-Bohm Effect ». *Australian Journal of Physics* 47.3 (1994), p. 245-252 (cf. p. 32).

[Badurina, 2020]   L. Badurina, E. Bentine, D. Blas, K. Bongs, D. Bortoletto, T. Bowcock et al. « AION: an atom interferometer observatory and network ». *Journal of Cosmology and Astroparticle Physics* 2020.05 (2020), p. 011 (cf. p. 8, 14, 16).

[Barrett, 2022]   B. Barrett, G. Condon, L. Chichet, L. Antoni-Micollier, R. Arguel, M. Rabault et al. « Testing the universality of free fall using correlated 39K–87Rb atom interferometers ». *AVS Quantum Science* 4.1 (2022), p. 014401 (cf. p. 15).

[Batelaan, 2015]   H. Batelaan et M. Becker. « Dispersionless forces and the Aharonov-Bohm effect ». *Europhysics Letters* 112.4 (2015), p. 40006 (cf. p. 24).

[Battelier, 2021]   Baptiste Battelier, Joël Bergé, Andrea Bertoldi, Luc Blanchet, Kai Bongs, Philippe Bouyer et al. « Exploring the foundations of the physical universe with space tests of the equivalence principle ». *Experimental Astronomy* 51.3 (2021), p. 1695-1736 (cf. p. 15).

[Baumann, 1988]   J. Baumann, R. Gähler, J. Kalus et W. Mampe. « Experimental limit for the charge of the free neutron ». *Phys. Rev. D* 37 (1988), p. 3107-3112 (cf. p. 58).

[Bause, 2020]   R. Bause, M. Li, A. Schindewolf, X.-Y. Chen, M. Duda, S. Kotochigova et al. « Tune-Out and Magic Wavelengths for Ground-State ^{23}Na^{40}K Molecules ». *Phys. Rev. Lett.* 125 (2020), p. 023201 (cf. p. 35).

[Becker, 2019]   Maria Becker, Giulio Guzzinati, Armand Béché, Johan Verbeeck et Herman Batelaan. « Asymmetry and non-dispersivity in the Aharonov-Bohm effect ». *Nature Communications* 10.1 (2019), p. 1700 (cf. p. 24, 31).

[Beguin, 2023]   Ashley Beguin. « Interférométrie atomique à grands transferts d'impulsion dans le régime de quasi-Bragg. » Theses. Université Toulouse 3 Paul Sabatier, 2023 (cf. p. 9, 45, 46, 53, 60).

[Béguin, 2023]   A. Béguin, T. Rodzinka, L. Calmels, B. Allard et A. Gauguet. « Atom Interferometry with Coherent Enhancement of Bragg Pulse Sequences ». *Phys. Rev. Lett.* 131 (2023), p. 143401 (cf. p. 50, 51).

[Béguin, 2022]   A. Béguin, T. Rodzinka, J. Vigué, B. Allard et A. Gauguet. « Characterization of an atom interferometer in the quasi-Bragg regime ». *Phys. Rev. A* 105 (2022), p. 033302 (cf. p. 46).

[Berman, 1997]   P.R. Berman. *Atom Interferometry*. Elsevier Science, 1997 (cf. p. 5, 7).

[Berry, 1999]   M V Berry. « Aharonov-Bohm beam deflection: Shelankov's formula, exact solution, asymptotics and an optical analogue ». *Journal of Physics A: Mathematical and General* 32.30 (1999), p. 5627 (cf. p. 31).

Bibliographie

[Berry, 1987]   M.V. BERRY. « The Adiabatic Phase and Pancharatnam's Phase for Polarized Light ». *Journal of Modern Optics* 34.11 (1987), p. 1401-1407 (cf. p. 39).

[Berry, 1984]   Michael Victor BERRY. « Quantal phase factors accompanying adiabatic changes ». *Proceedings of the Royal Society of London. A. Mathematical and Physical Sciences* 392.1802 (1984), p. 45-57 (cf. p. 24, 39).

[Bertoldi, 2019]   A. BERTOLDI, F. MINARDI et M. PREVEDELLI. « Phase shift in atom interferometers: Corrections for nonquadratic potentials and finite-duration laser pulses ». *Phys. Rev. A* 99 (2019), p. 033619 (cf. p. 6).

[Bezerra, 1991]   V B BEZERRA. « Gravitational Aharonov-Bohm effect in a locally flat spacetime ». *Classical and Quantum Gravity* 8.10 (1991), p. 1939 (cf. p. 31).

[Biedermann, 2015]   G. W. BIEDERMANN, X. WU, L. DESLAURIERS, S. ROY, C. MAHADESWARASWAMY et M. A. KASEVICH. « Testing gravity with cold-atom interferometers ». *Phys. Rev. A* 91 (2015), p. 033629 (cf. p. 14).

[Bongs, 2006]   K. BONGS, R. LAUNAY et M. A. KASEVICH. « High-order inertial phase shifts for time-domain atom interferometers ». *Applied Physics B* 84.4 (2006), p. 599-602 (cf. p. 6).

[Bonnin, 2013]   A. BONNIN, N. ZAHZAM, Y. BIDEL et A. BRESSON. « Simultaneous dual-species matter-wave accelerometer ». *Phys. Rev. A* 88 (2013), p. 043615 (cf. p. 15).

[Bordé, 1990]   Ch J BORDÉ. « Propagation of laser beams and of atomic systems ». *Les Houches Lectures, Session LIII* (1990), p. 287-380 (cf. p. 6).

[Bordé, 2002]   Ch J BORDÉ. « Atomic clocks and inertial sensors ». *Metrologia* 39.5 (2002), p. 435 (cf. p. 14).

[Bordé, 2008]   Ch. J. BORDÉ. « 5D optics for atomic clocks and gravito-inertial sensors ». *The European Physical Journal Special Topics* 163.1 (2008), p. 315-332 (cf. p. 6).

[Bordé, 1984]   Ch. J. BORDÉ, Ch. SALOMON, S. AVRILLIER, A. van LERBERGHE, Ch. BRÉANT, D. BASSI et al. « Optical Ramsey fringes with traveling waves ». *Phys. Rev. A* 30 (1984), p. 1836-1848 (cf. p. 5-7).

[Bordoux, 2019]   Maxime BORDOUX. « Développement d'une source de condensats de Bose-Einstein pour l'interférométrie atomique ». Theses. Université Toulouse III - Paul Sabatier, 2019 (cf. p. 9, 44).

[Bouchiat, 2011]   Marie-Anne BOUCHIAT et Claude BOUCHIAT. « Atomic interferometer measurements of Berry and Aharonov-Anandan phases for isolated spins $S > \frac{1}{2}$ nonlinearly coupled to external fields ». *Phys. Rev. A* 83 (2011), p. 052126 (cf. p. 57).

[Boulware, 1989]   David G. BOULWARE et S. DESER. « Aharonov-Bohm effect and the mass of the photon ». *Phys. Rev. Lett.* 63 (1989), p. 2319-2321 (cf. p. 31).

[Boyer, 2002]   Timothy H. BOYER. « Semiclassical Explanation of the Matteucci–Pozzi and Aharonov–Bohm Phase Shifts ». *Foundations of Physics* 32.1 (2002), p. 41-49 (cf. p. 24).

[Brand, 2020]   Christian BRAND, Filip KIAŁKA, Stephan TROYER, Christian KNOBLOCH, Ksenija SIMONOVI Ć, Benjamin A. STICKLER et al. « Bragg Diffraction of Large Organic Molecules ». *Phys. Rev. Lett.* 125 (2020), p. 033604 (cf. p. 5).

[Bressi, 2011]   G. BRESSI, G. CARUGNO, F. DELLA VALLE, G. GALEAZZI, G. RUOSO et G. SARTORI. « Testing the neutrality of matter by acoustic means in a spherical resonator ». *Phys. Rev. A* 83 (2011), p. 052101 (cf. p. 57, 58).

[Burke, 2008]   J. H. T. BURKE, B. DEISSLER, K. J. HUGHES et C. A. SACKETT. « Confinement effects in a guided-wave atom interferometer with millimeter-scale arm separation ». *Phys. Rev. A* 78 (2008), p. 023619 (cf. p. 17).

[Camp, 1991]   J. B. CAMP, T. W. DARLING et Ronald E. BROWN. « Macroscopic variations of surface potentials of conductors ». *Journal of Applied Physics* 69.10 (1991), p. 7126-7129 (cf. p. 61).

[Canuel, 2018]   B. CANUEL, A. BERTOLDI, L. AMAND, E. POZZO DI BORGO, T. CHANTRAIT, C. DANQUIGNY et al. « Exploring gravity with the MIGA large scale atom interferometer ». *Scientific Reports* 8.1 (2018), p. 14064 (cf. p. 14, 16).

[Caprez, 2007]   Adam CAPREZ, Brett BARWICK et Herman BATELAAN. « Macroscopic Test of the Aharonov-Bohm Effect ». *Phys. Rev. Lett.* 99 (2007), p. 210401 (cf. p. 24).

[Caprini, 2005]   C CAPRINI et P G FERREIRA. « Constraints on the electrical charge asymmetry of the universe ». *Journal of Cosmology and Astroparticle Physics* 2005.02 (2005), p. 006 (cf. p. 57, 62).

[Carnal, 1991]   O. CARNAL et J. MLYNEK. « Young's double-slit experiment with atoms: A simple atom interferometer ». *Phys. Rev. Lett.* 66 (1991), p. 2689-2692 (cf. p. 5).

[Cennini, 2003]   Giovanni CENNINI, Gunnar RITT, Carsten GECKELER et Martin WEITZ. « All-Optical Realization of an Atom Laser ». *Phys. Rev. Lett.* 91 (2003), p. 240408 (cf. p. 44).

[Champenois, 2001a]   C. Champenois, M. Büchner, R. Delhuille, R. Mathevet, C. Robilliard, C. Rizzo et al. « Atomic diffraction by a laser standing wave: Analysis using Bloch states ». *The European Physical Journal D - Atomic, Molecular, Optical and Plasma Physics* 13.2 (2001), p. 271-278 (cf. p. 11).

[Champenois, 1999]   Caroline Champenois. « Interférométrie atomique avec l'atome de lithium : analyse théorique et construction d'un interféromètre, applications. » Theses. Université Paul Sabatier - Toulouse III, 1999 (cf. p. 19).

[Champenois, 2001b]   Caroline Champenois, Matthias Büchner, Rémi Delhuille, Renaud Mathevet, Cécile Robilliard, Carlo Rizzo et al. « Matter Neutrality Test Using a Mach-Zehnder Interferometer ». Sous la dir. de Savely G. Karshenboim, F. Bassani, F.S. Pavone, M. Inguscio et T.W. Hänsch. Berlin, Heidelberg : Springer Berlin Heidelberg, 2001, p. 554-563 (cf. p. 32, 57-59).

[Chapman, 1995]   Michael S. Chapman, Troy D. Hammond, Alan Lenef, Jörg Schmiedmayer, Richard A. Rubenstein, Edward Smith et al. « Photon Scattering from Atoms in an Atom Interferometer: Coherence Lost and Regained ». *Phys. Rev. Lett.* 75 (1995), p. 3783-3787 (cf. p. 16).

[Charrière, 2012]   Renée Charrière, Malo Cadoret, Nassim Zahzam, Yannick Bidel et Alexandre Bresson. « Local gravity measurement with the combination of atom interferometry and Bloch oscillations ». *Phys. Rev. A* 85 (2012), p. 013639 (cf. p. 63).

[Chiarotti, 2022]   Mauro Chiarotti, Jonathan N. Tinsley, Satvika Bandarupally, Shamaila Manzoor, Michele Sacco, Leonardo Salvi et al. « Practical Limits for Large-Momentum-Transfer Clock Atom Interferometers ». *PRX Quantum* 3 (2022), p. 030348 (cf. p. 7).

[Chiow, 2011]   Sheng-wey Chiow, Tim Kovachy, Hui-Chun Chien et Mark A. Kasevich. « 102ℏk Large Area Atom Interferometers ». *Phys. Rev. Lett.* 107 (2011), p. 130403 (cf. p. 50, 51).

[Chiow, 2015]   Sheng-wey Chiow, Jason Williams et Nan Yu. « Laser-ranging long-baseline differential atom interferometers for space ». *Phys. Rev. A* 92 (2015), p. 063613 (cf. p. 14).

[Chu, 1986]   S. Chu, J. E. Bjorkholm, A. Ashkin, J. P. Gordon et L. W. Hollberg. « Proposal for optically cooling atoms to temperatures of the order of 10-6 K ». *Opt. Lett.* 11.2 (1986), p. 73-75 (cf. p. 45).

[Cimmino, 1989]   A. Cimmino, G. I. Opat, A. G. Klein, H. Kaiser, S. A. Werner, M. Arif et al. « Observation of the topological Aharonov-Casher phase shift by neutron interferometry ». *Phys. Rev. Lett.* 63 (1989), p. 380-383 (cf. p. 25, 30).

[Cladé, 2009]   P. Cladé, S. Guellati-Khélifa, F. Nez et F. Biraben. « Large Momentum Beam Splitter Using Bloch Oscillations ». *Phys. Rev. Lett.* 102 (2009), p. 240402 (cf. p. 50).

[Clauser, 1988]   John F. Clauser. « Ultra-high sensitivity accelerometers and gyroscopes using neutral atom matter-wave interferometry ». *Physica B+C* 151.1 (1988), p. 262-272 (cf. p. 13).

[Clément, 2009]   J.-F. Clément, J.-P. Brantut, M. Robert-de-Saint-Vincent, R. A. Nyman, A. Aspect, T. Bourdel et al. « All-optical runaway evaporation to Bose-Einstein condensation ». *Phys. Rev. A* 79 (2009), p. 061406 (cf. p. 43).

[Comparat, 2006]   D. Comparat, A. Fioretti, G. Stern, E. Dimova, B. Laburthe Tolra et P. Pillet. « Optimized production of large Bose-Einstein condensates ». *Phys. Rev. A* 73 (2006), p. 043410 (cf. p. 55).

[Condon, 2019]   G. Condon, M. Rabault, B. Barrett, L. Chichet, R. Arguel, H. Eneriz-Imaz et al. « All-Optical Bose-Einstein Condensates in Microgravity ». *Phys. Rev. Lett.* 123 (2019), p. 240402 (cf. p. 55).

[Copenhaver, 2019]   Eric Copenhaver, Kayleigh Cassella, Robert Berghaus et Holger Müller. « Measurement of a ^{7}Li tune-out wavelength by phase-patterned atom interferometry ». *Phys. Rev. A* 100 (2019), p. 063603 (cf. p. 35, 38).

[Corgier, 2020]   Robin Corgier, Sina Loriani, Holger Ahlers, Katerine Posso-Trujillo, Christian Schubert, Ernst M Rasel et al. « Interacting quantum mixtures for precision atom interferometry ». *New Journal of Physics* 22.12 (2020), p. 123008 (cf. p. 45, 63).

[Cronin, 2009]   Alexander D. Cronin, Jörg Schmiedmayer et David E. Pritchard. « Optics and interferometry with atoms and molecules ». *Rev. Mod. Phys.* 81 (2009), p. 1051-1129 (cf. p. 5).

[Damour, 2012]   Thibault Damour. « Theoretical aspects of the equivalence principle ». *Classical and Quantum Gravity* 29.18 (2012), p. 184001 (cf. p. 15).

[Danner, 2023]   Armin Danner, Hartmut Lemmel, Richard Wagner, Stephan Sponar et Yuji Hasegawa. « Neutron Interferometer Experiments Studying Fundamental Features of Quantum Mechanics ». *Atoms* 11.6 (2023) (cf. p. 16).

[Daszuta, 2012]   Boris DASZUTA et Mikkel F. ANDERSEN. « Atom interferometry using δ-kicked and finite-duration pulse sequences ». *Phys. Rev. A* 86 (2012), p. 043604 (cf. p. 54).

[Davisson, 1927]   C. DAVISSON et L. H. GERMER. « Diffraction of Electrons by a Crystal of Nickel ». *Phys. Rev.* 30 (1927), p. 705-740 (cf. p. 5).

[De Broglie, 1924]   Louis DE BROGLIE. « Recherches sur la théorie des quanta ». Thèse de doct. Migration-université en cours d'affectation, 1924 (cf. p. 5).

[Decamps, 2016]   Boris DECAMPS. « Atom interferometry : experiments with electromagnetic interactions and design of a Bose Einstein condensate setup ». Theses. Université Paul Sabatier - Toulouse III, 2016 (cf. p. 19, 43).

[Décamps, 2019]   B DÉCAMPS, M BORDOUX, J ALIBERT, B ALLARD et A GAUGUET. « Phase response of atom interferometers based on sequential Bragg diffractions ». *Journal of Physics B: Atomic, Molecular and Optical Physics* 52.1 (2019), p. 015003 (cf. p. 54).

[Décamps, 2016]   B. DÉCAMPS, J. GILLOT, J. VIGUÉ, A. GAUGUET et M. BÜCHNER. « Observation of Atom-Wave Beats Using a Kerr Modulator for Atom Waves ». *Phys. Rev. Lett.* 116 (2016), p. 053004 (cf. p. 32).

[Décamps, 2020]   B. DÉCAMPS, J. VIGUÉ, A. GAUGUET et M. BÜCHNER. « Measurement of the 671-nm tune-out wavelength of ^{7}Li by atom interferometry ». *Phys. Rev. A* 101 (2020), p. 033614 (cf. p. 9, 22, 35, 36, 61).

[Décamps, 2017]   Boris DÉCAMPS, Jonathan GILLOT, Alexandre GAUGUET, Jacques VIGUÉ et Matthias BÜCHNER. « Phase modulation of atom waves: theory and experiment using the atom optics analogue of the Kerr effect ». *The European Physical Journal D* 71.12 (2017), p. 334 (cf. p. 32, 34).

[Deissler, 2008]   B. DEISSLER, K. J. HUGHES, J. H. T. BURKE et C. A. SACKETT. « Measurement of the ac Stark shift with a guided matter-wave interferometer ». *Phys. Rev. A* 77 (2008), p. 031604 (cf. p. 17).

[Delhuille, 2002]   Rémi DELHUILLE. « Interférométrie atomique avec l'atome de lithium : Réalisation d'un interféromètre présentant un contraste et un flux élevés en vue de mesures de précision ». Theses. Université Paul Sabatier - Toulouse III, 2002 (cf. p. 19).

[Demirel, 2015]   Bülent DEMIREL, Stephan SPONAR et Yuji HASEGAWA. « Measurement of the spin–rotation coupling in neutron polarimetry ». *New Journal of Physics* 17.2 (2015), p. 023065 (cf. p. 63).

[Deng, 1999]   L. DENG, E. W. HAGLEY, J. DENSCHLAG, J. E. SIMSARIAN, Mark EDWARDS, Charles W. CLARK et al. « Temporal, Matter-Wave-Dispersion Talbot Effect ». *Phys. Rev. Lett.* 83 (1999), p. 5407-5411 (cf. p. 54).

[Deppner, 2021]   Christian DEPPNER, Waldemar HERR, Merle CORNELIUS, Peter STROMBERGER, Tammo STERNKE, Christoph GRZESCHIK et al. « Collective-Mode Enhanced Matter-Wave Optics ». *Phys. Rev. Lett.* 127 (2021), p. 100401 (cf. p. 45).

[Dimopoulos, 2007]   Savas DIMOPOULOS, Peter W. GRAHAM, Jason M. HOGAN et Mark A. KASEVICH. « Testing General Relativity with Atom Interferometry ». *Phys. Rev. Lett.* 98 (2007), p. 111102 (cf. p. 6, 16).

[Dimopoulos, 2008]   Savas DIMOPOULOS, Peter W. GRAHAM, Jason M. HOGAN et Mark A. KASEVICH. « General relativistic effects in atom interferometry ». *Phys. Rev. D* 78 (2008), p. 042003 (cf. p. 16).

[Dirac, 1948]   P. A. M. DIRAC. « The Theory of Magnetic Poles ». *Phys. Rev.* 74 (1948), p. 817-830 (cf. p. 62).

[Dowker, 1967]   J. S. DOWKER. « A gravitational Aharonov-Bohm effect ». *Il Nuovo Cimento B (1965-1970)* 52.1 (1967), p. 129-135 (cf. p. 31).

[Dowling, 1999]   Jonathan P. DOWLING, Colin P. WILLIAMS et J. D. FRANSON. « Maxwell Duality, Lorentz Invariance, and Topological Phase ». *Phys. Rev. Lett.* 83 (1999), p. 2486-2489 (cf. p. 26).

[Du, 2022]   Yufeng DU, Clara MURGUI, Kris PARDO, Yikun WANG et Kathryn M. ZUREK. « Atom interferometer tests of dark matter ». *Phys. Rev. D* 106 (2022), p. 095041 (cf. p. 16).

[Duan, 2014]   Xiao-Chun DUAN, Min-Kang ZHOU, De-Kai MAO, Hui-Bing YAO, Xiao-Bing DENG, Jun LUO et al. « Operating an atom-interferometry-based gravity gradiometer by the dual-fringe-locking method ». *Phys. Rev. A* 90 (2014), p. 023617 (cf. p. 14).

[Durfee, 2006]   D. S. DURFEE, Y. K. SHAHAM et M. A. KASEVICH. « Long-Term Stability of an Area-Reversible Atom-Interferometer Sagnac Gyroscope ». *Phys. Rev. Lett.* 97 (2006), p. 240801 (cf. p. 41).

[Durstberger-Rennhofer, 2011]   Katharina DURSTBERGER-RENNHOFER, Tobias JENKE et Hartmut ABELE. « Probing the neutron's electric neutrality with Ramsey spectroscopy of gravitational quantum states of ultracold neutrons ». *Phys. Rev. D* 84 (2011), p. 036004 (cf. p. 58).

[Dzuba, 2012]   V. A. DZUBA et V. V. FLAMBAUM. « Parity violation and electric dipole moments in atoms and molecules ». *International Journal of Modern Physics E* 21.11 (2012), p. 1230010 (cf. p. 35).

[Dzuba, 2006]   V. A. Dzuba, V. V. Flambaum et M. S. Safronova. « Breit interaction and parity nonconservation in many-electron atoms ». *Phys. Rev. A* 73 (2006), p. 022112 (cf. p. 34).

[Earman, 2019]   John Earman. « The role of idealizations in the Aharonov–Bohm effect ». *Synthese* 196.5 (2019), p. 1991-2019 (cf. p. 24).

[Ehrenberg, 1949]   W Ehrenberg et R E Siday. « The Refractive Index in Electron Optics and the Principles of Dynamics ». *Proceedings of the Physical Society. Section B* 62.1 (1949), p. 8 (cf. p. 23).

[Einstein, 1924]   Albert Einstein. « Concerning the aether ». *Verhandlungen der Schweizerischen Naturforschenden Gesellschaft* 105.2 (1924), p. 85-93 (cf. p. 57).

[Ekstrom, 1995]   Christopher R. Ekstrom, Jörg Schmiedmayer, Michael S. Chapman, Troy D. Hammond et David E. Pritchard. « Measurement of the electric polarizability of sodium with an atom interferometer ». *Phys. Rev. A* 51 (1995), p. 3883-3888 (cf. p. 16).

[Essig, 2013]   R. Essig, J. A. Jaros, W. Wester, P. Hansson Adrian, S. Andreas, T. Averett et al. *Dark Sectors and New, Light, Weakly-Coupled Particles.* 2013. arXiv : `1311.0029 [hep-ph]` (cf. p. 62).

[Estermann, 1930]   I. Estermann et O. Stern. « Beugung von Molekularstrahlen ». *Zeitschrift für Physik* 61.1 (1930), p. 95-125 (cf. p. 5).

[Fan, 2023]   X. Fan, T. G. Myers, B. A. D. Sukra et G. Gabrielse. « Measurement of the Electron Magnetic Moment ». *Phys. Rev. Lett.* 130 (2023), p. 071801 (cf. p. 15).

[Fang, 2016]   B Fang, I Dutta, P Gillot, D Savoie, J Lautier, B Cheng et al. « Metrology with Atom Interferometry: Inertial Sensors from Laboratory to Field Applications ». *Journal of Physics: Conference Series* 723.1 (2016), p. 012049 (cf. p. 8).

[Fein, 2019]   Yaakov Y. Fein, Philipp Geyer, Patrick Zwick, Filip Kiałka, Sebastian Pedalino, Marcel Mayor et al. « Quantum superposition of molecules beyond 25 kDa ». *Nature Physics* 15.12 (2019), p. 1242-1245 (cf. p. 5).

[Fekete, 2017]   J. Fekete, S. Chai, S. A. Gardiner et M. F. Andersen. « Resonant transfer of large momenta from finite-duration pulse sequences ». *Phys. Rev. A* 95 (2017), p. 033601 (cf. p. 54).

[Ferrari, 2006]   G. Ferrari, N. Poli, F. Sorrentino et G. M. Tino. « Long-Lived Bloch Oscillations with Bosonic Sr Atoms and Application to Gravity Measurement at the Micrometer Scale ». *Phys. Rev. Lett.* 97 (2006), p. 060402 (cf. p. 63).

[Fixler, 2007]   J. B. Fixler, G. T. Foster, J. M. McGuirk et M. A. Kasevich. « Atom Interferometer Measurement of the Newtonian Constant of Gravity ». *Science* 315.5808 (2007), p. 74-77 (cf. p. 14, 15, 63).

[Flambaum, 2005]   V. V. Flambaum et J. S. M. Ginges. « Radiative potential and calculations of QED radiative corrections to energy levels and electromagnetic amplitudes in many-electron atoms ». *Phys. Rev. A* 72 (2005), p. 052115 (cf. p. 34).

[Foot, 1993]   R Foot, H Lew et R R Volkas. « Electric-charge quantization ». *Journal of Physics G: Nuclear and Particle Physics* 19.3 (1993), p. 361 (cf. p. 57, 62).

[Foot, 1994]   R. Foot. « Electric charge quantization without anomalies? » *Phys. Rev. D* 49 (1994), p. 3617-3621 (cf. p. 62).

[Ford, 1981]   L H Ford et A Vilenkin. « A gravitational analogue of the Aharonov-Bohm effect ». *Journal of Physics A: Mathematical and General* 14.9 (1981), p. 2353 (cf. p. 31).

[Fray, 2004]   Sebastian Fray, Cristina Alvarez Diez, Theodor W. Hänsch et Martin Weitz. « Atomic Interferometer with Amplitude Gratings of Light and Its Applications to Atom Based Tests of the Equivalence Principle ». *Phys. Rev. Lett.* 93 (2004), p. 240404 (cf. p. 15).

[Freier, 2016]   C Freier, M Hauth, V Schkolnik, B Leykauf, M Schilling, H Wziontek et al. « Mobile quantum gravity sensor with unprecedented stability ». *Journal of Physics: Conference Series* 723.1 (2016), p. 012050 (cf. p. 8, 13).

[Garcion, 2021]   C. Garcion, N. Fabre, H. Bricha, F. Perales, S. Scheel, M. Ducloy et al. « Intermediate-Range Casimir-Polder Interaction Probed by High-Order Slow Atom Diffraction ». *Phys. Rev. Lett.* 127 (2021), p. 170402 (cf. p. 41).

[Gauguet, 2009]   A. Gauguet, B. Canuel, T. Lévèque, W. Chaibi et A. Landragin. « Characterization and limits of a cold-atom Sagnac interferometer ». *Phys. Rev. A* 80 (2009), p. 063604 (cf. p. 8).

[Gauguet, 2014]   Alexandre Gauguet. « Foreword ». *Comptes Rendus Physique* 15.10 (2014), p. 787-788 (cf. p. 14).

Bibliographie

[Gautier, 2022]   Romain GAUTIER, Mohamed GUESSOUM, Leonid A. SIDORENKOV, Quentin BOUTON, Arnaud LANDRAGIN et Remi GEIGER. « Accurate measurement of the Sagnac effect for matter waves ». *Science Advances* 8.23 (2022), eabn8009 (cf. p. 63).

[Gebbe, 2021]   Martina GEBBE, Jan-Niclas SIEMSS, Matthias GERSEMANN, Hauke MÜNTINGA, Sven HERRMANN, Claus LÄMMERZAHL et al. « Twin-lattice atom interferometry ». *Nature Communications* 12.1 (2021), p. 2544 (cf. p. 50).

[Geraci, 2016]   Andrew A. GERACI et Andrei DEREVIANKO. « Sensitivity of Atom Interferometry to Ultralight Scalar Field Dark Matter ». *Phys. Rev. Lett.* 117 (2016), p. 261301 (cf. p. 16).

[Gillot, 2013a]   J. GILLOT, S. LEPOUTRE, A. GAUGUET, M. BÜCHNER et J. VIGUÉ. « Measurement of the He-McKellar-Wilkens Topological Phase by Atom Interferometry and Test of Its Independence with Atom Velocity ». *Phys. Rev. Lett.* 111 (2013), p. 030401 (cf. p. 22, 29).

[Gillot, 2013b]   Jonathan GILLOT. « Expériences en interférométrie atomique: application à la mesure des phases géométriques He-McKellar-Wilkens et Aharonov-Casher ». Theses. Université Paul Sabatier - Toulouse III, 2013 (cf. p. 19).

[Gillot, 2013c]   Jonathan GILLOT, Alexandre GAUGUET, Matthias BÜCHNER et Jacques VIGUÉ. « Optical pumping of a lithium atomic beam for atom interferometry ». *The European Physical Journal D* 67.12 (2013), p. 263 (cf. p. 29).

[Gillot, 2014a]   Jonathan GILLOT, Steven LEPOUTRE, Alexandre GAUGUET, Jacques VIGUÉ et Matthias BÜCHNER. « Measurement of the Aharonov-Casher geometric phase with a separated-arm atom interferometer ». *The European Physical Journal D* 68.6 (2014), p. 168 (cf. p. 29).

[Gillot, 2014b]   P GILLOT, O FRANCIS, A LANDRAGIN, F Pereira Dos SANTOS et S MERLET. « Stability comparison of two absolute gravimeters: optical versus atomic interferometers ». *Metrologia* 51.5 (2014), p. L15 (cf. p. 13).

[Gochnauer, 2021]   Daniel GOCHNAUER, Tahiyat RAHMAN, Anna WIRTH-SINGH et Subhadeep GUPTA. « Interferometry in an Atomic Fountain with Ytterbium Bose–Einstein Condensates ». *Atoms* 9.3 (2021) (cf. p. 45).

[Goerz, 2023]   Michael H. GOERZ, Mark A. KASEVICH et Vladimir S. MALINOVSKY. « Robust Optimized Pulse Schemes for Atomic Fountain Interferometry ». *Atoms* 11.2 (2023) (cf. p. 56).

[Göklü, 2008]   Ertan GÖKLÜ et Claus LÄMMERZAHL. « Metric fluctuations and the weak equivalence principle ». *Classical and Quantum Gravity* 25.10 (2008), p. 105012 (cf. p. 15).

[Görlitz, 1995]   A. GÖRLITZ, B. SCHUH et A. WEIS. « Measurement of the Aharonov-Casher phase of aligned Rb atoms ». *Phys. Rev. A* 51 (1995), R4305-R4308 (cf. p. 27).

[Graham, 2016]   Peter W. GRAHAM, Jason M. HOGAN, Mark A. KASEVICH et Surjeet RAJENDRAN. « Resonant mode for gravitational wave detectors based on atom interferometry ». *Phys. Rev. D* 94 (2016), p. 104022 (cf. p. 7).

[Greenberger, 1981]   Daniel M. GREENBERGER, D. K. ATWOOD, J. ARTHUR, C. G. SHULL et M. SCHLENKER. « Is There an Aharonov-Bohm Effect for Neutrons? » *Phys. Rev. Lett.* 47 (1981), p. 751-754 (cf. p. 32, 59).

[Greenberger, 2012]   Daniel M. GREENBERGER, Wolfgang P. SCHLEICH et Ernst M. RASEL. « Relativistic effects in atom and neutron interferometry and the differences between them ». *Phys. Rev. A* 86 (2012), p. 063622 (cf. p. 16).

[Greve, 2022]   Graham P. GREVE, Chengyi LUO, Baochen WU et James K. THOMPSON. « Entanglement-enhanced matter-wave interferometry in a high-finesse cavity ». *Nature* 610.7932 (2022), p. 472-477 (cf. p. 63).

[Guéry-Odelin, 2019]   D. GUÉRY-ODELIN, A. RUSCHHAUPT, A. KIELY, E. TORRONTEGUI, S. MARTÍNEZ-GARAOT et J. G. MUGA. « Shortcuts to adiabaticity: Concepts, methods, and applications ». *Rev. Mod. Phys.* 91 (2019), p. 045001 (cf. p. 54).

[Gupta, 2002]   S. GUPTA, K. DIECKMANN, Z. HADZIBABIC et D. E. PRITCHARD. « Contrast Interferometry using Bose-Einstein Condensates to Measure h/m and α ». *Phys. Rev. Lett.* 89 (2002), p. 140401 (cf. p. 50).

[Gustavson, 2000]   T L GUSTAVSON, A LANDRAGIN et M A KASEVICH. « Rotation sensing with a dual atom-interferometer Sagnac gyroscope ». *Classical and Quantum Gravity* 17.12 (2000), p. 2385 (cf. p. 14, 41).

[Hagen, 1990]   C. R. HAGEN. « Exact equivalence of spin-1/2 Aharonov-Bohm and Aharonov-Casher effects ». *Phys. Rev. Lett.* 64 (1990), p. 2347-2349 (cf. p. 25).

[He, 1993]   Xiao-Gang HE et Bruce H. J. MCKELLAR. « Topological phase due to electric dipole moment and magnetic monopole interaction ». *Phys. Rev. A* 47 (1993), p. 3424-3425 (cf. p. 27).

[He, 2017]   Xiao-Gang HE et Bruce H. J. McKELLAR. « Relativistic dipole interaction and the topological nature for induced HMW and AC phases ». *Phys. Lett. A* 381 (2017), p. 1780-1783 (cf. p. 29).

[Heinz, 2020]   A. HEINZ, A. J. PARK, N. ŠANTI Ć, J. TRAUTMANN, S. G. PORSEV, M. S. SAFRONOVA et al. « State-Dependent Optical Lattices for the Strontium Optical Qubit ». *Phys. Rev. Lett.* 124 (2020), p. 203201 (cf. p. 35).

[Heisenberg, 1925]   W. HEISENBERG. « Über quantentheoretische Umdeutung kinematischer und mechanischer Beziehungen. » *Zeitschrift für Physik* 33.1 (1925), p. 879-893 (cf. p. 5).

[Henson, 2022]   B. M. HENSON, J. A. ROSS, K. F. THOMAS, C. N. KUHN, D. K. SHIN, S. S. HODGMAN et al. « Measurement of a helium tune-out frequency: an independent test of quantum electrodynamics ». *Science* 376.6589 (2022), p. 199-203 (cf. p. 35, 38).

[Herold, 2012]   C. D. HEROLD, V. D. VAIDYA, X. LI, S. L. ROLSTON, J. V. PORTO et M. S. SAFRONOVA. « Precision Measurement of Transition Matrix Elements via Light Shift Cancellation ». *Phys. Rev. Lett.* 109 (2012), p. 243003 (cf. p. 35).

[HILLAS, 1959]   A. M. HILLAS et T. E. CRANSHAW. « A Comparison of the Charges of the Electron, Proton and Neutron ». *Nature* 184.4690 (1959), p. 892-893 (cf. p. 58).

[Hohensee, 2012]   Michael A. HOHENSEE, Brian ESTEY, Paul HAMILTON, Anton ZEILINGER et Holger MÜLLER. « Force-Free Gravitational Redshift: Proposed Gravitational Aharonov-Bohm Experiment ». *Phys. Rev. Lett.* 108 (2012), p. 230404 (cf. p. 32, 57, 63).

[Hosten, 2016]   Onur HOSTEN, Nils J. ENGELSEN, Rajiv KRISHNAKUMAR et Mark A. KASEVICH. « Measurement noise 100 times lower than the quantum-projection limit using entangled atoms ». *Nature* 529.7587 (2016), p. 505-508 (cf. p. 63).

[Hu, 2017a]   Jiazhong HU, Alban URVOY, Zachary VENDEIRO, Valentin CRÉPEL, Wenlan CHEN et Vladan VULETIĆ. « Creation of a Bose-condensed gas of ^{87}Rb by laser cooling ». *Science* 358.6366 (2017), p. 1078-1080 (cf. p. 55).

[Hu, 2017b]   Liang HU, Nicola POLI, Leonardo SALVI et Guglielmo M. TINO. « Atom Interferometry with the Sr Optical Clock Transition ». *Phys. Rev. Lett.* 119 (2017), p. 263601 (cf. p. 8).

[Hu, 2013]   Zhong-Kun HU, Bu-Liang SUN, Xiao-Chun DUAN, Min-Kang ZHOU, Le-Le CHEN, Su ZHAN et al. « Demonstration of an ultrahigh-sensitivity atom-interferometry absolute gravimeter ». *Phys. Rev. A* 88 (2013), p. 043610 (cf. p. 8).

[Hughes, 1988]   V. W. HUGHES, L. J. FRASER et E. R. CARLSON. « The electrical neutrality of atoms ». *Zeitschrift für Physik D Atoms, Molecules and Clusters* 10.2 (1988), p. 145-151 (cf. p. 58).

[Huntington, 2023]   William HUNTINGTON, Jeremy GLICK, Michael BORYSOW et Daniel J. HEINZEN. « Intense continuous cold-atom source ». *Phys. Rev. A* 107 (2023), p. 013302 (cf. p. 41).

[Imhof, 2017]   Eric IMHOF, Benjamin K. STUHL, Brian KASCH, Bethany KROESE, Spencer E. OLSON et Matthew B. SQUIRES. « Two-dimensional grating magneto-optical trap ». *Phys. Rev. A* 96 (2017), p. 033636 (cf. p. 65, 66).

[Jackson, 1999]   John David JACKSON. *Classical electrodynamics.* 3rd ed. New York, NY : Wiley, 1999 (cf. p. 25, 27).

[Jacquey, 2007]   M. JACQUEY, M. BÜCHNER, G. TRÉNEC et J. VIGUÉ. « First Measurements of the Index of Refraction of Gases for Lithium Atomic Waves ». *Phys. Rev. Lett.* 98 (2007), p. 240405 (cf. p. 22).

[Jacquey, 2006]   Marion JACQUEY. « Expériences d interférométrie atomique avec l'atome de lithium ». Theses. Université Paul Sabatier - Toulouse III, 2006 (cf. p. 19).

[Jaeckel, 2010]   Joerg JAECKEL et Andreas RINGWALD. « The Low-Energy Frontier of Particle Physics ». *Annual Review of Nuclear and Particle Science* 60.1 (2010), p. 405-437 (cf. p. 62).

[Jaekel, 2013]   M-T JAEKEL, B LAMINE et S REYNAUD. « Phases and relativity in atomic gravimetry ». *Classical and Quantum Gravity* 30.6 (2013), p. 065006 (cf. p. 6).

[Jansen, 2007]   M. A. H. M. JANSEN, K. F. E. M. DOMEN, H. C. W. BEIJERINCK et K. A. H. van LEEUWEN. « Off-resonance atomic Bragg scattering ». *Phys. Rev. A* 76 (2007), p. 053629 (cf. p. 11).

[Jentsch, 2004]   C. JENTSCH, T. MÜLLER, E. M. RASEL et W. ERTMER. « HYPER: A Satellite Mission in Fundamental Physics Based on High Precision Atom Interferometry ». *General Relativity and Gravitation* 36.10 (2004), p. 2197-2221 (cf. p. 16).

[Kang, 2015]   Kicheon KANG. « Locality of the Aharonov-Bohm-Casher effect ». *Phys. Rev. A* 91 (2015), p. 052116 (cf. p. 24).

[Kao, 2017]   Wil Kao, Yijun Tang, Nathaniel Q. Burdick et Benjamin L. Lev. « Anisotropic dependence of tune-out wavelength near Dy 741-nm transition ». *Opt. Express* 25.4 (2017), p. 3411-3419 (cf. p. 35).

[Karcher, 2018]   R Karcher, A Imanaliev, S Merlet et F Pereira Dos Santos. « Improving the accuracy of atom interferometers with ultracold sources ». *New Journal of Physics* 20.11 (2018), p. 113041 (cf. p. 14).

[Kasevich, 1991]   Mark Kasevich et Steven Chu. « Atomic interferometry using stimulated Raman transitions ». *Phys. Rev. Lett.* 67 (1991), p. 181-184 (cf. p. 5).

[Keith, 1991]   David W. Keith, Christopher R. Ekstrom, Quentin A. Turchette et David E. Pritchard. « An interferometer for atoms ». *Phys. Rev. Lett.* 66 (1991), p. 2693-2696 (cf. p. 5, 7, 16).

[Keller, 1999]   C. Keller, J. Schmiedmayer, A. Zeilinger, T. Nonn, S. Dürr et G. Rempe. « Adiabatic following in standing-wave diffraction of atoms ». *Applied Physics B* 69.4 (1999), p. 303-309 (cf. p. 11).

[Kim, 2020]   Minjeong Kim, Remy Notermans, Chris Overstreet, Joseph Curti, Peter Asenbaum et Mark A. Kasevich. « 40W, 780nm laser system with compensated dual beam splitters for atom interferometry ». *Opt. Lett.* 45.23 (2020), p. 6555-6558 (cf. p. 56).

[King, 1960]   John G. King. « Search for a Small Charge Carried by Molecules ». *Phys. Rev. Lett.* 5 (1960), p. 562-565 (cf. p. 58).

[Kinoshita, 2005]   Toshiya Kinoshita, Trevor Wenger et David S. Weiss. « All-optical Bose-Einstein condensation using a compressible crossed dipole trap ». *Phys. Rev. A* 71 (2005), p. 011602 (cf. p. 55).

[Kirsten-Siemß, 2023]   J.-N. Kirsten-Siemss, F. Fitzek, C. Schubert, E. M. Rasel, N. Gaaloul et K. Hammerer. « Large-Momentum-Transfer Atom Interferometers with μrad-Accuracy Using Bragg Diffraction ». *Phys. Rev. Lett.* 131 (2023), p. 033602 (cf. p. 49, 50).

[Klein, 1986]   A.G. Klein. « Topological effects in neutron optics ». *Physica B+C* 137.1 (1986), p. 230-234 (cf. p. 25).

[Kleinert, 2015]   Stephan Kleinert, Endre Kajari, Albert Roura et Wolfgang P. Schleich. « Representation-free description of light-pulse atom interferometry including non-inertial effects ». *Physics Reports* 605 (2015), p. 1-50 (cf. p. 6).

[Kobakhidze, 2007]   Archil Kobakhidze et Bruce H. J. McKellar. « Particle interference as a test of Lorentz-violating electrodynamics ». *Phys. Rev. D* 76 (2007), p. 093004 (cf. p. 31).

[Kokorowski, 2001]   David A. Kokorowski, Alexander D. Cronin, Tony D. Roberts et David E. Pritchard. « From Single- to Multiple-Photon Decoherence in an Atom Interferometer ». *Phys. Rev. Lett.* 86 (2001), p. 2191-2195 (cf. p. 16).

[Kostelecký, 2011]   V. Alan Kostelecký et Jay D. Tasson. « Matter-gravity couplings and Lorentz violation ». *Phys. Rev. D* 83 (2011), p. 016013 (cf. p. 15).

[Kovachy, 2015a]   T. Kovachy, P. Asenbaum, C. Overstreet, C. A. Donnelly, S. M. Dickerson, A. Sugarbaker et al. « Quantum superposition at the half-metre scale ». *Nature* 528.7583 (2015), p. 530-533 (cf. p. 17, 41, 56).

[Kovachy, 2010]   Tim Kovachy, Jason M. Hogan, David M. S. Johnson et Mark A. Kasevich. « Optical lattices as waveguides and beam splitters for atom interferometry: An analytical treatment and proposal of applications ». *Phys. Rev. A* 82 (2010), p. 013638 (cf. p. 63).

[Kovachy, 2015b]   Tim Kovachy, Jason M. Hogan, Alex Sugarbaker, Susannah M. Dickerson, Christine A. Donnelly, Chris Overstreet et al. « Matter Wave Lensing to Picokelvin Temperatures ». *Phys. Rev. Lett.* 114 (2015), p. 143004 (cf. p. 45).

[Lamine, 2002]   B. Lamine, M. -T. Jaekel et S. Reynaud. « Gravitational decoherence of atomic interferometers ». *The European Physical Journal D - Atomic, Molecular, Optical and Plasma Physics* 20.2 (2002), p. 165-176 (cf. p. 6).

[Lammerzahl, 2007]   C. Lammerzahl, A. Macias et H. Muller. « Limits to differences in active and passive charges ». *Phys. Rev. A* 75 (2007), p. 052104 (cf. p. 57, 62).

[LeBlanc, 2007]   L. J. LeBlanc et J. H. Thywissen. « Species-specific optical lattices ». *Phys. Rev. A* 75 (2007), p. 053612 (cf. p. 35).

[Leonard, 2017]   R. H. Leonard, A. J. Fallon, C. A. Sackett et M. S. Safronova. « Erratum: High-precision measurements of the ^{87}RbD-line tune-out wavelength [Phys. Rev. A 92, 052501 (2015)] ». *Phys. Rev. A* 95 (2017), p. 059901 (cf. p. 17, 35, 38).

[Lepoutre, 2013a]   S. Lepoutre, A. Gauguet, M. Büchner et J. Vigué. « Test of the He-McKellar-Wilkens topological phase by atom interferometry. I. Theoretical discussion ». *Phys. Rev. A* 88 (2013), p. 043627 (cf. p. 29).

[Lepoutre, 2012] S. Lepoutre, A. Gauguet, G. Trénec, M. Büchner et J. Vigué. « He-McKellar-Wilkens Topological Phase in Atom Interferometry ». *Phys. Rev. Lett.* 109 (2012), p. 120404 (cf. p. 22, 29).

[Lepoutre, 2013b] S. Lepoutre, J. Gillot, A. Gauguet, M. Büchner et J. Vigué. « Test of the He-McKellar-Wilkens topological phase by atom interferometry. II. The experiment and its results ». *Phys. Rev. A* 88 (2013), p. 043628 (cf. p. 29).

[Lepoutre, 2009] S. Lepoutre, H. Jelassi, V. P. A. Lonij, G. Trénec, M. Büchner, A. D. Cronin et al. « Dispersive atom interferometry phase shifts due to atom-surface interactions ». *Europhysics Letters* 88.2 (2009), p. 20002 (cf. p. 22).

[Lepoutre, 2011] Steven Lepoutre. « Mesures de précision par interférométrie atomique. Interaction de Van der Waals et phase géométrique de He-McKellar-Wilkens ». Theses. Université Paul Sabatier - Toulouse III, 2011 (cf. p. 9, 19, 29).

[Lévèque, 2022] T. Lévèque, C. Fallet, J. Lefebve, A. Piquereau, A. Gauguet, B. Battelier et al. *CARIOQA: Definition of a Quantum Pathfinder Mission*. 2022. arXiv : 2211.01215 [physics.atom-ph] (cf. p. 14).

[Li, 2022] Xiang Li, Thors Hans Hansson et Wei Ku. « Gauge-independent description of the Aharonov-Bohm effect ». *Phys. Rev. A* 106 (2022), p. 032217 (cf. p. 24).

[Lin, 2009] Y.-J. Lin, A. R. Perry, R. L. Compton, I. B. Spielman et J. V. Porto. « Rapid production of ^{87}Rb Bose-Einstein condensates in a combined magnetic and optical potential ». *Phys. Rev. A* 79 (2009), p. 063631 (cf. p. 55).

[Loriani, 2019] Sina Loriani, Alexander Friedrich, Christian Ufrecht, Fabio Di Pumpo, Stephan Kleinert, Sven Abend et al. « Interference of clocks: A quantum twin paradox ». *Science Advances* 5.10 (2019), eaax8966 (cf. p. 6).

[Louie, 2023] Garrett Louie, Zilin Chen, Tejas Deshpande et Timothy Kovachy. « Robust atom optics for Bragg atom interferometry ». *New Journal of Physics* 25.8 (2023), p. 083017 (cf. p. 56).

[Luo, 2016] Yukun Luo, Shuhua Yan, Qingqing Hu, Aiai Jia, Chunhua Wei et Jun Yang. « Contrast enhancement via shaped Raman pulses for thermal coldatom cloud interferometry ». *The European Physical Journal D* 70.12 (2016), p. 262 (cf. p. 56).

[Malinovsky, 2003] Vladimir S. Malinovsky et Paul R. Berman. « Momentum transfer using chirped standing-wave fields: Bragg scattering ». *Phys. Rev. A* 68 (2003), p. 023610 (cf. p. 50).

[Manicchia, 2023] Michael P. Manicchia, Jeffrey G. Lee et Frank A. Narducci. « Characterization of a Continuous Beam Cold Atom Ramsey Interferometer ». *Atoms* 11.3 (2023) (cf. p. 41).

[Marinelli, 1984] M. Marinelli et G. Morpurgo. « The electric neutrality of matter: A summary ». *Physics Letters B* 137.5 (1984), p. 439-442 (cf. p. 58).

[Marletto, 2020] Chiara Marletto et Vlatko Vedral. « Aharonov-Bohm Phase is Locally Generated Like All Other Quantum Phases ». *Phys. Rev. Lett.* 125 (2020), p. 040401 (cf. p. 24, 31, 63).

[Marton, 1952] L. Marton. « Electron Interferometer ». *Phys. Rev.* 85 (1952), p. 1057-1058 (cf. p. 5).

[Mashhoon, 1988] Bahram Mashhoon. « Neutron interferometry in a rotating frame of reference ». *Phys. Rev. Lett.* 61 (1988), p. 2639-2642 (cf. p. 63).

[McDonald, 2013] G. D. McDonald, C. C. N. Kuhn, S. Bennetts, J. E. Debs, K. S. Hardman, M. Johnsson et al. « 80$\hbar k$ momentum separation with Bloch oscillations in an optically guided atom interferometer ». *Phys. Rev. A* 88 (2013), p. 053620 (cf. p. 45).

[McGilligan, 2015] J. P. McGilligan, P. F. Griffin, E. Riis et A. S. Arnold. « Phase-space properties of magneto-optical traps utilising micro-fabricated gratings. » *Opt. Express* 23.7 (2015), p. 8948-8959 (cf. p. 65, 66).

[McGilligan, 2017] James P. McGilligan, Paul F. Griffin, Rachel Elvin, Stuart J. Ingleby, Erling Riis et Aidan S. Arnold. « Grating chips for quantum technologies ». *Scientific Reports* 7.1 (2017), p. 384 (cf. p. 65, 66).

[McGuirk, 2000] J. M. McGuirk, M. J. Snadden et M. A. Kasevich. « Large Area Light-Pulse Atom Interferometry ». *Phys. Rev. Lett.* 85 (2000), p. 4498-4501 (cf. p. 50).

[McKellar, 2014] B. H. J. McKellar, X-G. He et A. G. Klein. « Topological phases reviewed: The Aharonov Bohm, Aharonov Casher, and He McKellar Wilkens phases ». *AIP Conference Proceedings* 1588.1 (2014) (cf. p. 24, 29, 63).

[McKellar, 2016] Bruce H. J. McKellar. « Aharonov–Bohm types of phases in Maxwell and Yang–Mills field theories ». *International Journal of Modern Physics A* 31.07 (2016), p. 1630004 (cf. p. 24, 29).

[Ménoret, 2018]   Vincent MÉNORET, Pierre VERMEULEN, Nicolas LE MOIGNE, Sylvain BONVALOT, Philippe BOUYER, Arnaud LANDRAGIN et al. « Gravity measurements below 10-9 g with a transportable absolute quantum gravimeter ». *Scientific Reports* 8.1 (2018), p. 12300 (cf. p. 14).

[Merlet, 2021]   Sébastien MERLET, Pierre GILLOT, Bing CHENG, Romain KARCHER, Almazbek IMANALIEV, Ludger TIMMEN et al. « Calibration of a superconducting gravimeter with an absolute atom gravimeter ». *Journal of Geodesy* 95.5 (2021), p. 62 (cf. p. 14).

[Meystre, 2001]   P. MEYSTRE. *Atom Optics*. Series on Atoms and Plasmas. Springer, 2001 (cf. p. 9).

[Miffre, 2006a]   A MIFFRE, M JACQUEY, M BÜCHNER, G TRÉNEC et J VIGUÉ. « Atom interferometry ». *Physica Scripta* 74.2 (2006), p. C15 (cf. p. 5).

[Miffre, 2006b]   A. MIFFRE, M. JACQUEY, M. BÜCHNER, G. TRÉNEC et J. VIGUÉ. « Atom interferometry measurement of the electric polarizability of lithium ». *The European Physical Journal D - Atomic, Molecular, Optical and Plasma Physics* 38.2 (2006), p. 353 (cf. p. 22).

[Miffre, 2005]   Alain MIFFRE. « Expériences d'interférométrie atomique avec le lithium. Mesure de précision de la polarisabilité électrique ». Theses. Université Paul Sabatier - Toulouse III, 2005 (cf. p. 19).

[Mohapatra, 2008]   Ashok K. MOHAPATRA, Mark G. BASON, Björn BUTSCHER, Kevin J. WEATHERILL et Charles S. ADAMS. « A giant electro-optic effect using polarizable dark states ». *Nature Physics* 4.11 (2008), p. 890-894 (cf. p. 61).

[Mohr, 2016]   Peter J MOHR, David B NEWELL et Barry N TAYLOR. « CODATA recommended values of the fundamental physical constants: 2014 ». *Journal of Physical and Chemical Reference Data* 45.4 (2016) (cf. p. 15).

[Möllenstedt, 1955]   G. MÖLLENSTEDT et H. DÜKER. « Fresnelscher Interferenzversuch mit einem Biprisma fur Elektronenwellen ». *Naturwissenschaften* 42.2 (1955), p. 41-41 (cf. p. 5).

[Moore, 2021]   David C MOORE et Andrew A GERACI. « Searching for new physics using optically levitated sensors ». *Quantum Science and Technology* 6.1 (2021), p. 014008 (cf. p. 58, 62).

[Moore, 1995]   F. L. MOORE, J. C. ROBINSON, C. F. BHARUCHA, Bala SUNDARAM et M. G. RAIZEN. « Atom Optics Realization of the Quantum δ-Kicked Rotor ». *Phys. Rev. Lett.* 75 (1995), p. 4598-4601 (cf. p. 54).

[Morel, 2020]   Léo MOREL, Zhibin YAO, Pierre CLADÉ et Saida GUELLATI-KHÉLIFA. « Determination of the fine-structure constant with an accuracy of 81 parts per trillion ». *Nature* 588.7836 (2020), p. 61-65 (cf. p. 8, 15).

[Morinaga, 1999]   M. MORINAGA, I. BOUCHOULE, J.-C. KARAM et C. SALOMON. « Manipulation of Motional Quantum States of Neutral Atoms ». *Phys. Rev. Lett.* 83 (1999), p. 4037-4040 (cf. p. 45).

[Moshinsky, 1952]   Marcos MOSHINSKY. « Diffraction in Time ». *Phys. Rev.* 88 (1952), p. 625-631 (cf. p. 32).

[Mount, 2010]   Brianna J MOUNT, Matthew REDSHAW et Edmund G MYERS. « Atomic masses of 6 Li, 23 Na, 39, 41 K, 85, 87 Rb, and 133 Cs ». *Physical Review. A* 82.4 (2010), p. 042513-042513 (cf. p. 15).

[Müller, 2008]   H. MÜLLER, S.-w. CHIOW et S. CHU. « Atom-wave diffraction between the Raman-Nath and the Bragg regime: Effective Rabi frequency, losses, and phase shifts ». *Phys. Rev. A* 77 (2008), p. 023609 (cf. p. 11).

[Nicholson, 2015]   T. L. NICHOLSON, S. L. CAMPBELL, R. B. HUTSON, G. E. MARTI, B. J. BLOOM, R. L. MCNALLY et al. « Systematic evaluation of an atomic clock at 2 ×10-18 total uncertainty ». *Nature Communications* 6.1 (2015), p. 6896 (cf. p. 35).

[Niebauer, 1995]   T M NIEBAUER, G S SASAGAWA, J E FALLER, R HILT et F KLOPPING. « A new generation of absolute gravimeters ». *Metrologia* 32.3 (1995), p. 159 (cf. p. 13).

[Nshii, 2013]   C. C. NSHII, M. VANGELEYN, J. P. COTTER, P. F. GRIFFIN, E. A. HINDS, C. N. IRONSIDE et al. « A surface-patterned chip as a strong source of ultracold atoms for quantum technologies ». *Nature Nanotechnology* 8.5 (2013), p. 321-324 (cf. p. 65).

[Olariu, 1985]   S. OLARIU et I. Iovitzu POPESCU. « The quantum effects of electromagnetic fluxes ». *Rev. Mod. Phys.* 57 (1985), p. 339-436 (cf. p. 23).

[Oliveira, 1962]   C. G. de OLIVEIRA et J. TIOMNO. « Representations of Dirac equation in general relativity ». *Il Nuovo Cimento (1955-1965)* 24.4 (1962), p. 672-687 (cf. p. 63).

[Osterwalder, 1999]   A. OSTERWALDER et F. MERKT. « Using High Rydberg States as Electric Field Sensors ». *Phys. Rev. Lett.* 82 (1999), p. 1831-1834 (cf. p. 61).

[Overstreet, 2022]   Chris OVERSTREET, Peter ASENBAUM, Joseph CURTI, Minjeong KIM et Mark A. KASEVICH. « Observation of a gravitational Aharonov-Bohm effect ». *Science* 375.6577 (2022), p. 226-229 (cf. p. 17, 32, 57, 63).

[Overstreet, 2021] Chris OVERSTREET, Peter ASENBAUM et Mark A. KASEVICH. « Physically significant phase shifts in matter-wave interferometry ». *American Journal of Physics* 89.3 (2021), p. 324-332 (cf. p. 6).

[Overstreet, 2023] Chris OVERSTREET, Joseph CURTI, Minjeong KIM, Peter ASENBAUM, Mark A. KASEVICH et Flaminia GIACOMINI. « Inference of gravitational field superposition from quantum measurements ». *Phys. Rev. D* 108 (2023), p. 084038 (cf. p. 6, 32).

[Pagel, 2020] Zachary PAGEL, Weicheng ZHONG, Richard H. PARKER, Christopher T. OLUND, Norman Y. YAO et Holger MÜLLER. « Symmetric Bloch oscillations of matter waves ». *Phys. Rev. A* 102 (2020), p. 053312 (cf. p. 50).

[Pancharatnam, 1956] S. PANCHARATNAM. « Generalized theory of interference, and its applications ». *Proceedings of the Indian Academy of Sciences - Section A* 44.5 (1956), p. 247-262 (cf. p. 39).

[Parker, 2016] Richard H. PARKER, Chenghui YU, Brian ESTEY, Weicheng ZHONG, Eric HUANG et Holger MÜLLER. « Controlling the multiport nature of Bragg diffraction in atom interferometry ». *Phys. Rev. A* 94 (2016), p. 053618 (cf. p. 15, 49).

[Pearle, 2017] Philip PEARLE et Anthony RIZZI. « Quantum-mechanical inclusion of the source in the Aharonov-Bohm effects ». *Phys. Rev. A* 95 (2017), p. 052123 (cf. p. 24).

[Perreault, 2005] John D. PERREAULT et Alexander D. CRONIN. « Observation of Atom Wave Phase Shifts Induced by Van Der Waals Atom-Surface Interactions ». *Phys. Rev. Lett.* 95 (2005), p. 133201 (cf. p. 17).

[Peshkin, 2014] M. PESHKIN et A. TONOMURA. *The Aharonov-Bohm Effect.* Lecture Notes in Physics. Springer Berlin Heidelberg, 2014 (cf. p. 23).

[Peshkin, 1999] Murray PESHKIN. « Force-Free Interactions and Nondispersive Phase Shifts in Interferometry ». *Foundations of Physics* 29.3 (1999), p. 481-489 (cf. p. 24).

[Phillips, 1982] William D. PHILLIPS et Harold METCALF. « Laser Deceleration of an Atomic Beam ». *Foundations of Quantum Mechanics in the Light of New Technology.* 48 (1982), p. 596-599 (cf. p. 41).

[Piccard, 1925] A PICCARD et E KESSLER. « Determination of the ratio between the electrostatic charges of the proton and of the electron ». *Arch. Sci. Phys. Nat* 7 (1925), p. 340-342 (cf. p. 57, 58).

[Pippa Storey, 1994] PIPPA STOREY et CLAUDE COHEN-TANNOUDJI. « The Feynman path integral approach to atomic interferometry. A tutorial ». *J. Phys. II France* 4.11 (1994), p. 1999-2027 (cf. p. 6).

[Plotkin-Swing, 2018] Benjamin PLOTKIN-SWING, Daniel GOCHNAUER, Katherine E. MCALPINE, Eric S. COOPER, Alan O. JAMISON et Subhadeep GUPTA. « Three-Path Atom Interferometry with Large Momentum Separation ». *Phys. Rev. Lett.* 121 (2018), p. 133201 (cf. p. 50, 51).

[Quinn, 2000] Terry QUINN. « Measuring big G ». *Nature* 408.6815 (2000), p. 919-920 (cf. p. 15).

[Quinn, 2013] Terry QUINN, Harold PARKS, Clive SPEAKE et Richard DAVIS. « Improved Determination of *G* Using Two Methods ». *Phys. Rev. Lett.* 111 (2013), p. 101102 (cf. p. 15).

[Qureshi, 2023] Izma QURESHI, Tasawar ABBAS, Muhammad IMRAN et Rameez-ul ISLAM. « Exploring wave–particle behaviors of entangled Bragg diffracted neutral atoms ». *Journal of Mathematical Physics* 64.1 (2023), p. 012101 (cf. p. 63).

[Raffelt, 1999] Georg G RAFFELT. « Limits on neutrino electromagnetic properties — an update ». *Physics Reports* 320.1 (1999), p. 319-327 (cf. p. 62).

[Rahman, 2023] Tahiyat RAHMAN, Anna WIRTH-SINGH, Andrew IVANOV, Daniel GOCHNAUER, Emmett HOUGH et Subhadeep GUPTA. *Bloch Oscillation Phases investigated by Multi-path Stuckelberg Atom Interferometry.* 2023. arXiv : 2308.04134 [physics.atom-ph] (cf. p. 54).

[Raman, 1936] C. V. RAMAN et N. S. NAGENDRA NATH. « The diffraction of light by high frequency sound waves ». *Proc. Indian Sci.* A2 (1936), p. 406 (cf. p. 11).

[Ramsey, 1950] Norman F. RAMSEY. « A Molecular Beam Resonance Method with Separated Oscillating Fields ». *Phys. Rev.* 78 (1950), p. 695-699 (cf. p. 5).

[Ratkata, 2021] Apichayaporn RATKATA, Philip D. GREGORY, Andrew D. INNES, Alex J. MATTHIES, Lewis A. MCARD, Jonathan M. MORTLOCK et al. « Measurement of the tune-out wavelength for ^{133}Cs at 880 nm ». *Phys. Rev. A* 104 (2021), p. 052813 (cf. p. 35).

[Rauch, 1974] H. RAUCH, W. TREIMER et U. BONSE. « Test of a single crystal neutron interferometer ». *Physics Letters A* 47.5 (1974), p. 369-371 (cf. p. 5).

[Rauch, 2015] Helmut RAUCH et Samuel A. WERNER. *Neutron Interferometry: Lessons in Experimental Quantum Mechanics, Wave-Particle Duality, and Entanglement.* Oxford University Press, 2015 (cf. p. 5, 16).

[Riehle, 1988]   F. RIEHLE, J. ISHIKAWA et J. HELMCKE. « Suppression of a Recoil Component in Nonlinear Doppler-Free Spectroscopy ». *Phys. Rev. Lett.* 61 (1988), p. 2092-2095 (cf. p. 6, 7).

[Riehle, 1991]   F. RIEHLE, Th. KISTERS, A. WITTE, J. HELMCKE et Ch. J. BORDÉ. « Optical Ramsey spectroscopy in a rotating frame: Sagnac effect in a matter-wave interferometer ». *Phys. Rev. Lett.* 67 (1991), p. 177-180 (cf. p. 5).

[Rosi, 2014]   G. ROSI, F. SORRENTINO, L. CACCIAPUOTI, M. PREVEDELLI et G. M. TINO. « Precision measurement of the Newtonian gravitational constant using cold atoms ». *Nature* 510.7506 (2014), p. 518-521 (cf. p. 8, 15, 63).

[Roy, 2016]   Richard ROY, Alaina GREEN, Ryan BOWLER et Subhadeep GUPTA. « Rapid cooling to quantum degeneracy in dynamically shaped atom traps ». *Phys. Rev. A* 93 (2016), p. 043403 (cf. p. 55).

[Rudolph, 2015]   Jan RUDOLPH, Waldemar HERR, Christoph GRZESCHIK, Tammo STERNKE, Alexander GROTE, Manuel POPP et al. « A high-flux BEC source for mobile atom interferometers ». *New Journal of Physics* 17.6 (2015), p. 065001 (cf. p. 55, 66).

[Rudolph, 2020]   Jan RUDOLPH, Thomas WILKASON, Megan NANTEL, Hunter SWAN, Connor M. HOLLAND, Yijun JIANG et al. « Large Momentum Transfer Clock Atom Interferometry on the 689 nm Intercombination Line of Strontium ». *Phys. Rev. Lett.* 124 (2020), p. 083604 (cf. p. 8, 50).

[Ryutov, 2007]   D D RYUTOV. « Using plasma physics to weigh the photon ». *Plasma Physics and Controlled Fusion* 49.12B (2007), B429 (cf. p. 31).

[Safronova, 2012]   Marianna S. SAFRONOVA, Mikhail G. KOZLOV et Charles W. CLARK. « Blackbody radiation shifts in optical atomic clocks ». *IEEE Transactions on Ultrasonics, Ferroelectrics, and Frequency Control* 59.3 (2012), p. 439-447 (cf. p. 35).

[Salvi, 2018]   Leonardo SALVI, Nicola POLI, Vladan VULETIĆ et Guglielmo M. TINO. « Squeezing on Momentum States for Atom Interferometry ». *Phys. Rev. Lett.* 120 (2018), p. 033601 (cf. p. 63).

[Sangster, 1993]   Karin SANGSTER, E. A. HINDS, Stephen M. BARNETT et Erling RIIS. « Measurement of the Aharonov-Casher phase in an atomic system ». *Phys. Rev. Lett.* 71 (1993), p. 3641-3644 (cf. p. 27).

[Savoie, 2018]   D. SAVOIE, M. ALTORIO, B. FANG, L. A. SIDORENKOV, R. GEIGER et A. LANDRAGIN. « Interleaved atom interferometry for high-sensitivity inertial measurements ». *Science Advances* 4.12 (2018), eaau7948 (cf. p. 14).

[Saywell, 2023]   J. C. SAYWELL, M. S. CAREY, P. S. LIGHT, S. S. SZIGETI, A. R. MILNE, K. GILL et al. *Enhancing the sensitivity of atom-interferometric inertial sensors in dynamic environments using robust control.* 2023. arXiv : 2303.03683 [quant-ph] (cf. p. 56).

[Saywell, 2020]   Jack SAYWELL, Max CAREY, Ilya KUPROV et Tim FREEGARDE. « Biselective pulses for large-area atom interferometry ». *Phys. Rev. A* 101 (2020), p. 063625 (cf. p. 56).

[Schlamminger, 2008]   S. SCHLAMMINGER, K.-Y. CHOI, T. A. WAGNER, J. H. GUNDLACH et E. G. ADELBERGER. « Test of the Equivalence Principle Using a Rotating Torsion Balance ». *Phys. Rev. Lett.* 100 (2008), p. 041101 (cf. p. 16).

[Schlippert, 2014]   D. SCHLIPPERT, J. HARTWIG, H. ALBERS, L. L. RICHARDSON, C. SCHUBERT, A. ROURA et al. « Quantum Test of the Universality of Free Fall ». *Phys. Rev. Lett.* 112 (2014), p. 203002 (cf. p. 15).

[Schlippert, 2020]   D. SCHLIPPERT, C. MEINERS, R.J. RENGELINK, C. SCHUBERT, D. TELL, E. WODEY et al. « Matter-Wave Interferometry for Inertial Sensing and Tests of Fundamental Physics ». *CPT and Lorentz Symmetry.* Singapore : World Scientific, 2020, p. 37-40 (cf. p. 8, 14, 16).

[Schmidt, 2016]   Felix SCHMIDT, Daniel MAYER, Michael HOHMANN, Tobias LAUSCH, Farina KINDERMANN et Artur WIDERA. « Precision measurement of the ^{87}Rb tune-out wavelength in the hyperfine ground state $F = 1$ at 790 nm ». *Phys. Rev. A* 93 (2016), p. 022507 (cf. p. 35).

[Schmiedmayer, 1995]   Jörg SCHMIEDMAYER, Michael S. CHAPMAN, Christopher R. EKSTROM, Troy D. HAMMOND, Stefan WEHINGER et David E. PRITCHARD. « Index of Refraction of Various Gases for Sodium Matter Waves ». *Phys. Rev. Lett.* 74 (1995), p. 1043-1047 (cf. p. 16).

[Schreck, 2021]   Florian SCHRECK et Klaasjan van DRUTEN. « Laser cooling for quantum gases ». *Nature Physics* 17.12 (2021), p. 1296-1304 (cf. p. 55).

[Schrödinger, 1926]   E. SCHRÖDINGER. « An Undulatory Theory of the Mechanics of Atoms and Molecules ». *Phys. Rev.* 28 (1926), p. 1049-1070 (cf. p. 5).

[Schubert, 2021]   Christian SCHUBERT, Sven ABEND, Matthias GERSEMANN, Martina GEBBE, Dennis SCHLIPPERT, Peter BERG et al. « Multi-loop atomic Sagnac interferometry ». *Scientific Reports* 11.1 (2021), p. 16121 (cf. p. 7, 63).

[Sengupta, 2000]   Sujan SENGUPTA. « Binary pulsar PSR B1913+16 constrains the electron-proton charge asymmetry ». *Physics Letters B* 484.3 (2000), p. 275-277 (cf. p. 62).

[Sengupta, 1996]   Sujan SENGUPTA et Palash B. PAL. « Constraints on cosmic electric charge asymmetry and neutrino charge from the microwave background ». *Physics Letters B* 365.1 (1996), p. 175-177 (cf. p. 62).

[Sidorenkov, 2020]   L. A. SIDORENKOV, R. GAUTIER, M. ALTORIO, R. GEIGER et A. LANDRAGIN. « Tailoring Multiloop Atom Interferometers with Adjustable Momentum Transfer ». *Phys. Rev. Lett.* 125 (2020), p. 213201 (cf. p. 7).

[Sorrentino, 2014]   F. SORRENTINO, Q. BODART, L. CACCIAPUOTI, Y.-H. LIEN, M. PREVEDELLI, G. ROSI et al. « Sensitivity limits of a Raman atom interferometer as a gravity gradiometer ». *Phys. Rev. A* 89 (2014), p. 023607 (cf. p. 14).

[Spavieri, 2007]   G. SPAVIERI et M. RODRIGUEZ. « Photon mass and quantum effects of the Aharonov-Bohm type ». *Phys. Rev. A* 75 (2007), p. 052113 (cf. p. 31).

[Stover, 1967]   R. W. STOVER, T. I. MORAN et J. W. TRISCHKA. « Search for an Electron-Proton Charge Inequality by Charge Measurements on an Isolated Macroscopic Body ». *Phys. Rev.* 164 (1967), p. 1599-1609 (cf. p. 58).

[Streed, 2006]   Erik W. STREED, Ananth P. CHIKKATUR, Todd L. GUSTAVSON, Micah BOYD, Yoshio TORII, Dominik SCHNEBLE et al. « Large atom number Bose-Einstein condensate machines ». *Review of Scientific Instruments* 77.2 (2006), p. 023106 (cf. p. 55).

[Szigeti, 2021]   Stuart S. SZIGETI, Onur HOSTEN et Simon A. HAINE. « Improving cold-atom sensors with quantum entanglement: Prospects and challenges ». *Applied Physics Letters* 118.14 (2021), p. 140501 (cf. p. 14).

[Tang, 2013]   Li-Yan TANG, M. W. J. BROMLEY, Z.-C. YAN et J. MITROY. « Dynamic Stark shift of the ^{7}Li($2s \to 3s$) transition ». *Phys. Rev. A* 87 (2013), p. 032507 (cf. p. 38).

[Tarallo, 2014]   M. G. TARALLO, T. MAZZONI, N. POLI, D. V. SUTYRIN, X. ZHANG et G. M. TINO. « Test of Einstein Equivalence Principle for 0-Spin and Half-Integer-Spin Atoms: Search for Spin-Gravity Coupling Effects ». *Phys. Rev. Lett.* 113 (2014), p. 023005 (cf. p. 15).

[Thiele, 2015]   T. THIELE, J. DEIGLMAYR, M. STAMMEIER, J.-A. AGNER, H. SCHMUTZ, F. MERKT et al. « Imaging electric fields in the vicinity of cryogenic surfaces using Rydberg atoms ». *Phys. Rev. A* 92 (2015), p. 063425 (cf. p. 61).

[Thomson, 1928]   George Paget THOMSON. « Experiments on the diffraction of cathode rays ». *Proceedings of the Royal Society of London. Series A, containing papers of a mathematical and physical character* 117.778 (1928), p. 600-609 (cf. p. 5).

[Tiesinga, 2021]   Eite TIESINGA, Peter J. MOHR, David B. NEWELL et Barry N. TAYLOR. « CODATA recommended values of the fundamental physical constants: 2018 ». *Rev. Mod. Phys.* 93 (2021), p. 025010 (cf. p. 15).

[Tino, 2014]   G.M. TINO et M.A. KASEVICH. *Atom Interferometry.* IOS Press, 2014 (cf. p. 5).

[Tonomura, 1986]   Akira TONOMURA, Nobuyuki OSAKABE, Tsuyoshi MATSUDA, Takeshi KAWASAKI, Junji ENDO, Shinichiro YANO et al. « Evidence for Aharonov-Bohm effect with magnetic field completely shielded from electron wave ». *Phys. Rev. Lett.* 56 (1986), p. 792-795 (cf. p. 23).

[Touboul, 2017]   Pierre TOUBOUL, Gilles MÉTRIS, Manuel RODRIGUES, Yves ANDRÉ, Quentin BAGHI, Joël BERGÉ et al. « MICROSCOPE Mission: First Results of a Space Test of the Equivalence Principle ». *Phys. Rev. Lett.* 119 (2017), p. 231101 (cf. p. 16).

[Tourrenc, 1977]   P. TOURRENC. « Geometric structure of charged fields ». *Phys. Rev. D* 16 (1977), p. 3421-3426 (cf. p. 24).

[Trubko, 2017]   Raisa TRUBKO, Maxwell D. GREGOIRE, William F. HOLMGREN et Alexander D. CRONIN. « Potassium tune-out-wavelength measurement using atom interferometry and a multipass optical cavity ». *Phys. Rev. A* 95 (2017), p. 052507 (cf. p. 17, 35).

[Ufrecht, 2020]   Christian UFRECHT et Enno GIESE. « Perturbative operator approach to high-precision light-pulse atom interferometry ». *Phys. Rev. A* 101 (2020), p. 053615 (cf. p. 6).

[Unnikrishnan, 2004]   C S UNNIKRISHNAN et G T GILLIES. « The electrical neutrality of atoms and of bulk matter ». *Metrologia* 41.5 (2004), S125 (cf. p. 57).

[Uys, 2005]   Hermann UYS, John D. PERREAULT et Alexander D. CRONIN. « Matter-Wave Decoherence due to a Gas Environment in an Atom Interferometer ». *Phys. Rev. Lett.* 95 (2005), p. 150403 (cf. p. 17).

[Vaidman, 2012]   Lev VAIDMAN. « Role of potentials in the Aharonov-Bohm effect ». *Phys. Rev. A* 86 (2012), p. 040101 (cf. p. 24).

[Wei, 1995]   Haiqing WEI, Rushan HAN et Xiuqing WEI. « Quantum Phase of Induced Dipoles Moving in a Magnetic Field ». *Phys. Rev. Lett.* 75 (1995), p. 2071-2073 (cf. p. 28).

[Weiss, 1994]   D. S. WEISS, B. C. YOUNG et S. CHU. « Precision measurement of $\hbar/mCs$ based on photon recoil using laser-cooled atoms and atomic interferometry ». *Applied Physics B* 59.3 (1994), p. 217-256 (cf. p. 6).

[Wicht, 2002]   Andreas WICHT, Joel M HENSLEY, Edina SARAJLIC et Steven CHU. « A preliminary measurement of the fine structure constant based on atom interferometry ». *Physica scripta* 2002.T102 (2002), p. 82 (cf. p. 15).

[Wilkason, 2022]   Thomas WILKASON, Megan NANTEL, Jan RUDOLPH, Yijun JIANG, Benjamin E. GARBER, Hunter SWAN et al. « Atom Interferometry with Floquet Atom Optics ». *Phys. Rev. Lett.* 129 (2022), p. 183202 (cf. p. 50).

[Wilkens, 1994]   Martin WILKENS. « Quantum phase of a moving dipole ». *Phys. Rev. Lett.* 72 (1994), p. 5-8 (cf. p. 27).

[Witten, 1979]   E. WITTEN. « Dyons of charge $e\vartheta/2\pi$ ». *Physics Letters B* 86.3 (1979), p. 283-287 (cf. p. 62).

[Wolf, 2004]   Peter WOLF, Sébastien BIZE, André CLAIRON, Giorgio SANTARELLI, Michael E. TOBAR et André N. LUITEN. « Improved test of Lorentz invariance in electrodynamics ». *Phys. Rev. D* 70 (2004), p. 051902 (cf. p. 31).

[Wolf, 2000]   Steffen WOLF, Steven J. OLIVER et David S. WEISS. « Suppression of Recoil Heating by an Optical Lattice ». *Phys. Rev. Lett.* 85 (2000), p. 4249-4252 (cf. p. 55).

[Wu, 1975]   Tai Tsun WU et Chen Ning YANG. « Concept of nonintegrable phase factors and global formulation of gauge fields ». *Phys. Rev. D* 12 (1975), p. 3845-3857 (cf. p. 23, 24, 31).

[Xu, 2019]   Victoria XU, Matt JAFFE, Cristian D. PANDA, Sofus L. KRISTENSEN, Logan W. CLARK et Holger MÜLLER. « Probing gravity by holding atoms for 20 seconds ». *Science* 366.6466 (2019), p. 745-749 (cf. p. 63).

[Xue, 2015]   Hongbo XUE, Yanying FENG, Shu CHEN, Xiaojia WANG, Xueshu YAN, Zhikun JIANG et al. « A continuous cold atomic beam interferometer ». *Journal of Applied Physics* 117.9 (2015), p. 094901 (cf. p. 41).

[Yamashita, 2017]   Kazuya YAMASHITA, Kouhei HANASAKI, Akihiro ANDO, Masahiro TAKAHAMA et Toshiya KINOSHITA. « All-optical production of a large Bose-Einstein condensate in a double compressible crossed dipole trap ». *Phys. Rev. A* 95 (2017), p. 013609 (cf. p. 55).

[Yanagimachi, 2002]   Shinya YANAGIMACHI, Masaki KAJIRO, Mamoru MACHIYA et Atsuo MORINAGA. « Direct measurement of the Aharonov-Casher phase and tensor Stark polarizability using a calcium atomic polarization interferometer ». *Phys. Rev. A* 65 (2002), p. 042104 (cf. p. 27).

[Young, 1997]   Brenton C. YOUNG, Mark A. KASEVICH et Steven CHU. « Precision Atom Interferometry with Light Pulses ». *Atom Interferometry*. Elsevier Science, 1997, p. 363 (cf. p. 58).

[Zeilinger, 1983]   A. ZEILINGER, M.A. HORNE et C.G. SHULL. « Search for Unorthodox Phenomena by Neutron Interference Experiments ». *Foundations of Quantum Mechanics in the Light of New Technology*. Phys. Soc. Japan, Tokyo (1983), p. 289-293 (cf. p. 31).

[Zeilinger, 1986]   Anton ZEILINGER. « Generalized Aharonov-Bohm Experiments with Neutrons ». Sous la dir. de Vittorio GORINI et Alberto FRIGERIO. Boston, MA : Springer US, 1986, p. 311-318 (cf. p. 24, 32).

[Zeiske, 1995]   K. ZEISKE, G. ZINNER, F. RIEHLE et J. HELMCKE. « Atom interferometry in a static electric field: Measurement of the Aharonov-Casher phase ». *Applied Physics B* 60.2 (1995), p. 205-209 (cf. p. 27).

[Zhan, 2020]   Ming-Sheng ZHAN, Jin WANG, Wei-Tou NI, Dong-Feng GAO, Gang WANG, Ling-Xiang HE et al. « ZAIGA: Zhaoshan long-baseline atom interferometer gravitation antenna ». *International Journal of Modern Physics D* 29.04 (2020), p. 1940005 (cf. p. 14, 16).

[Zhang, 2016]   Xian ZHANG, Ruben Pablo del AGUILA, Tommaso MAZZONI, Nicola POLI et Guglielmo M. TINO. « Trapped-atom interferometer with ultracold Sr atoms ». *Phys. Rev. A* 94 (2016), p. 043608 (cf. p. 63).

[Zhou, 2021]   Lin ZHOU, Chuan HE, Si-Tong YAN, Xi CHEN, Dong-Feng GAO, Wei-Tao DUAN et al. « Joint mass-and-energy test of the equivalence principle at the 10^{-10} level using atoms with specified mass and internal energy ». *Phys. Rev. A* 104 (2021), p. 022822 (cf. p. 15).

[Zych, 2011]   Magdalena ZYCH, Fabio COSTA, Igor PIKOVSKI et Časlav BRUKNER. « Quantum interferometric visibility as a witness of general relativistic proper time ». *Nature Communications* 2.1 (2011), p. 505 (cf. p. 6, 16).

[Zygelman, 2015]   B. ZYGELMAN. « Geometric-phase atom optics and interferometry ». *Phys. Rev. A* 92 (2015), p. 043620 (cf. p. 57, 63).

Curriculum Vitae

Alexandre GAUGUET

Associate Professor - Maître de conférences - section 30

French nationality

Date of birth : 15th of november 1980

05 61 55 60 32

Education

2008 : PhD in Physics, Université Paris 6, Paris, France.

2004 : DEA "Lasers et Matière" (Master in Physics), Université Paris 11, Orsay.

2003 : Maîtrise de physique, Université Bretagne Sud, Lorient.

2002 : Licence de physique, Université Bretagne Sud (Bachelor of Science - Physics), Lorient.

Positions

2010 - 2024 : Associate Professor (Maître de conf.), Université Toulouse 3, Toulouse, France.
Laboratoire Collisions Agrégats Réactivité (LCAR) UMR5589.
Since 2014, I head the atom interferometer team.

2008 - 2010: Postdoctoral fellow, Durham University, United Kingdom.
ATMOL group of C.S. Adams.
Topics: Interactions in Rydberg gases for the manipulation of non-classical states of light.

2007 - 2008: Teaching and Research fellow (ATER), Université Paris 13, Villetaneuse, France.
Metrology, Molecules and fundamental tests group of A. Amy-Klein.

Topics: Measurement of the Boltzmann constant with molecular spectroscopy, supervisor Christophe Daussy.

2004 - 2007: PhD student, Université Paris 6, Paris Observatory, Paris, France.
SYRTE Laboratory, Atom interferometry and inertial sensors group of A. Landragin.
Topics: Cold atom gyroscope: Study of limiting stability and systematic effects associated with laser beam splitters. Supervisors A. Landragin and Ph. Tuckey.

Teaching activities

I have carried out all of my teaching activities at the University of Toulouse 3. For 3 years (2014-2017), I benefited from a teaching reduction through a CNRS delegation. Between 2018 and 2024, I have a full teaching load (192h).

Institutional responsabilies

2012-2024 : Organisation of LCAR Seminars

2014-2016 : Member of the "Science de la Matière" council at Toulouse 3 University

2016-2020 : Member of the Labe-NanoX Scientific Council.

2018-2024 : Labex FIRST-TF correspondent for the LCAR

2018-2024 : Equipex Refimeve correspondent for the LCAR

2019-2024 : Member of the local board of the "Société Française de Physique".

Collaborations

B. Battelier, LP2N, Talence, France. 3D Inertial Sensors Development.

V. Menoret, Exail, Talence, France. 3D Inertial Sensors Development.

O. Gauthier-Lafaye, Toulouse, France. Developing Cold Atom Sources on Hybrid Chips.

N. Gaaloul, Hanover, Germany. Simulations of Atom-Optics with Large Momentum Transfer.

B. Canuel, Talence, France. Development of LMT gradiometer.

F. Pereira dos Santos, SYRTE, Paris, France. Constructing Arbitrary Waveform Synthesizers for Driving Optical Lattices.

Student Supervisions

Name	Supervision	Years
J. Gillot	co-supervision (30%)	2010 - 2013
B. Décamps	co-supervision (30%)	2013 - 2016
J. Alibert	co-supervision (50%)	2014 - 2017
M. Bordoux	supervision (100%)	2016-2019
A. Béguin	co-supervision (50%)	2019-2023
T. Rodzinka	co-supervision (50%)	2020 - anticipated 2024
R. Calviac	co-supervision (25%)	2020 - anticipated 2024
L. Calmels	co-supervision (50%)	2022 - anticipated 2025
S. Beldjoudi	co-supervision (50%)	2023 - anticipated 2026

TABLE 5.5 – PhD students

Name	Degree	Duration (month)	Year
S. Beldjoudi	M2	5	2023
C. Franck	M1	2	2022
L. Calmels	M2	5	2022
L. Becker	M1	2	2021
L. Loranca	M2	5	2021
T. Rodzinka	M2	5	2020
A. Béguin	M2	5	2019
P. Lassègues	M2	5	2019
V. Combette	M1	2	2019
P. Azam	M2	4	2018
P. Lassègues	M1	2	2018
V. Czamler	M1	2	2017
J. Junca	M2	5	2017
M. Bordoux	M2	6	2016
E. Gréco	M2	6	2016
L. Lehman	M2	5	2015
R. Corgier	M2	4	2015
J. Alibert	M2	5	2014
R. Picard	L3	3	2014
B. Décamps	M2	4	2013
I. Braud	M2	4	2013
H. Astier	L3	2	2013
D. Sordes	M1	4	2012
A. Omar	M2	4	2012

TABLE 5.6 – Masters and undergraduate internships

Publications and conferences

Publications

1. B. Canuel, F. Leduc, D. Holleville, A. Gauguet, J. Fils, A. Virdis, A. Clairon, N. Dimarcq, Ch. J. Bordé, A. Landragin, and P. Bouyer. Six-Axis Inertial Sensor Using Cold-Atom Interferometry. Phys. Rev. Lett., 97 :010402, Jul 2006.

2. X. Baillard, A. Gauguet, S. Bize, P. Lemonde, Ph. Laurent, A. Clairon, and P. Rosenbusch. Interference-filter-stabilized external-cavity diode lasers. Optics Communications, 266(2) :609-613, 2006.

3. A. Gauguet, B. Canuel, F. Leduc, D. Holleville, N. Dimarcq, A. Clairon, and A. Landragin. Caractérisation d'un gyromètre à atomes froids. J. Phys. IV France, 135 :357?358, 2006.

4. P. Cheinet, B. Canuel, F. Pereira Dos Santos, A. Gauguet, F. Yver-Leduc, and A. Landragin. Measurement of the Sensitivity Function in a Time-Domain Atomic Interferometer. Instrumentation and Measurement, IEEE Transactions on, 57(6) :1141-1148, june 2008.

5. A. Gauguet, T.E. Mehlstäubler, T. Lévèque, J. LeGouët, W.Chaibi, B. Canuel, A. Clairon, F. Pereira Dos Santos, and A. Landragin. Off-resonant Raman transition impact in an atom interferometer. Phys. Rev. A, 78 :043615, Oct 2008.

6. K. Djerroud, C. Lemarchand, A. Gauguet, C. Daussy, S. Briaudeau, B. Darquié, O. Lopez, A. Amy-Klein, C. Chardonnet, and C.J. Bordé. Measurement of the Boltzmann constant by the Doppler broadening technique at a 3,8x10-5 accuracy level. C. R. Phys., 10 :883?893, 2009. LNE and EraNet/IMERA.

7. A. Gauguet, B. Canuel, T. Lévèque, W. Chaibi, and A. Landragin. Characterization and limits of a cold-atom Sagnac interferometer. Phys. Rev. A, 80 :063604, Dec 2009.

8. T. Lévèque, A. Gauguet, F. Michaud, F. Pereira Dos Santos, and A. Landragin. Enhancing the Area of a Raman Atom Interferometer Using a Versatile Double- Diffraction Technique. Phys Rev Lett, 103 :080405, Aug 2009.

9. T. Lévèque, A. Gauguet, W. Chaibi, and A. Landragin. Low noise amplification of an optically carried microwave signal : application to atom interferometry. Appl. Phys. B : Lasers Opt., 101 :723-729, 2010. 10.1007/s00340-010-4082-y.

10. J. D. Pritchard, D. Maxwell, A. Gauguet, K. J. Weatherill, M. P. A. Jones, and C. S. Adams. Cooperative Atom-Light Interaction in a Blockaded Rydberg Ensemble. Phys Rev

Lett, 105 :193603, Nov 2010.

11. J D Pritchard, A Gauguet, K J Weatherill, and C S Adams. Optical non- linearity in a dynamical Rydberg gas. J. Phys. B : At., Mol. Opt. Phys., 44(18) :184019, 2011.

12. S Sevincli, C Ates, T Pohl, H Schempp, C S Hofmann, G Guenter, T Am- thor, M Weidemueller, J D Pritchard, D Maxwell, A Gauguet, K J Weatherill, M P A Jones, and C S Adams. Quantum interference in interacting three-level Rydberg gases : coherent population trapping and electromagnetically induced transparency. J. Phys. B : At., Mol. Opt. Phys., 44(18) :184018, 2011.

13. M Tanasittikosol, J D Pritchard, D Maxwell, A Gauguet, K J Weatherill, R M Potvliege, and C S Adams. Microwave dressing of Rydberg dark states. J. Phys. B : At., Mol. Opt. Phys., 44(18) :184020, 2011.

14. S. Lepoutre, A. Gauguet, G. Trénec, M. Büchner, and J. Vigué. He- McKellar-Wilkens Topological Phase in Atom Interferometry. Phys. Rev. Lett., 109 :120404, Sep 2012.

15. J. Gillot, A. Gauguet, M. Büchner, and J. Vigué. Optical pumping of a lithium atomic beam for atom interferometry. The European Physical Journal D, 67(12) :1?11, 2013.

16. J. Gillot, C. Lemarchand, I. Braud, B. Decamps, A. Gauguet, J. Vigué, and M. Büchner. Note : A passively cooled heat pipe for spectroscopy. Review of Scientific Instruments, 84(10) :106109, 2013.

17. J. Gillot, S. Lepoutre, A. Gauguet, M. Büchner, and J. Vigué. Measurement of the He-McKellar-Wilkens Topological Phase by Atom Interferometry and Test of Its Independence with Atom Velocity. Phys. Rev. Lett., 111 : 030401, Jul 2013.

18. S. Lepoutre, A. Gauguet, M. Büchner, and J. Vigué. Test of the He-McKellar- Wilkens topological phase by atom interferometry. I. Theoretical discussion. Phys. Rev. A, 88 :043627, Oct 2013.

19. S. Lepoutre, J. Gillot, A. Gauguet, M. Büchner, and J. Vigué. Test of the He- McKellar-Wilkens topological phase by atom interferometry. II. The experiment and its results. Phys. Rev. A, 88 :043628, Oct 2013.

20. D. Maxwell, D. J. Szwer, D. Paredes-Barato, H. Busche, J. D. Pritchard, A. Gauguet, K. J. Weatherill, M. P. A. Jones, and C. S. Adams. Storage and Control of Optical Photons Using Rydberg Polaritons. Phys. Rev. Lett., 110 :103001, Mar 2013.

21. Brynle Barrett, Rémy Geiger, Indranil Dutta, Matthieu Meunier, Benjamin Canuel, Alexandre Gauguet, Philippe Bouyer, and Arnaud Landragin. The Sagnac effect : 20 years of development in matter-wave interferometry. Comptes Rendus Physique, 16(3), 2014.

22. Jonathan Gillot, Steven Lepoutre, Alexandre Gauguet, Jacques Vigué, and Matthias Büchner. Measurement of the Aharonov-Casher geometric phase with a separated-arm atom interferometer. The European Physical Journal D, 68(6), 2014.

23. D. Maxwell, D. J. Szwer, D. Paredes-Barato, H. Busche, J. D. Pritchard, A. Gauguet, M. P. A. Jones, and C. S. Adams. Microwave control of the interaction between two optical photons. Phys. Rev. A, 89 :043827, Apr 2014.

24. B. Decamps, J. Gillot, J. Vigue, A. Gauguet, M. Buchner, Observation of Atom-Wave Beats Using a Kerr Modulator for Atom Waves. Phys. Rev. Lett., 116 : 053004, Feb 2016.

25. B. Decamps, A Gauguet, J Vigue, M Buchner, Pancharatnam phase: A tool for atom optics, Phys. rev. a 96 :013624 (2017).

26. J. Alibert, B. Décamps, M. Bordoux, B. Allard, and A. Gauguet, A millimeter magnetic trap for a dual (85Rb and 87Rb) species atom interferometer, RSI 88, 113115 (2017).

27. B. Decamps, J. Gillot, A. Gauguet, J. Vigue and M. Buchner, Phase modulation of atom waves: theory and experiment using the atom optics analogue of the Kerr effect, EPJD 71 (12), 734 (2017).

28. B. Décamps, M. Bordoux, J. Alibert, B. Allard and A. Gauguet, Phase response of atom interferometers based on sequential Bragg diffractions J. Phys. B: At. Mol. Opt. Phys. 52 015003 (2019).

29. El-Neaj, et al. AEDGE: Atomic Experiment for Dark Matter and Gravity Exploration in Space. EPJ Quantum Technol. 7, 6 (2020).

30. B. Décamps, J. Vigué, A. Gauguet, M. Büchner, Measurement of the 671-nm tune-out wavelength of ^7Li by atom interferometry. Phys. Rev. A, 101, 033614 (2020).

31. A. Béguin, T. Rodzinka, J. Vigué, B. Allard, A. Gauguet, Characterization of an atom interferometer in the quasi-Bragg regime. Phys. Rev. A, 105, 033302 (2022).

32. S. Abend et al. Technology roadmap for cold-atoms based quantum inertial sensor in space, AVS Quantum Sci 5, 019201 (2023).

33. A. Béguin, T. Rodzinka, L. Calmels, B. Allard, A. Gauguet, Atom interferometry with coherent enhancement of Bragg pulse sequences. Phys. Rev. Lett., 131, 143401 (2023).

Conferences

1. Journées de Broglie 2023, Paris, France, 2023: invited talk.

2. Very-Long-Baseline Atom Interferometry, Geneva, Switzerland, 2023: invited talk.

3. FOMO, Trieste, Italia, 2022: talk.

4. ONERA seminar, Paris, France, 2021: talk.

5. SYRTE seminar, Paris, France, 2021: talk.

6. Quantum Technology Workshop, Montpellier, France, 2021: invited talk.

7. RTS-CNES, Paris, France, 2019: invited talk.

8. GDR atomes froids, Toulouse, France, 2018: invited talk.

9. SFP, Orsay, France, 2017: talk.

10. IRSAMC seminar, Toulouse, France, 2016: invited talk.

11. FOMO, Chania, Greece, 2014: invited talk.

12. Journées Capteurs Embarquées, Nailloux, France, 2013: invited talk.

13. Sagnac Effect 100 years later, Paris, France, 2013: organizer.

14. IRSAMC seminar, Toulouse, France, 2012: invited talk.

15. LCAR seminar, Toulouse, France, 2009: invited talk.

16. Phlam seminar, Lille, France, 2009: invited talk.

17. ATMOL seminar, Durham, UK, 2008: invited talk.

18. INLN seminar, Nice, France, 2007: invited talk.

19. YAO, Hanover, Germany, 2005: talk.